Applied Materials Today 31 (2023) 101775

Contents lists available at ScienceDirect

Applied Materials Today

journal homepage: www.elsevier.com/locate/apmt

Designing stable lead halide perovskite nanocrystals: From a single particle to nanocomposites

Cynthia Collantes [a], William Teixeira [a], Victoria González Pedro [a,b,*], Maria-José Bañuls [a,b], Ángel Maquieira [a,b]

[a] Instituto Interuniversitario de Investigación de Reconocimiento Molecular y Desarrollo Tecnológico (IDM), Universitat Politècnica de València-Universitat de València, Camino de Vera s/n, València E46022, Spain
[b] Departamento de Química, Universitat Politècnica de València, Camino de Vera s/n, València E46022, Spain

ARTICLE INFO

Keywords:
Lead halide perovskite
Surface chemistry
Stability drawbacks
Core-shell nanoparticles
Nanocomposites

ABSTRACT

Metal halide perovskite nanocrystals have attracted substantial interest given their easy manufacturing, superior Photoluminiscence Quantum Yield and striking optical properties. Despite the huge potential of such materials, their practical implementation and future technological applications need to overcome stability drawbacks: spontaneous degradation, which is accelerated by external stressors (i.e., moisture, oxygen, heat, light, and their combinations), poor phase stability and loss of their colloidal stability due to ligand lability. Within this framework, the understanding of their surface chemistry features and ligand-binding patterns plays a key role in improving the robustness and stability of perovskite nanocrystals. This review presents a comprehensive study of state-of-the-art and current challenges in surface chemistry, interface engineering and encapsulation methodologies for stabilizing lead halide perovskite nanoparticles. We first introduced lead halide perovskite structural and optical properties and a brief discussion of synthesis methods. Next, we explored recent developments in encapsulation methods in different protective matrices comprising from core-shell to macroscale nanocomposites. We also analyzed the advantages and shortcomings of each approach according to their final applications. Finally, we concluded with a discussion of open research challenges and future directions in the aforementioned aspects.

1. Introduction

Lead halide perovskites (LHP) have emerged in the last decade as a new type of materials family that exhibits superior optical features for a myriad of optoelectronic applications, including solar cells, high-efficiency LEDs, imaging labels, high-color-purity displays, low-threshold optical amplifiers and lasers [1,2].

One of the main attractive features of LHP nanocrystals (NCs) is their "defect tolerance", which enables their synthesis under mild conditions. This means that the optical and electronical properties of perovskite appear to behave as if they do not have electronic traps, despite structural characterization suggesting the presence of a high density of structural defects. Several theoretical studies reveal that intrinsic defects, such as vacancies or surface-related sites, have a negligible effect on materials' optical and electrical properties because their defect energy levels are located entirely in either the valence band (VB) or the conduction band (CB) manifolds, but not in the bandgap itself, therefore, preserve a clean bandgap electronic transition [3,4]. This fact is of critical importance in the properties of perovskite NCs because it implies the difference to conventional chalcogenide and metal pnictides (i.e., InP) semiconductors whose properties very much depend on lattice defects.

Unfortunately, bulk perovskite structures present a smaller photoluminescence compared to the nanocrystal counterparts. This fact is mainly addressed in accordance with smaller exciton binding energies, lowering electron-hole capture rates and higher recombination rates through bulk grain-to-grain surfaces and their deleterious effect on the PLQY [5]. Therefore, research has turned its attention to study perovskite NCs because they present larger exciton binding energies, a superior PLQY, and shape- and size-dependent optical and electronic properties that differ from their bulk counterparts due to the quantum confinement regime [6,7].

* Corresponding author at: Instituto Interuniversitario de Investigación de Reconocimiento Molecular y Desarrollo Tecnológico (IDM), Universitat Politècnica de València-Universitat de València, Camino de Vera s/n, València E46022, Spain.
E-mail address: vigonpe@upv.es (V. González Pedro).

https://doi.org/10.1016/j.apmt.2023.101775
Received 2 November 2022; Received in revised form 3 February 2023; Accepted 11 February 2023
Available online 22 February 2023

Since the pioneering colloidal synthesis of LHP NCs, countless innovate synthesis and processing have delivered materials that have been tested in solar cells, [8,9] solar concentrators [10], visible light communications [11], electroluminescent diodes [12], photodetectors [13], and photocatalysis [14]. Besides all this, their PLQY, together with higher-order nonlinear optical properties, [15] make them promising and versatile luminophores for *in vitro* bioimaging and biosensing purposes[16,17], and also for super-resolution imaging applications that go beyond optical diffraction limits [18]. Despite such rapid advancements in material syntheses and device applications, poor chemical, structural and colloidal stability because of their soft ionic binding nature and ligand lability hinders their implementation. Hence gaining knowledge and answering questions about interface properties, surface stability issues and ligand-to-surface bonding mechanisms will enable the design of "tailored-made" NCs designed according to the needs of the final purpose that remain stable in different chemical environments.

This article aims to cover the recent advances made in designing stable LHP NCs by performing an extensive analysis of the state of art of surface functionalization strategies and discussing the strengths and weakness of different approaches. This manuscript is structured in the following sections. First, it includes a brief introduction to LHP NC to provide an understanding of their nature, crystal structures and properties, as well as a summary and analysis of the different strategies to synthesize LHP NCs. Then it provides a comprehensive explanation of approaches for improving the stability of LHP, including post-synthetic modifications and the formation of core-shell nanoparticles (NPs) at a single particle level, and the formation of easily processable macroscale composites. The last section deals with the recent progress made in colloidal LHP applications by considering their advantages and disadvantages as to their bulk counterparts. We finish this review with our vision of the future of this field.

2. Colloidal semiconductor perovskite nanocrystals

2.1. Discovery and brief history of colloidal perovskite NCs

In the early 1980s, the discovery of quantum-sized effects in the optical spectra of nanometer-sized semiconductors triggered research into the synthesis of colloidal semiconductor NCs, often referred as Quantum Dots (QDs) [19]. Their large PLQY, multiphoton absorption properties and size-tunable band gaps have enabled their exploitation in a wide range of applications in far-ranging fields,such as optoelectronics and life sciences [20,21]. Nearly all of the work has focused to date on binary compounds, designated as II-VI (Zn, Cd, Hg), III-V (InP and InAs), IV-VI (Pb and Sn chalcogenides) and multinary compounds (e.g. copper zinc tin sulfide, copper indium gallium selenide, etc.).

One of the major limitations that semiconductor NCs face is the presence of detrimental shallow electronic surface defects on their large surface area, which arises from undercoordinated surface sites and deviations from bulk stoichiometry on the surface, and lead to the formation of trap states for charge carriers. Therefore, attaining high-performance QDs requires the rational control of these surface defects and, therefore, involves intricate synthetic methodologies and the development of elaborate NCs heterostructures with both inorganic and organic passivating agents.

Consequently, the several works that described the defect-tolerant nature of metal halide perovskites in 2012 encouraged the scientific community to study the colloidal synthesis of metal halide perovskite as a new type of nanomaterials that encompass the concomitant optoelectronic properties of colloidal NCs and the absence of detrimental structural defects. This hypothesis has been well-proven by the pioneer synthetic works described by Schmidt et al. [22] and Protesescu et al. [6]. The former described 6 nm-sized $CH_3NH_3PbBr_3$ NCs prepared by the reverse microemulsion methodology, which give a PLQY of 20%. Soon after in 2015, Protesescu et al. synthesized monodispersed colloidal NCs prepared by hot injection methodologies with a large PLQY of ~90%, and achieved without any additional post-synthetic treatment, and with tunable emission properties across the entire visible spectral range, by varying the ratio of the halide precursors, PL with a narrow full width at the half-maximum (fwhm), namely below 15 nm. Also in 2015, Zhang et al. [23] synthesized $CH_3NH_3PbX_3$ NCs by a supersaturated recrystallization methodology in the presence of surfactants. From this work, it is remarkably that LHP NCs exhibit very big PLQYs close to unity despite being prepared by a reprecipitation method at room temperature without further surface passivation other than the original ligand coverage. This behavior was totally unexpected and indicated that many things that we have learned from studying conventional semiconductor QDs compounds have to be thought over again because LHP behave differently. In line with these ideas, we direct readers to recent reviews for a comprehensive comparison of LHP NCs to well-established QDs [24]. Hereafter, we refer LHP as NCs instead of QDs, because in most cases they present weak confinement regime where the size effect on the band gap is small.

Thus, easy synthesis procedures together with fascinating properties, as well as the many questions that have arisen in light of these initial results, have made perovskite NCs an appealing topic for the scientific community.

2.2. Structure and general properties of perovskite NCs

2.2.1. Composition, crystal structure and defect tolerance

The classic 3D metal halide perovskite (MHP) adopts an ideal general formula ABX_3, and consists in a cubic array of corner-sharing BX_6 octahedra, where B is a 6-fold coordinated metal cation (Pb^{2+}, Sn^{2+} or Ge^{2+}) surrounded by halides (namely chloride, bromide, iodide, or their mixture). The A-site is commonly occupied by monovalent organic cations of methylammonium ($CH_3NH_3^+$, MA) and formamidinium ($CH(NH_2)_2^+$, FA), as well as inorganic cations of cesium Cs^+ and rubidium Rb^+, located in cuboctahedra voids.

The relative ion size requirements to stabilize the cubic structure are quite stringent. The commonest rule to predict the stability of 3D structures is the Goldschmidt tolerance factor, t, calculated as follows:

$$t = (r_A + r_B) \Big/ \sqrt{2(r_B + r_X)} \quad (1)$$

where r_A, r_B, and r_X represent the radii of ions A, B and X, respectively. In general, stable 3D perovskite structures are formed when t is between 0.8 and 1 [25]. With LHP, due to the higher covalency of their bonding as regards their fluoride and oxide counterparts, the formation of sTable 3D perovskites is restrained for $t \geq 0.89$. For this reason, only a limited number of A-cations (Cs, MA, and FA) can produce sTable 3D structures. The perovskites at the edge of the tolerance factor requirement, such as $FAPbI_3$ ($t \sim 1$) and $CsPbI_3$ ($t \sim 0.8$), easily undergo phase transition at room temperature (RT) to stabler 1D hexagonal and orthorhombic phases [26,27] (yellow phases). When t is calculated to be beyond these two ranges, the 3D LHP collapse to nonperovskite or lower-symmetry distorted versions, in which the coordination numbers of A cations, B cations, or both, lower (Fig. 1A).

Another critical parameter to predict spatial restrictions is the octahedral factor, μ, which is defined as $\mu = r_B/r_X$, and describes the stability of the $[BX_6]^{2-}$ octahedral. The stability range for μ lies between 0.442 and 0.895. Tolerance and octahedral factors are currently a smart tool to predict stability and to discover novel possible perovskite structures. The combined structural map for all known LHP compounds (Fig. 1B) indicates a clear-cutoff at $0.88 < t < 1.1$ and $0.41 < \mu < 0.89$. [26]

In addition, one of the most striking properties of LHP, which has been ascribed to their success as high-performance semiconductors, is their good tolerance to defects. The term "defect tolerance" refers to the ability to preserve a clean band gap even in the presence of a high concentration of defects. Such behavior is attributed mainly to two factors. First, the nature of electronic structures of halide perovskites,

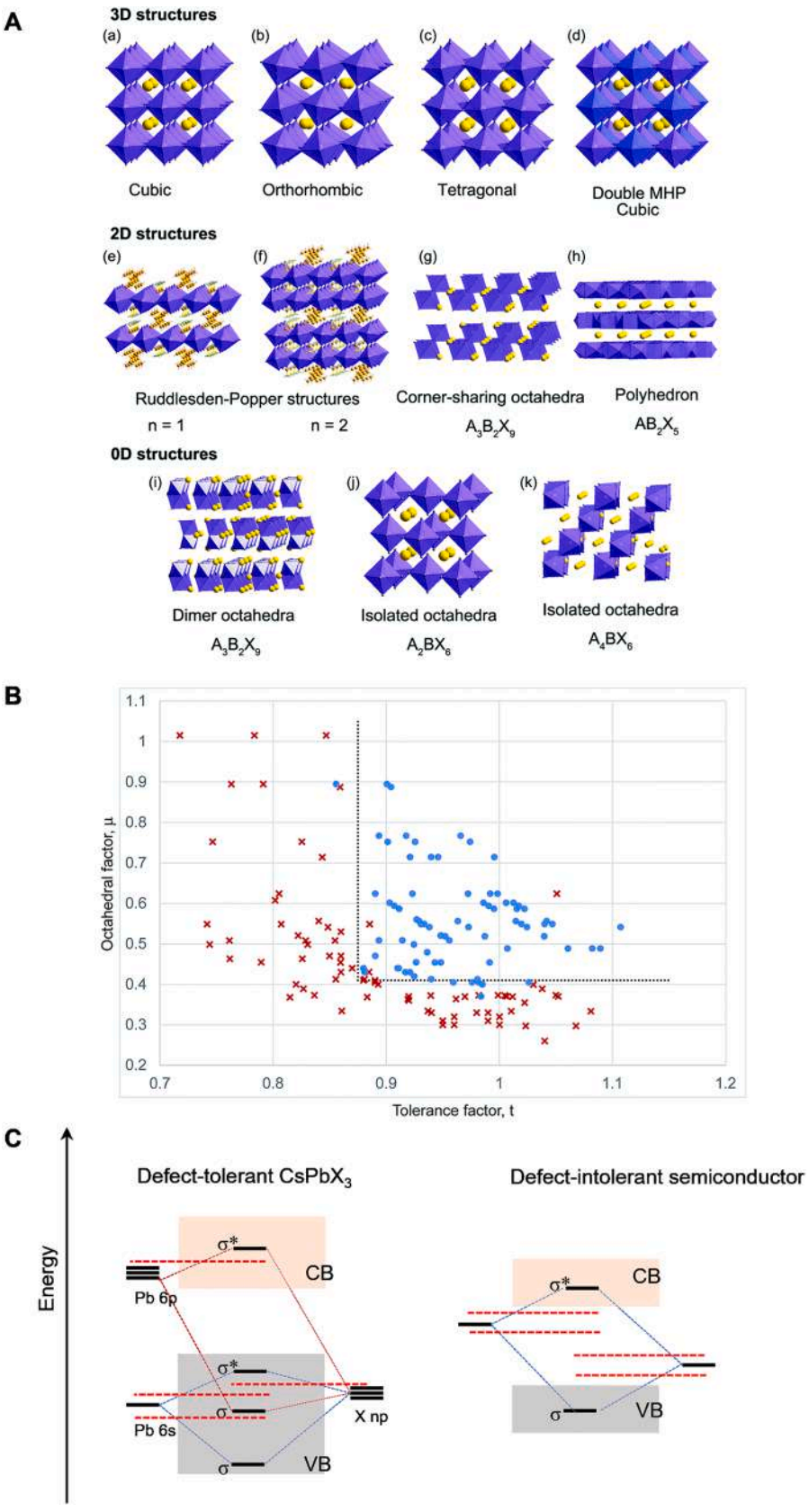

Fig. 1. A) Schematic sketch of ideal 3D-cubic LHP and 3D distorted orthorhombic and tetragonal structures and perovskite-related 2D and 0D structures. (reproduced from Ref. [28] with permission from the Royal Society of Chemistry). (B) The T-μ plot of LHP. Reprinted with permission from Ref. [26] Copyright 2016 American Chemical Society. Blue dots represent the LHP compositions that adopt the perovskite structure at room temperature and pressure, while red crosses denote the inorganic compounds that do not form perovskites. (C) A simplified diagram of the electronic band structure of defect-intolerant and defect-tolerant semiconductors.

where the conduction band forms from the antibonding orbitals and structural defects tend to have energy levels that fall in the CB and VB, respectively, rather than lying in the bandgap itself [29]. This starkly contrasts with conventional defect-intolerant semiconductors, such as Si, CdSe, or GaAs, where the bandgap is formed between bonding and antibonding orbitals, and point defects emerge as weak bonding or nonbonding states in the bandgap (Fig. 1C).

Second, another consideration for explaining clean bandgaps is related to the energy of defect formation in LHP. Interstitial and anti-site defects, which would form deep trap states in the electronic structure (Fig. 2B), have high formation energies and are almost absent because the ions in the perovskite lattice are energetically difficult to misplace [30,31]., whereas defects with low formation energies, such as vacancies A-site and halide vacancies, have transition energies slightly above (below) the valence (conduction) band; e.g., for $CH_3NH_3PbI_3$, A-site vacancies $V_{CH3NH3PbI3}$ have transition energies lower than 0.05 eV above the valence band [32].

To date, most of the progress in MHP NCs has been made in lead $APbX_3$ with a cubic or pseudo-cubic 3D crystal structure. However, the poor stability and intrinsic toxicity of this class of halide perovskites has stimulated research into other structures and compositions, such as those defined as "perovskite-related structures", the so-called 0D and 2D structures. [28,33,34] (Fig. 1A)

2.2.2. Optical properties

Compositional band gap tunability. From the very beginning, one of the most noteworthy features of LHP is their composition engineering of their band gap. A broad spectral range can be covered by a selective presynthetic mixture of the Cl/Br and Br/I ratios (Fig. 2A). This easy tunability is associated with valence band edge energy shifts because the halide component changes, with only minor changes to the conduction band edge due to their stronger ionic nature, with Pb orbitals contributing with ~70–90% [35,36].

The A-cation also has a significant effect on the band gap of perovskites. For instance, in lead halide perovskite, as the A-cation size diminishes, the bandgap blue- shifts because of the distortion of the cubic crystal structure due to lattice contraction and the concomitant increase in the tilting angle of the Pb-X-Pb bonds (Fig. 2B). Thus iodide perovskites have been shown to shift from 690 nm for Cs^+ to 734 nm for MA^+ and 784 nm for FA^+ [37–40].

Besides all this, the B-site cation also plays an important role in the final optical properties of MHP NCs. It has been described that the substitution of Pb^{2+} for Sn^{2+} or Ge^{2+} results in a strong red shift of their bandgap and PL emission. [41–43] This fact is attributed to their higher electronegativity as regards Pb^{2+}. However, Sn-based and Ge-based perovskites suffer from extremely poor stability caused by ready $B^{2+} \rightarrow B^{4+}$ oxidation, and only a single study of Ge-based perovskites has been reported to date [44].

PLQY, emission and confinement properties. LHP NCs, unlike their chalcogenide based QDs predecessors, typically present big PLQYs, even in the absence of passivation shells. PLQYs up to 70–95% have been described for bromide and iodide species of cesium, methylammonium and formamidinium lead halide perovskites [37,39,45–47]. In contrast, they present small excitonic Bohr radii (example, 5–12 nm for Cs-based NCs [6] and 1.5–3 nm [48]. for hybrid NCs). Consequently, many reported LHP NCs display only a weak quantum confinement compared to conventional QDs. (Fig. 3).

Chloride-based LHP present much smaller PLQYs ($\leq$ 20%). This is likely attributed to the small size of the chloride anion, which results in lattice shrinkage and crystal structure distortion, or is due to the fact that defects in Cl-perovskites are not as benign as in their Br and I perovskites. Therefore, they might act as electronic nonradiative traps.

A strategy to obtain strong blue luminescent LHP perovskite NCs is to dope bromide perovskites with additional ions. For instance, partially exchanging the Pb^{2+} ions in $CsPbBr_3$ NCs with several other divalent cations, such as Sn^{2+}, Cd^{2+} and Zn^{2+}, results in a blue-shift of PL bands, and a PLQY over 60% is maintained (Fig. 4A). [49]

Another method to obtain blue-emitting LHP NCs is the synthesis of $CsPbX_3$ 2D nanoplatelets (NPLs), which exhibits strong-confinement effects [47,50,51]. In these nanostructures, a pronounced blue-shift of absorption onsets (up to 170 nm) has been reported when their thicknesses drop to five monolayers [52]. Several works have demonstrated how their PL emission properties can be tuned throughout the visible range by synthetically adjusting crystal sizes [53–56] (Fig. 4B).

Other critical parameters, especially for emitting applications, are Stokes shifts and fwhm widths. For LHP, the reported Stokes shifts are small (5–15 nm) and size-dependent [57]. Several studies have also demonstrated that Stokes shift can also be engineered by doping NCs with transition metal elements to achieve extremely high Stokes shift values of ~200 nm for $CsPbCl_3$ NCs doped with Mn^{2+} ions (Fig. 5) [10, 58,59]. Another strategy to reduce Stokes shift is to reduce NCs dimensions due to the aforementioned size-dependent confinement properties. [60] Regarding fwhm width, LHP exhibit narrow width lines within the 12–40 nm range, which is comparable to the best CdSe-QD systems currently used in commercially lighting technologies.

Nonlinear optics. One of the most fascinating properties of LHP is their multiphoton absorption. This means that the photons whose energy goes below the bandgap ($h\nu \leq EG$) can also be used to generate an electron-hole pair. This phenomenon was first described by Wang et al. who found that $CsPbBr_3$ NCs exhibit strong nonlinear absorption and emission, as well as a two-photon absorption cross-section as high as $\sim 1.2 \times 10^5$ GM at 800 nm, which were two orders of magnitude larger than that observed in conventional semiconductor QDs (Fig 6A) [61]. With MA-based NCs, the reported absorption cross-sections are even one order of magnitude higher. Chen et al. reported absorption cross sections for up to five-photon in both MA- and Cs-containing bromide perovskite NCs encapsulated in $(OA)_2PbBr_4$ shells. [15] The observation of nonlinear optics is especially appealing for many applications like photovoltaics because more of the solar spectrum can be used to generate a current or optical bioimaging, where the use of near infrared sources (NIR) sources reduces autofluorescence, and also tissue and cell damage.

Due to their large absorption cross-sections, LHPs are shown to be promising as an inexpensive optical gain medium and stable amplified spontaneous emission (ASE). In 2015, the first ASE and lasing in MHP nanocrystals of $CsPbX_3$ was demonstrated with low pump thresholds down to 5 ± 2 μJ cm^{-2} [63]. Over the past 3-4 years, many reports have focused on the study of the mechanism of optical amplification in LHPs [64,65]. However, the intrinsic mechanism underlying the optical gain in LHPs remains poorly studied and, it is still under debate whether the single- or biexciton regime is realized in LHPs at threshold excitation fluencies or if free carriers are the dominant mechanism in the stimulated emission process

Another interesting nonlinear phenomenon is the so-called quantum cutting effect. This consists in a particular case of a down conversion energy process that typically occurs in bulk crystals doped with rare earth ions, in which a high-energy photon is absorbed and converted into two lower-energy photons or more, with consequent PLQY values exceeding the unity. This phenomenon has also been observed in Ce-doped and Yb-doped LHP NCs, with PLQYs up to 170% in the NIR (Fig 6B) [62].

2.3. Synthesis of LHP colloidal NCs

Since the first report of colloidal LHP NCs, several synthesis methods have been developed in response to requirements of NCs stability and applications. The particle size, dimensionality and morphological

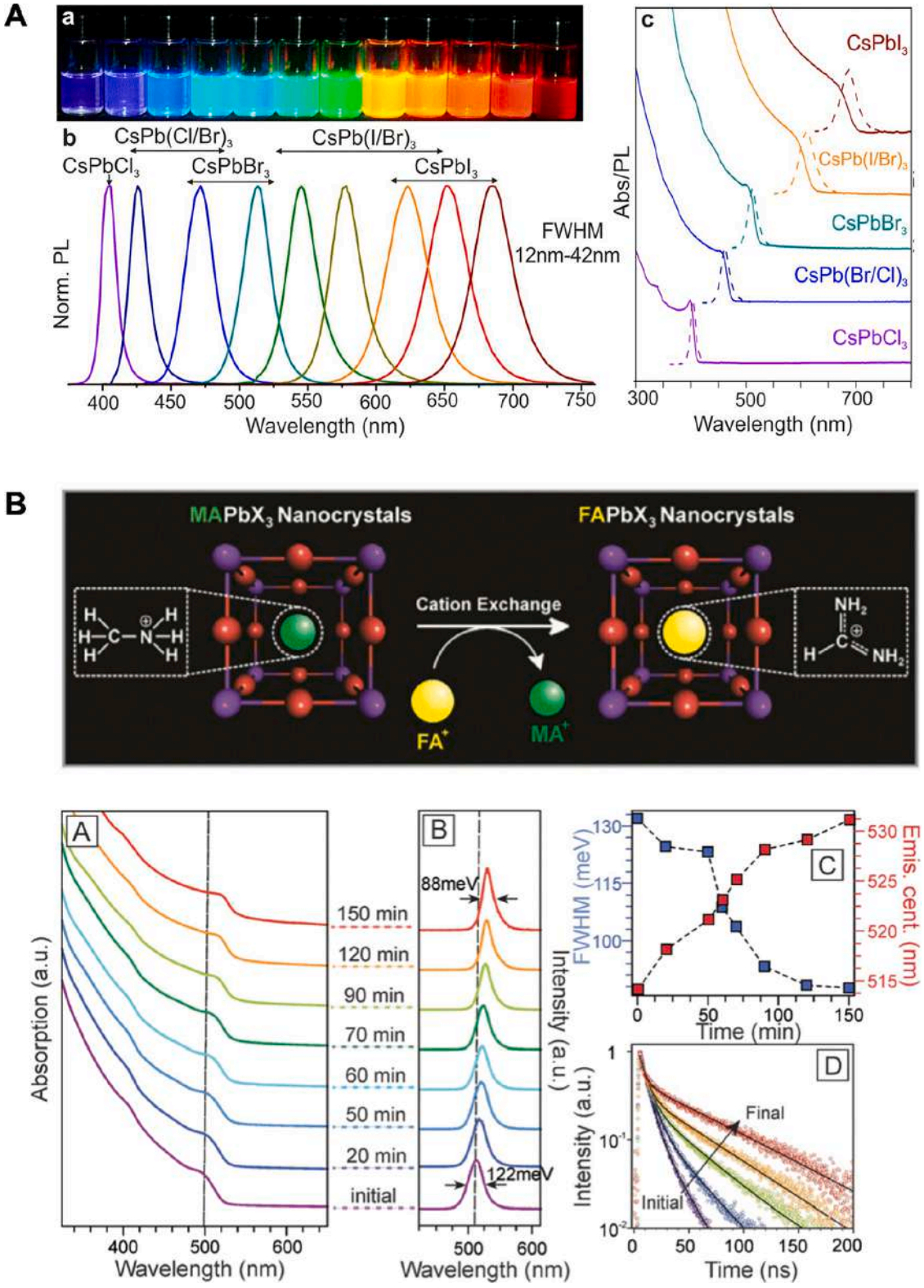

Fig. 2. Panel A. Colloidal perovskite $CsPbX_3$ NCs (X = Cl, Br, I) with composition-tunable bandgap energies along the entire visible spectrum. Adapted with permission from Ref. [6] Copyright 2015 American Chemical Society). Panel B Evolution of the optical properties of MHP NCs during the $MA^+ \rightarrow FA^+$ cation exchange reaction. (A) and (B) Absorption and PL spectra. (C) and (D) PL peak position shift (red square), FWHM (blue square) and lifetime curve decays as a function of reaction time. (Reproduced from Ref. [40] with permission from the Royal Society of Chemistry).

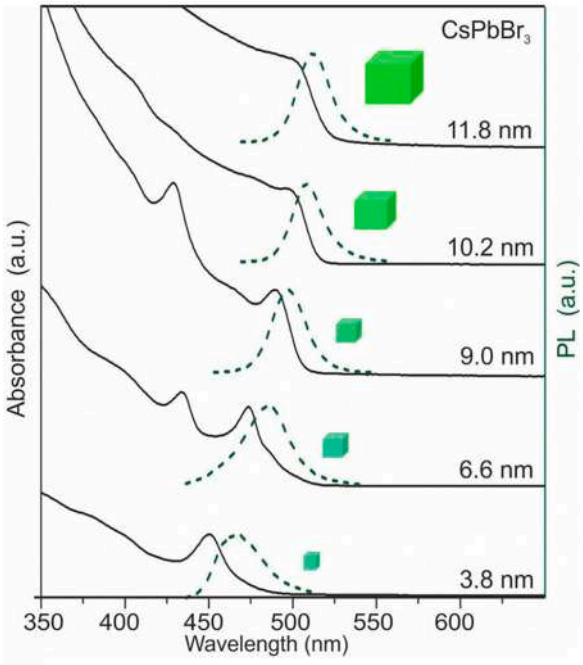

Fig. 3. Size confinement effects in the absorption and emission spectra of $CsPbBr_3$ NCs. Adapted from Ref. [6] Copyright 2015 American Chemical Society.

features, as well as optoelectronic properties like bandgap, emission wavelength and charge mobility, can easily be customized by controlling the experimental conditions, including the concentration and amount of the perovskite reaction temperature, environmental conditions and reaction time. These approaches include: a) bottom-up methods, such as hot-injection, solvent-induced precipitation, ligand-assisted reprecipitation (LARP), ultrasonication, chemical deposition, solvothermal, spray pyrolysis and microwave-assisted methods; b) top-down approaches, such as wet ball milling or laser ablation (Fig. 7) [66].

Pérez-Prieto et al. pioneered the wet chemistry colloidal synthesis of hybrid metal halide NCs [22]. In their work, 6 nm-sized $MAPbBr_3$ NCs were obtained by a reverse microemulsion technique, also referred to as 'solvent-induced precipitation'. Mixing a small amount of a polar solvent in a nonpolar solvent generates reverse micelles (i.e.: a polar core and a hydrophobic shell). Given that perovskite precursors are soluble in polar solvents, but are insoluble in nonpolar solvents, reverse micelle cores act as suitable confined nucleation sites for crystal growth. The presence of capping ligands helps to control the morphology and crystal size by, thus, preserving the excellent optoelectronic properties of the resulting NCs, with a PLQY of 87% [45]. Table 1 summarizes the LHP's optical and structural features for different strategies described in the state-of-the-art.

Zhang et al. [23] also obtained brightly luminescent colloidal 3.3 nm-sized $MAPbBr_3$ NCs with a PLQY of up to 70% by a slightly different approach known as LARP. This method is based on the supersaturated recrystallization principle, which consists of inducing a high salt saturation state from a solution of ions in equilibrium by reducing its solubility, e.g.: cooling down the solution, evaporating the solvent or adding a miscible cosolvent, where the solubility of ions is low, also termed 'antisolvent'. Under such conditions, spontaneous precipitation and crystallization reactions occur until the system once again reaches an equilibrium state. This strategy was extended to different halide and A^+ cation compositions with PLQYs of around 70–90% being described. In addition, LARP is a low-cost method and is convenient for scale-up production [67].

The hot-injection (HI) method was developed by Kovalenko et al. [6] for the preparation of cesium lead-halide colloidal NCs. It was inspired by the approach typically employed for classic colloidal cadmium chalcogenide QDs, such as CdSe and PbSe. This method consists of the rapid injection of precursor Cs-oleate into a PbX_2 solution containing oleylamine (OLA), oleic acid (OA) and octadecene (ODE) at high temperature in an inert atmosphere, which makes HI not as cost-effective as LARP. After injection, rapid nucleation occurs with the simultaneous formation of small nuclei. Then the reaction solution is ice bath-cooled to stop crystal growth, and results in a narrow size distribution of NCs. The HI method was further extended to MA- and FA-based LHP NC systems by replacing Cs-oleate with MA or FA cations [68]. PLQYs near unity are reported for the HI methodology, and both shape and particle size can be tuned by adjusting the reaction conditions (i.e. ligand concentration, temperature, etc.) [73].

Interest in exploring yet more new synthesis strategies has not been waned. In the same year, Seokjin et al. [70] and Protesescu et al. [71] reported a ligand-assisted wet ball milling method to produce LHP NCs. This grinding method, performed in the presence of a solvent and organic ligands, involves mechanical friction between high-hardness zirconia balls and the ground material (bulk perovskite or salt precursors), which generates a final powder on the micron- and nanoscale. Compared to HI, wet ball milling has its shortcomings, such as broader size distribution, presence of impurities, and a mixed population of NCs and NPLs. Despite this fact, it is considered a green chemistry approach because it does not require high temperatures and consumes minimal quantities of solvents. Besides, its production yield is bigger than what typical bottom-up approaches can offer. So it seems interesting for scalability purposes given the increasing demands for their use in optoelectronic applications [70].

Ahmadian-Yadzi et al. [69]. reported using spray-pyrolysis as an alternative method. They prepared methylammonium lead halide perovskite particles by aerosolizing a precursor solution, which turned into pure and crystalline perovskite powders after heat treatment. A limitation of these methodologies is the production of a heterogeneous population of large NCs ($>$ 500 nm) beyond a wide size range with poor colloidal stability.

Rosa-Pardo et al. [72]. also showed interest in applying top-down methods and recently explored laser ablation to obtain NCs from a micrometer-sized single $MAPbBr_3$ crystal by pulsed-laser irradiation. Unlike wet ball milling, this approach enables a narrow size distribution of NCs (4–8 nm) to be obtained, which is similar to that reported for the NCs obtained by the HI methodology.

As we face the need to develop enviro-friendly, stable and efficient perovskite materials for future imaging and optoelectronic applications, interest in searching for lead-free halide perovskites with comparable optical and electronic properties has lately increased [74]. For this purpose, several metal cations, which are less or nontoxic, have been explored as Pb substitutes at the B-site, including Group 14 elements (Sn and Ge)[75,76], Group 15 elements adjacent to Pb (Sb and Bi)[77,78], double elements (Bi combined with Ag) and rare-earth elements (Eu, Yb) [79,80].

3. Interface engineering: coatings and surface modification strategies

One of the major limitations of LHP NCs is related to their chemical stability. With LHP, the experimentally measured formation enthalpies of $MAPbI_3$, by means of acid-solution calorimetry, show that $MAPbI_3$ is thermodynamically unstable and prone to decompose to its halide precursors ($MAPbI_3 \rightarrow MAI$ and PbI_2). [81] This finding correlates with the theoretical predictions by first-principles calculations, which claim that $MAPbI_3$ spontaneously decompose and this process is greatly accelerated by moisture, oxygen, heat, light, and their combination [82–85]. When I^- is replaced with Br^- or Cl^- or organic cation MA^+ with inorganic Cs^+, perovskites become stabler and do not spontaneously decompose. [82,86,87] Yet due to the strong ionic bonding nature, they are unstable in essentially all polar solvents and sensitive to

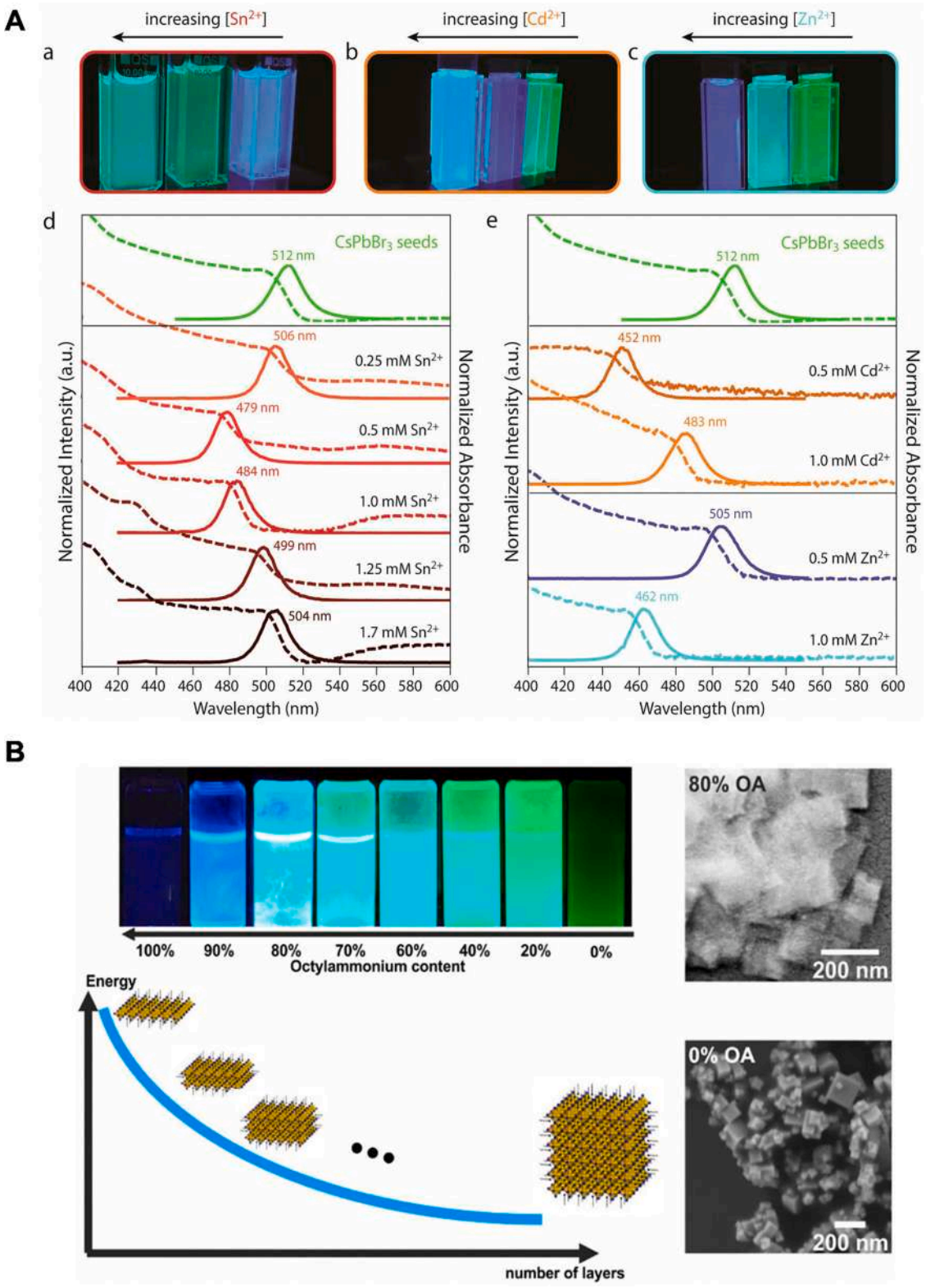

Fig. 4. Strategies to obtain strong blue luminescent perovskite NCs. A) By doping lead bromide perovskites with other additional cations. B) By exploiting quantum confinement properties. Adapted from Ref. [49] and [50] Copyright 2015. American Chemical Society).

environmental moisture [84].

In structural stability terms with iodide LHP, the $CsPbI_3$ 3D-orthorhombic and $FAPbI_3$ 3D-cubic phases are metastable at room temperature and tend to convert into wide band gap 1D-orthorhombic ($CsPbI_3$) and 1D-hexagonal ($FAPbI_3$) phases [88–92]. These transitions take from several months for FA-based ones to weeks for Cs-based ones. This poor phase stability, combined with the poor chemical stability of $MAPbI_3$ NCs, makes it difficult to obtain stable NCs with PL in red and near-infrared spectral regions, and has been termed as the "perovskite red wall" [27].

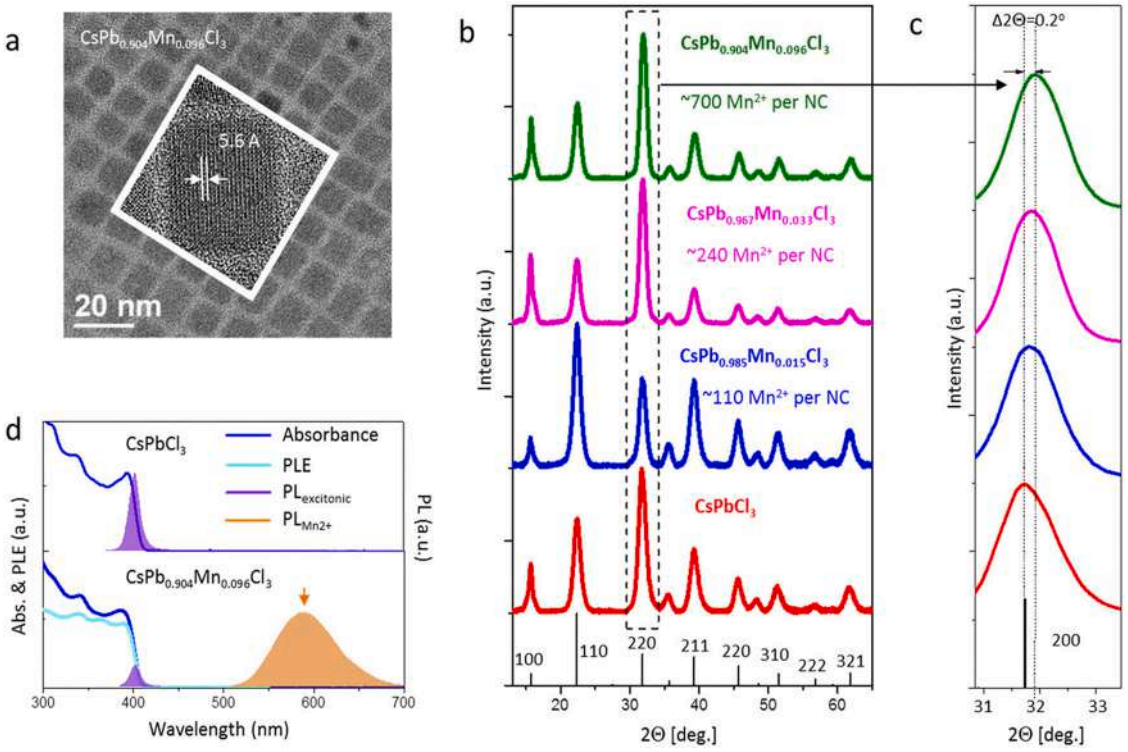

Fig. 5. Structural and spectral characterizations of undoped and Mn-doped $CsPbCl_3$ NCs. Doped NCs obtain a higher Stokes shift value (~ 200 nm) when addressing the Mn^{2+} d–d transition. Adapted from Ref. [59] Copyright 2016 American Chemical Society.

From the thermal stability perspective, LHP exhibit moderate thermal decomposition temperatures of 150–200 °C for $MAPbI_3$ and 290−300 °C for $FAPbI_3$ [93]. In addition, another formidable challenge in LHP arises from the labile and highly dynamic nature of the ligand shell, which causes desorption of capping ligands and loss of colloidal stability [94]. These drawbacks have led to intense research into perovskite surfaces and ligand chemistries, and to the development of encapsulation strategies inside inorganic and polymeric coatings to stabilize them, which we consider in detail below.

3.1. *Surface chemistry of LHP NCs*

Before discussing LHP NCs post-synthetic chemical modifications and encapsulation strategies, we first introduce the first insight into LHP surface features. Fig. 8A schematically depicts the principal perovskite ligand-binding motifs. Considering the different synthetic routes of LHP, it is accepted that alkylammonium ligands attach to the perovskite surface through hydrogen bonding and electrostatic interactions with halide anions, while oleate ligands do so by chelate binding with Cs^+ and Pb^{2+} dangling bonds [6,23,94]. However, more in-depth studies carried out by means of a Nuclear Overhauser Effect Spectroscopy (NOESY) NMR analysis have pointed out that, due to their strong ionic nature, $CsPbBr_3$ NCs prefer ionic ligands like NH_3^+ and Br^- instead of those with a more covalent nature, such as oleates (Fig. 8B) [94]. In addition, further experimental and theoretical works suggest that the surface of perovskite NCs is terminated by lead bromide, and surface Cs^+ are replaced with oleylammonium chains, which stabilize the nanocrystal by three hydrogen bonds forming between the $-NH_3^+$ moiety and the surrounding Br^- on the surface of NCs [54,95,96].

LHP surfaces present low energy formation of halide vacancies, which entails the creation of naked Pb^{2+} atoms on the surface of NCs, and has been demonstrated to be deleterious to NCs' optical performance [31,32,97]. Therefore, the effective repair of lead-rich surfaces via the passivation of under-coordinated Pb^{2+} with Br^- or small molecules like thiocyanates confers perovskite NCs with the resulting PLQY near unity [98,99]. Along these lines, Alpert *et al.* screened surface trap passivation efficacy for $CsPbX_3$ NCs of over 20 ligands with different binding motifs, including alkylammonium and oleate X-type ligands and phosphines, pyridine, thiophene, or amines Z-type ligands. Of them, tri-n-butylphosphine demonstrated effective surface trap passivation for $CsPbX_3$, while thiophene, pyridine and dodecanethiol (DDT) appeared to improve the PLQY of $CsPbI_3$ NCs (Fig. 9) [100]. These data agree well with a previous report on colloidal NCs and thin films. [99,101–107]

Compared to the classic chalcogenide QDs, LHP are more ionic in nature and interactions with capping ligands are extremely dynamic. This results in the rapid desorption of the protective ligand shell upon the isolation and purification of colloids, which is observed as loss of colloidal stability and a rapid drop in PLQY. In addition, loss of the ligand shell is accelerated by the Bronsted acid-base neutralization reaction between oleate and alkylammonium olefins. This eventually leads to loss of structural integrity, i.e., sintering of NCs in bulk polycrystalline materials [108,109]. An effective strategy to address such an issue is to use zwitterionic capping ligands, such as lecithin and benzene sulfonic acid, whose cationic and anionic groups have no possibility of mutual or external neutralization and, furthermore, their attachment to the NC surface is kinetically stabilized by the chelate effect [109,110].

Another interesting ligand is didodecyl dimethylammonium bromide (DDAB), which has been demonstrated to replace original OLA ligands and provide very stable LHP NC films [111]. This is due to dual surface trap passivation via the surface repair of Br^- vacancies and the ionic interaction of quaternary cation with surface bromides. Potassium-oleate (K^+-oleate) has also been introduced to protect and passivate the surface of LHP NCs by filling Cs^+ vacancies with K^+, which leads to an enhancement of optical properties and of the photo and thermal stability of LHP NCs [112].

In all these protocols, the presence of insulating long-chain aliphatic molecules hinders the exploitation of such NCs in optoelectronic applications. To overcome this issue, short aromatic ligands, such as benzoic acid or 4- phenylbutylamine in an appropriate (co)solvent (e.g., octane and benzene), can be utilized as safe media to remove the long-chain

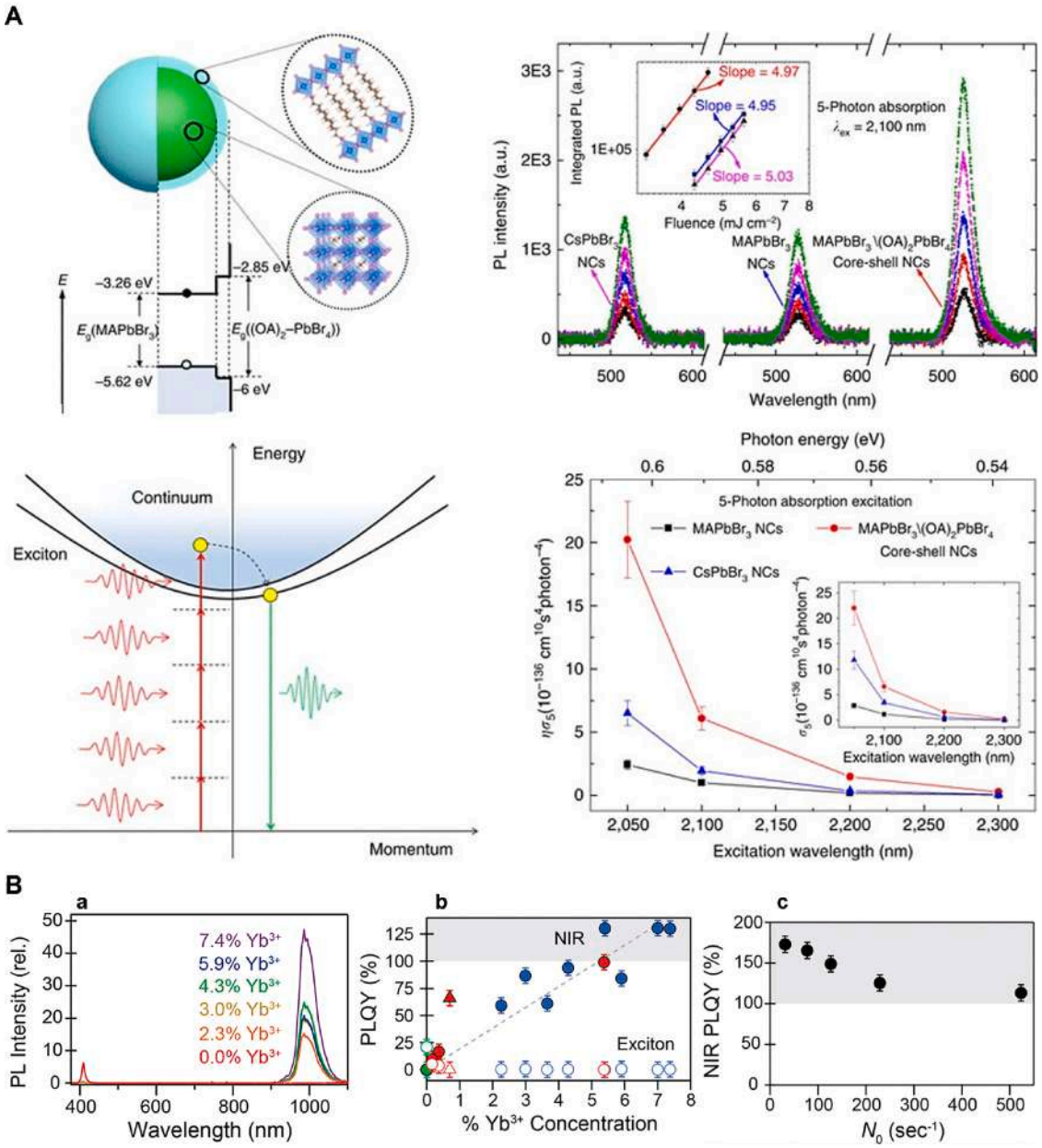

Fig. 6. A) Core-shell multidimensional NCs with 3D $MAPbBr_3$ as a core and 2D $(OA)_2PbBr_4$ as a shell, which exhibit giant 5-photon action cross-sections. Reproduced with permission from Ref [15]., Springer Nature Ltd. (B) Optical properties of Yb^{3+}: $CsPbCl_3$ NCs, including room-temperature PL spectra (a), exciton (open) and NIR (closed) PLQYs plotted as a function of the Yb^{3+} concentration. $\lambda_{exc} = 375$ nm, excitation, $N_0 = 369\ s^{-1}$ and (c) NIR PLQYs of a sample of 5.2% Yb^{3+}-doped $CsPbCl_3$ NCs plotted as a function of the photoexcitation rate. The experimental NIR PLQY reaches 170% at its highest value. Reproduced from Ref [62]. Copyright 2018 American Chemical Society.

aliphatic molecules present on the surface of the as-synthesized NCs [113]. In addition, Wheeler et al. have reported the post-synthetic modification of $CsPbI_3$ NCs with methylacetate and formamidinium iodide to exchange electronic-insulating olefin ligands for shorter molecules to prepare functional electronically coupled films [114].

3.2. Ligand assisted phase transitions

Due to the soft nature of LHP NCs, the interaction with ligands can induce a phase transformation accompanied by shape evolution. For instance, with 3D $CsPbBr_3$ NCs, transformation to lead-depleted 0D Cs_4PbBr_6 is held in the presence of amine or alkyl-thiol ligands [115–119]. In addition, this transformation process can be reversed by the addition of OA [116], lead bromide [120], Prussian Blue, [121] maleic anhydride[122] or water traces [123].

Another example of the phase transformation of 3D $CsPbBr_3$ to 2D $CsPb_2Br_5$ can occur in the presence of DDAB via ligand exchange and the exfoliation/reorganization of $CsPbBr_3$ NCs [124]. A similar conversion can occur under $PbBr_2$-rich conditions ($CsPbBr_3 + PbBr_2 \rightarrow CsPb_2Br_5$) [119,125].

Further to ligand-assisted phase transformation, other extrinsic factors can induce phase conversion, such as heat [121,126], light [127–129], pressure[130,131] and water [132,133].

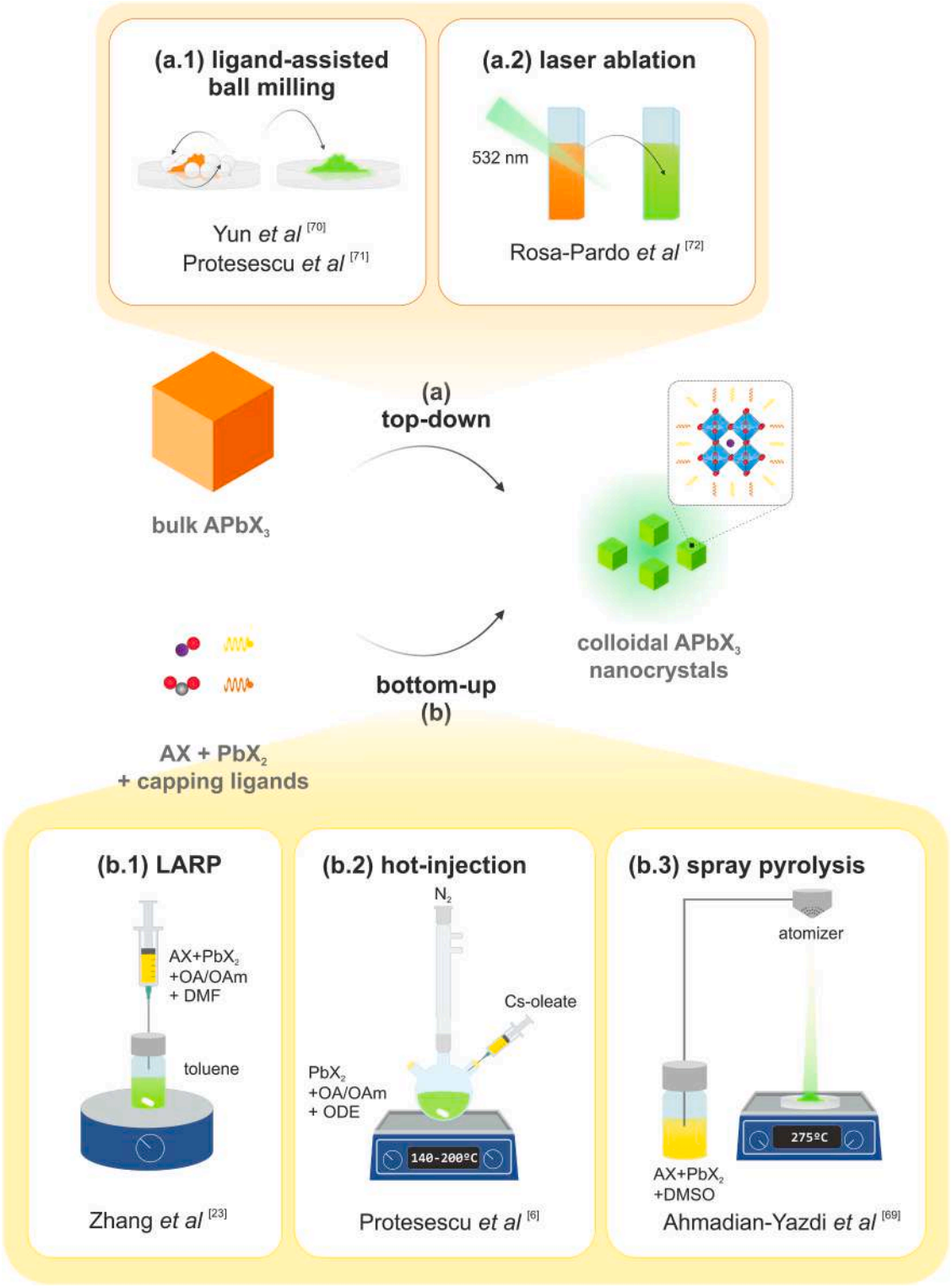

Fig. 7. Scheme of the most representative top-down and bottom-up synthetic strategies of LHP NCs.

4. Synthetic strategies toward improving the stability of lead halide perovskite nanocrystals

The ability to manipulate NCs' surfaces is essential for their future technological development. However, the surface manipulation of LHP has proven particularly challenging compared to that of more established inorganic materials due to their highly dynamic surface chemistry and low material formation energy threshold. Most conventional chemical manipulation methods that address the LHP surface result in the transformation or dissolution of the LHP crystal. This section seeks to summarize recent developments in encapsulation methods of LHP, which go from the development of core-shell NPs to the fabrication of macroscale composites by assessing the strengths and weaknesses of each strategy.

Table 1
Summary of the optical features reported of the most representative top-down and bottom-up LHP synthetic strategies described in the literature.

Synthesis method	Composition (AbX_3)	NCs size (nm)	PLQY (%)	FHWM (nm)	Refs.
Solvent-induced precipitation	$MAPbBr_3$	6	20%	25	[22]
Ligand-assisted reprecipitation	$MAPbBr_3$	3.3	70%	21	[23]
	$CsPbX_3$ (X = Cl, Br, I)	8–10	70–95%	18–35	[67]
Hot-injection	$CsPbX_3$ (X = Cl, Br, I)	4–15	50–90%	12–42	[6]
	$MAPbX_3$, (*X* = Br, I)	10–35	15–50%	19–22	[68]
Spray pyrolysis	$MAPbI_3$	> 100	N. A.	N. A.	[69]
Ligand-assisted ball milling	$APbBr_3$ (*A* = MA, FA)	20	25%	–	[70]
	$APbBr_3$ (A = Cs, FA)	N. A.	75–80%	27–34	[71]
Laser ablation	MAPbX (*X* = Br, I)	4–8	6–67%	32–76	[72]

4.1. *Improving the stability of LHP at a single particle level*

The ability to reliably improve the stability of LHP NCs while retaining their individual nanometer size represents a critical step that underpins future advances in optoelectronic applications or as a luminescent probe. Here we review and analyze the different approaches described in the literature to obtain LHP NCs with improved water stability, while preserving NP individuality. They go from the bottom-up synthesis of core-shell nanocomposites to the top-down preparation of water-stable LHP from larger crystals. Fig. 10 is the schematic diagram of the principal LHP stabilization strategies. Table 2 describes the stability, optical and structural features of state-of-art data compilation.

4.1.1. *Modification or replacement of the native ligand*

A common strategy to improve the stability of LHP NCs is to decorate their surface with ligands, which offer steric hindrance and, hence, hinder the diffusion of water molecules to the perovskite core by avoiding their decomposition, and by also preserving colloidal and structural stability.

Along these lines, one interesting approach is the replacement of oleylamine synthetic precursor in the HI methodology by the commonly known trioctylphosphine (TOP) and trioctylphosphine oxide (TOPO). Apart from the stronger steric effect of the TOP ligand owing to their multibranched nature, under these conditions the reaction environment is free of amines, which avoids the neutralization reaction with OAs and subsequent ligand losses. In addition, according to the hard and soft acid and base (HSAB) theory, phosphine ligands allegedly possess stronger bonding with Pb^{2+} compared to OA and OLA, which enables ligand shell stabilization toward moisture (Fig 11A) [134–136]. TOP-$CsPbBr_3$ withstands exposure to ethanol in room light for 30 days with no significant fluorescent quenching.

An alternative strategy consists in ligand replacement in the LARP synthesis procedure. By using thiol appended polyhedral oligomeric silsesquioxane (POSS), which provides steric hindrance, $CsPbX_3$~~NCs NPs~~, which preserve their luminescence after 10 storage weeks under ambient conditions, were achieved (Fig 11B) [45,137]. The use of strong bonding tetradecylphosphonic acid as a LARP precursor provides $CsPbBr_3$ NCs coated with alkylphosphates, which retain 75% of their relative PL after dispersion in water for 5 h or heated to 375 K (100 °C). [138] In a similar approach, highly hydrophobic synthetic precursors, such as fluorocarbon alkoxysilanes, also enable the direct synthesis of $CsPbBr_3$ in water, which exhibits a big absolute PLQY (~80%) with PL lasting for weeks. [139] However, the resulting NPs exhibit marked size variations and polydispersity.

Most of the studies in the literature that report these methods describe stability in a mixture of water and nonprotic solvents, which indicates that water diffusion and perovskite decomposition are not prevented. Thus, further research that seeks more robust shells is mandatory. In addition, the described final products are suspensions and aggregates with high polydispersity and a broad size distribution due to their hydrophobic ligand nature, which negatively affects the use and processing of perovskite NCs in most applications.

Finally, ligand exchange has been successfully demonstrated to preserve the structural stability of LHP. For example, the replacement of OA with an alkyl phosphinic acid leads to phase-stable cubic perovskite $CsPbI_3$ NCs being obtained, whose structural stability remains for over 20 days [143]. In an alternative approach, their post-synthetic passivation process by using a bidentate ligand, namely 2,2′-iminodibenzoic acid, renders passivated NCs, which exhibit narrow red PL with an exceptional PLQY ~~quantum yield~~ (close to unity) and substantially improved phase stability (Fig 11C) [144].

4.1.2. *Encapsulation in amphiphilic lipidic micelles*

Lipid core micelles are a well-known and thoroughly studied system used for the encapsulation of QDs and organic molecules, such as organic dyes or drugs, which enables their transfer and dispersion in aqueous media.

This strategy with LHP NCs is very challenging because it pursues the stabilization and dispersion of a hydrophilic core in polar media (unlike QDs or organic molecule, which are highly insoluble in water, and LHP are strongly ionic and water-sensitive in nature). Thus to date, the use of amphiphilic molecules has proven useful only for providing robust shells with improved structural stability (i.e. reduced detachment of surface ligands and NCs sintering in bulk crystals) [109,110].

Notwithstanding, very few works have demonstrated the effective encapsulation of LHP and nanoparticle stabilization in water by using amphiphilic micelles. For instance, Gomez et al. developed a smart strategy based on their encapsulation in solid lipid nanoparticles (made of lipids that are solid at room temperature) and stabilized by emulsifiers in water. By this methodology, $CsPbX_3$ NCs encapsulated inside stearic acid solid lipid NPs, which preserve their water stability for a period longer than 2 months, have been reported (Fig. 12) [145]. By a different approach, Yang et al. reported $CsPbBr_3$ NCs encapsulated in phospholipidic micelles that bore different hydrophilic heads, which preserve their PL in water for days, and even under alkaline or acid conditions [17].

The main drawback of this strategy is the formation of polydisperse emulsion with a wide particle size distribution and heterogeneous NCs shapes (nanoplatelets, nanorods, etc.). Thus future research is necessary into the ligand design and development of double layered lipidic micelles, which produce monodisperse NCs while preserving their structural and optical properties in water media.

Other works have used micelle-forming polymer derivates for the growth and encapsulation of water-stable polymer NCs, which are considered to be more stable than their surfactant counterparts. Works related to polymeric micelles are discussed later in the polymer coating section.

4.1.3. *Encapsulation with inorganic materials*

Silica shell. Significant interest has been shown for nearly 20 years in overcoating inorganic NCs with silica (SiO_2), which is chemically stable and transparent in the whole visible region, can protect materials against moisture-induced damage and possesses facile surface modification with different functional groups to enable the further functionalization of the outer surface of NCs, irrespectively of the core material and its surface chemistry.

Normally, the silica shell is formed by the sol-gel approach, which consists in the basic hydrolysis of a silicon alkoxide precursor (tetramethylorthosilicate (TMOS) or tetraethylorthosilicate (TEOS)), followed

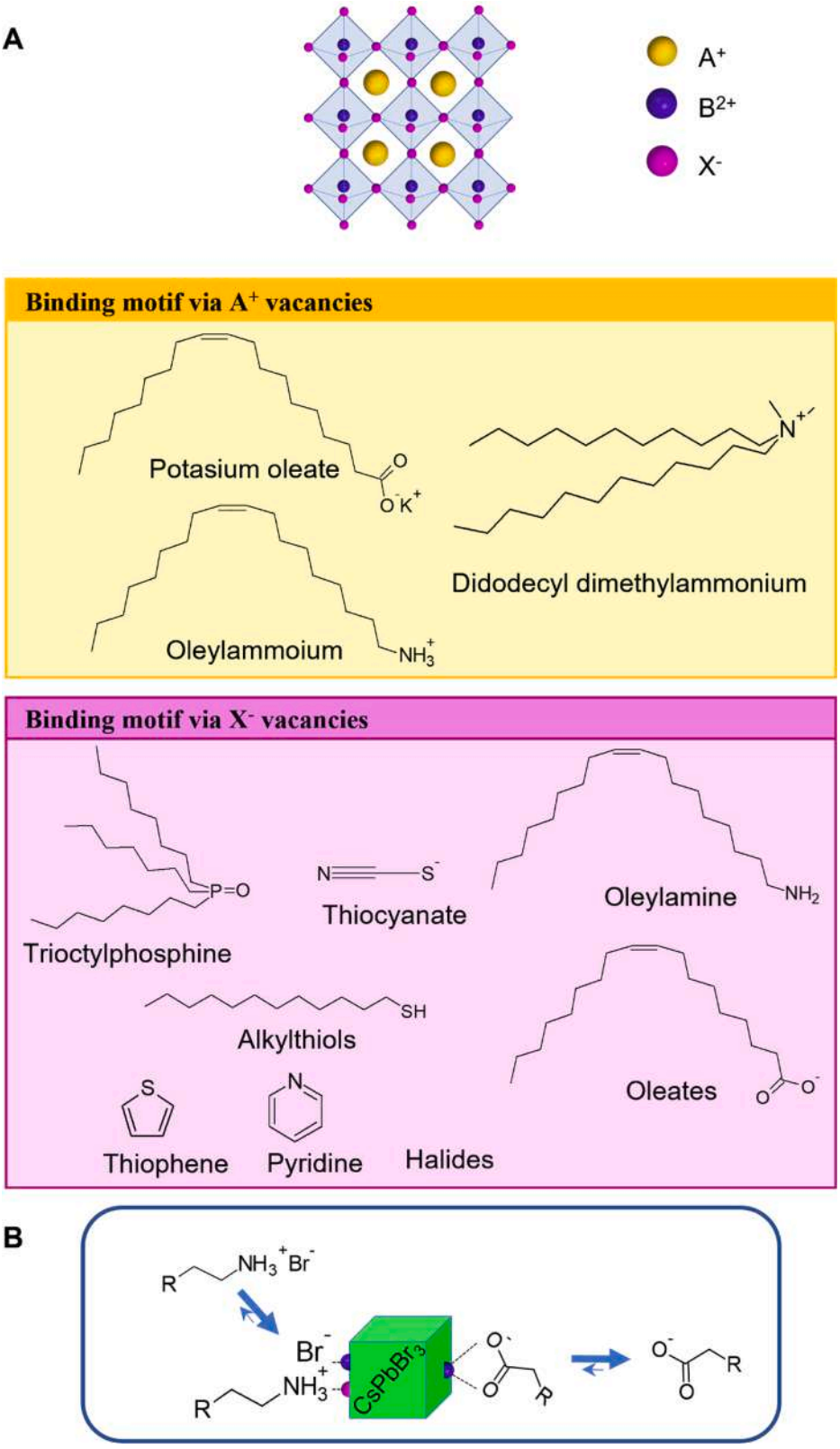

Fig. 8. A) Schematic representation of the most important metalhalide perovskite-ligand-binding motifs. (B) Illustration of the dynamic surface stabilization of the $CsPbBr_3$ NCs governed by the preferential attachment of oleylammonium bromide species.

by room-temperature condensation in a silica network. It is worth mentioning that, when perovskite encapsulation methodologies started being investigated, extending sol-gel procedures to LHP seemed difficult because of the harsh operating conditions and water-sensitive perovskites' nature. Recently however, many smart innovative solutions to prepare core-shell LHP@SiO_2 NPs by adapting and softening previous methodologies have been reported.

By adapting "water in oil" sol-gel methods using triton x-100 tenside

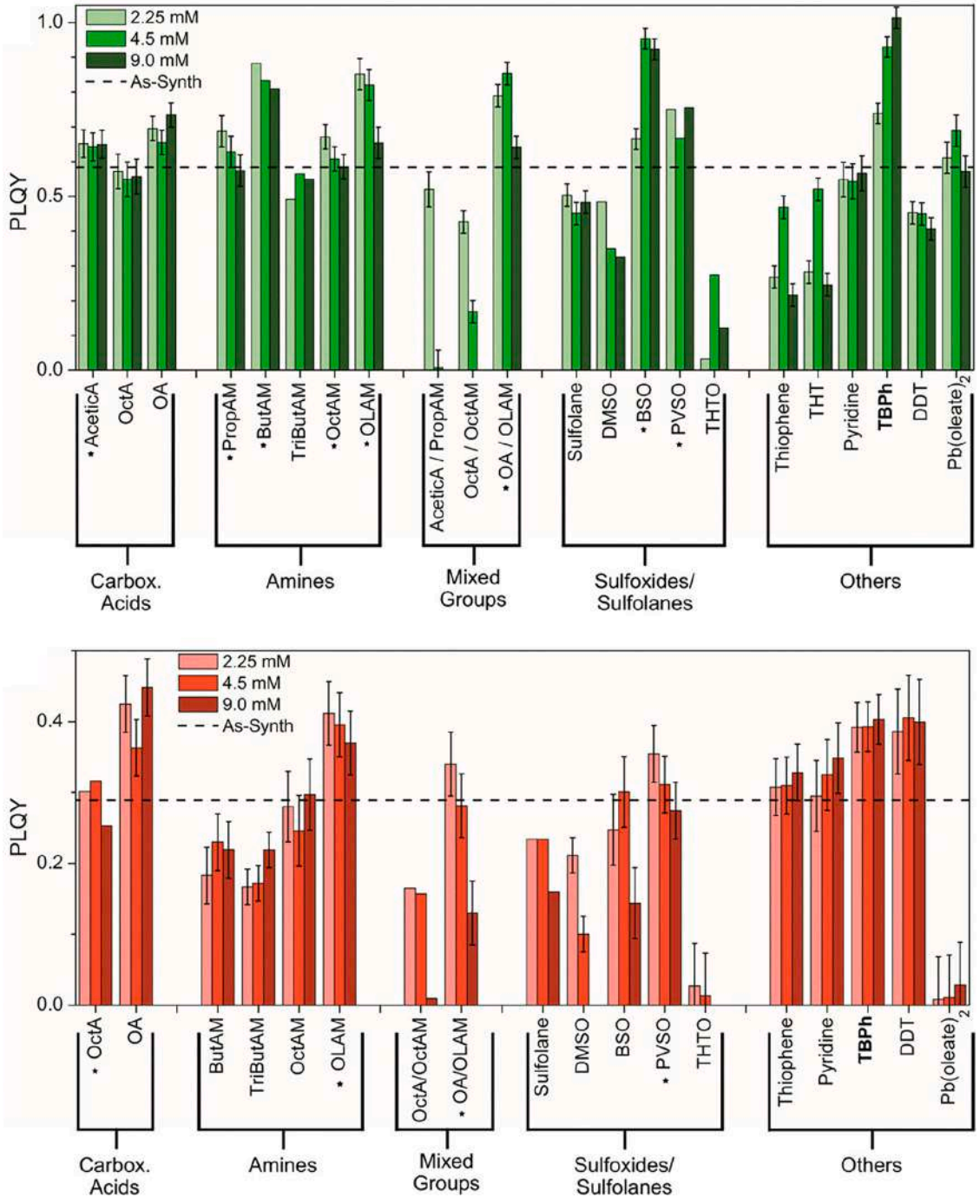

Fig. 9. PLQY values reported for $CsPbBr_3$ (green panel) and $CsPbI_3$ (red panel) NCs originally capped with the OA and alkylamine mixture in response to the addition of ligands of different natures. Dotted lines represent the PLQY of the as-synthesized NCs. Reproduced from Ref. [100] Copyright 2018 American Chemical Society.

and adjusting reaction water conditions, highly water soluble and stable $CsPbX_3@SiO_2$ nanocomposites can be obtained. Even in the absence of an alkaline catalyst and using solvent water traces or controlling the humidity environment for alkoxide precursors hydrolysis, SiO_2 and, also TiO_2 encapsulated NPs without decreasing the PLQY ~~quantum yield~~, have been reported. (Method A. Fig. 13) [152,153]

In a similar approach, by replacing TMOS and TEOS with (3-mercaptopropyl) trimethoxysilane silica source, silane molecules first physically adsorb on the surface of $CsPbBr_3$ NCs, and then hydrolyze and condense to form a silica shell overcoating. This method reports water-resistant $CsPbBr_3$ nanodots of 170 nm encapsulated in silica shells that keep 50% of their original emission yield in water for over 6 weeks. [151] However, it is true that PLQY in water media are not provided and these methods generally lead to the formation of silica nanocomposite with several LHP cores inwardly rather than proper core-shell NPs. [147]

An innovative approach to obtain a silica protective overcoating at a single particle level is the encapsulation of *in situ*-synthesized perovskite NCs (Fig. 13. Method B). Following this strategy, the addition of TMOS or TEOS and ammonia traces in the LARP methodology leads to the formation of core-shell NPs with a core size of around 10.5 nm and a shell thickness of about 7.7 nm, which preserve their PLQY (~90%) and present enhanced stability in water, even against ultrasonication treatment. In this methodology, the silica network is formed on the LHP NCs'

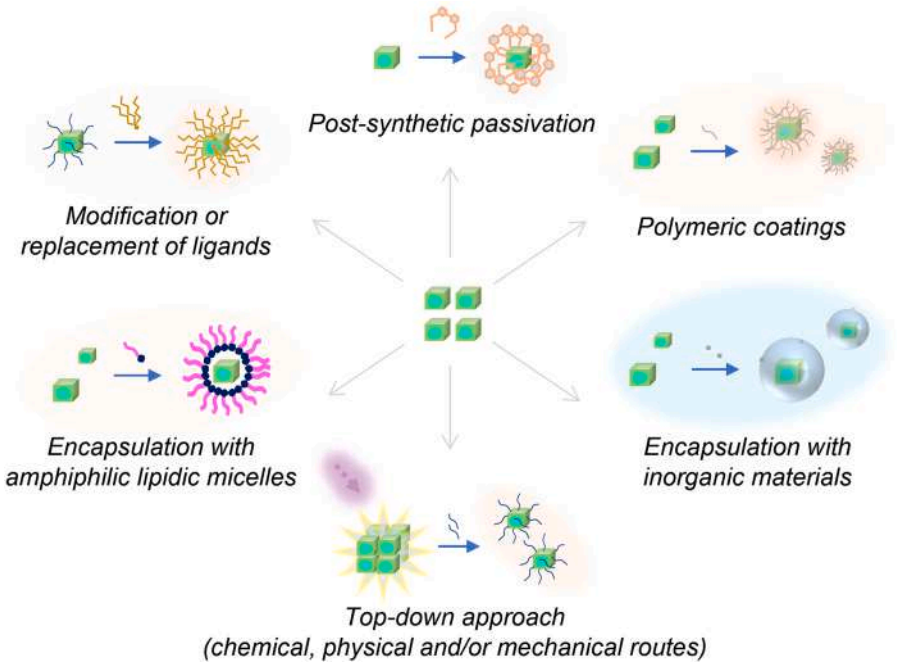

Fig. 10. Schematic representation of encapsulation strategies to obtain perovskite NCs with improved stability at a single particle level.

surface through the water oil interface, which enables controlled shell formation at a single particle level. [148] In addition, this strategy has also proven effective for the encapsulation of $CsPbBr_3$:Sn and Cs_4PbBr_6:Sn NCs [180]. Notwithstanding, estimating PLQY in water and the accurate study of colloidal features and size distribution still need to be solved.

As an alternative approach, Huicheng et al. combined water-triggered (0D) Cs_4PbBr_6 to (3D) $CsPbBr_3$ NCs phase transformation and sol-gel methods to $CsPbBr_3@SiO_2$ Janus NPs with enhanced water stability [123]. They also demonstrated that this is a universal strategy that can be extended to other perovskite compositions and other shell oxides, such as $CsPbBr_3@Ta_2O_5$ [149]. Although the described NPs combine the advantages of both materials, in this method perovskite NCs are not encapsulated and, thus, stability issues in water are not fully addressed. In a recent work, Rossi et al. exploit the transforming properties of $CsPbBr_3$ NCs to successfully prepare spherical $CsPbBr_3@SiO_2$ core-shell NPs. However, they are poor emitters (PLQY< 2%) (Fig. 13. Method C). [122]

Cheng et al. have reported the direct synthesis of $CsPbBr_3$ NPs in ethanol solvent *via* the preformation of TEOS/APTES micelles in an acid catalyzed sol-gel process, which then act as nanoreactors for $CsPbBr_3$ NCs formation. By this methodology, monodisperse quasi-spherical $CsPbBr_3$ NCs were obtained with an average diameter of 5.2 nm, which retain their PL in ethanol after 34 days (Fig. 13. Method D) [146].

From a different perspective, another interesting route to effectively provide LHP NCs protected by silica shields is the infiltration of MHP precursors in hollow silica nanospheres and subsequent *in situ* LHP growth. By this methodology, an average 20 nm diameter of $MAPbBr_3@SiO_2$ NPs, which remain stable in water solvent for 30 days, has been described (Fig. 13. Method E) [155].

In summary, significant advances have been made in the fundamental understanding of the underlying silica growth chemistry, and new avenues have opened out to the rational design of robust and efficient core-shell NPs with potential for many fields, such as fluorescent labels for bioimaging, biosensing and molecular detection. Despite the continuous advancements made in this strategy, most of the reported methods have led to macroscale composites or a broad NPs size distribution due to the softening of silica growth conditions. In addition, a structural and monodispersity study is still needed for synthesized core-shell NPs in water, while the PLQY in water media has not yet been properly estimated.

Other inorganic shells. Apart from silica, several works have described effective LHP encapsulation within other well-known metal oxide frameworks, such as ZnO and Al_2O_3, which are extensively used for encapsulating predecessor QDs. For instance, by a pre-protection strategy of $CsPbBr_3$ NCs with Na^+ cations that fills Cs^+ vacancies, and a subsequent Al_2O_3 coating by means of sol-gel procedures, water-stable mulberry-like nanocomposite particles have been obtained (Fig. 14A). The pre-protection step avoids damage under harsh alumina growth conditions. [156] $CsPbBr_3@$ $NaYF_4$ and $CsPbBr_3@$ ZnO with enhanced water stability have been obtained by simple solution phase methods heating fresh synthesized $CsPbBr_3$ NCs with inorganic salt precursors and surfactants (Fig. 14B). [157]

Another option to improve LHP water resistance is the formation of a peripherical water insoluble M(OH)x passivating layer. This protective hydroxide layer can be obtained by the post-synthetic aqueous treatment of LHP powders. [158,159] By this method, $MAPbBr_3@Pb(OH)_2$ rod-like shape NCs with average particles sizes of up to 4 μm and 12–70% PLQYs have been described.

The shell can also be made of different metal sulfide materials. Although this line has been less explored, there are already several promising studies that describe efficient encapsulation in Ag_2S, [161] ZnS [162,181] and CdS (Fig. 14D). [182,183]

Although not properly encapsulated, there have also been reports about $CsPbX_3$ NCs decorated with metal aggregates (Ag or Au). This occurs as a result of the reaction within perovskite NCs with M(I) halide salts, and Ag or Ag nanoparticles are deposited on the surface of perovskites *via* the reduction of Au^{1+} or Ag^{1+} ions by the surfactant ligand shell to produce Au-$CsPbX_3$ and Ag-$CsPbX_3$ heterostructures. These NCs exhibit enhanced light harvesting because of the scattering effect of metal, but no evidence of water resistance improvements has been provided for these systems. [164,165] Interestingly, these metal-$CsPbBr_3$ heterostructures can maintain PLQY of 70%, unlike similar Au–Cd chalcogenide heterostructures for which band-edge luminescence is quenched by the presence of metal.

Finally, several works capitalize the phase transformation ability of LHP to create perovskite-related structure shells that exhibit higher

Table 2
Summary of the optical, structural and stability features of LHP NCs stabilized at a single particle level. (N.P. Value is not provided).

Modification or replacement of the native ligand					
LHP/shell	PLQY (%)	Particle size (nm)	PLQY (water) (%)	Stability	Refs.
$CsPbBr_3$/TOPO+oleic acid	64–71 (dimethylbencene)	22.7 ± 2.6	N.P.	30 days (ethanol)	[134]
$CsPbX_3$/TOPO	N.P.	9–14	N.P.	2 h (ethanol)	[135]
$CsPbX_3$/TOP	75–86 (hexane)	9 ± 1	60–74 (hexane: water)	52 h (hexane:water)	[136]
$CsPbX_3$/ polyhedral oligomeric silsesquioxane	45–62 (toluene)	12–15	N.P.	10 storage weeks under ambient conditions	[137]
$MAPbBr_3$/ adamantylammoniun	~100 (toluene)	Nanoplatelets 44 × 35 nm^2	N.P.	120 min (water:toluene)	[45]
$CsPbBr_3$/alkylphosphates	68 (toluene)	≤ 10	N.P.	5 h (water)	[138]
$CsPbBr_3$/Cs_4PbBr_6/ perfluorooctyltriethoxylsilane	N.P.	Rectangle-shaped 20–100	80	8 days (water) 1 day (phosphate buffer solution, PBS)	[139]
$APbBr_3$/ oleylammonium lead bromide-terminated surface	95–99 (hexane)	8.4 ± 0.62 ($CsPbBr_3$) 14.2 ± 1.2 ($MAPbBr_3$) 11.9 ± 1.4 ($FAPbBr_3$)	N.P.	$CsPbBr_3$: 65% of original PL intensity (hexane:water) $MAPbBr_3$ and $CsPbBr_3$: 85% of original PL intensity (storage under ambient conditions)	[140]
$Cs_3Bi_2Br_9$	N.P.	4.80 ± 1.24	37 (ethanol) 42 (ethanol:water)	30 storage days under ambient conditions 8 h (ethanol:water)	[141]
$CsPbBr_3$/N-doped graphene quantum dots	35.2 (paraxylene)	15.3–35.7	33.6	7 days (water)	[142]
$CsPbI_3$/ alkyl phosphinic acid	N.P.	9.5–12.1	N.P.	Structural and phase stability for 20 days	[143]
CsPbI3/ 2,2′- iminodibenzoic acid	95 ± 2 (octane)	12 ± 1.5	N.P.	Structural and phase stability for 15 days	[144]
Encapsulation in phospholipid micelles					
$CsPbBr_3$/phospholipids	N. P.	255.3	N.P.	original PL intensity (water) after 27 days 96 h (acid and alkaline media)	[17]
$CsPbX_3$/stearic acid	52 $CsPbCl_3$ 85 $CsPbBr_3$ 33 $CsPbBr_xI_{1-x}$	700 ± 240	13 $CsPbBr_3$ 9 $CsPbBr_xI_{1-x}$	% of original PL intensity after 100 h (water) ~30–40 for $CsPbBr_3$ ~90–95 for $CsPbBr_xI_{1-x}$	[145]
Encapsulation with inorganic materials					
$CsPbBr_3$/SiO_2	N.P.	5.2	61.2 (ethanol)	34 days (PLQY~38%)	[146]
$CsPbX_3$/SiO_2	9.1 $CsPbCl_3$ 84 $CsPbBr_3$ 45 $CsPbI_3$ (cyclohexane)	120	59.4 $CsPb(Cl_{0.5}Br_{0.5})_3$ 82 $CsPbBr_3$ 73 $CsPb(Br_{0.3}I_{0.7})_3$	60 of original PL intensity (water) after 100 h	[147]
$CsPbBr_3$/SiO_2	90 (toluene)	25–30	N.P.	100% of original PL after 40 min (sonication, water)	[148]
Silica Shell	PLQY (%)	Particle size (nm)	PLQY (water) (%)	Stability	Ref.
$CsPbBr_3$/SiO_2 $CsPbX_3$/Ta_2O_5	80–85 (hexane)	Janus NPs 11.2 ($CsPbBr_3$) 3.4–12.6 (SiO_2)	N.P.	80% of its original PL intensity (hexane: water)	[149]
$CsPbBr_3$/SiO_2	N.P.	14–19.4	N.P.	35.8% of its original PL intensity after 48 h (toluene:water) Still luminescent in water after 48 h (not reported value)	[150]
$CsPbBr_3$@SiO_2	78 (toluene)	170	N.P.	50% of its original PL intensity after 20 days (water)	[151]
$MAPbBr_3$/SiO_2	89 (toluene)	150	N.P.	80% of its original PL intensity after 7 days (powder at 80% relative humidity; RH)	[152]
$CsPbBr_3$/TiO_2	N.P.	22	N.P.	85% of its original PL intensity after 3 months (water)	[153]
$CsPbBr_3$@SiO_2	48 (powder)	200–1000 Pore size 2–7	N.P.	N.P.	[154]
($MAPbBr_3$@SiO_2/poly (vinylidene fluoride)	85.5 (powder)	Hollow nanosphere 20.7 Cavity 3.7–9.9	N.P.	100% of its original PL intensity after 60 ambient storage days 60% of its original PL intensity after 2 h (water)	[155]

(*continued on next page*)

Table 2 (*continued*)

Modification or replacement of the native ligand					
LHP/shell	PLQY (%)	Particle size (nm)	PLQY (water) (%)	Stability	Refs.
LHP/other inorganic shells	PLQY (%)	Particle size (nm)	PLQY (water) (%)	Stability	Ref.
$CsPbX_3$@Al_2O_3	N.P.	300 nm-thick with lengths of up to several micrometers (rods) <1 μm (mulberry structures)	N.P.	100% of original PL intensity after 40 min (water, sonication)	[156]
$CsPbBr_3$@ZnO $CsPbBr_3$@$NaYF_4$	N.P.	$CsPbBr_3$@ZnO 200-nm thicked 600-nm length $CsPbBr_3$@$NaYF_4$ 50–500	N.P.	Stable in water and ethanol solvents. Time-stability test not afforded	[157]
$MAPbBr_3$@PbBr(OH)	N.P.	Rod-like shape 1.5 × 4 μm	71.54	% of original PL intensity 90% (1 year, water), 80% (100 °C, water) 50% (60 h, UV)	[158]
$Cs_3Bi_2Br_9$/BiOBr	46.4% (toluene)	< 100 nm	N.P.	130% of original PL after 50 h (toluene: water)	[159]
$APbX_3$@$Pb(OH)_2$	$MAPbBr_3$@$Pb(OH)_2$ 11.7 $MAPbBr_{3-x}Cl_x$@Pb $(OH)_2$ 8.3 $CsPbBr_3$@$Pb(OH)_2$ 53.9	Rod-like shape >100 μm length	$MAPbBr_3$@$Pb(OH)_2$ 11.7 $MAPbBr_{3-x}Cl_x$@Pb $(OH)_2$ 5.1 $CsPbBr_3$@$Pb(OH)_2$ 53.7	% original PL intensity after 6 months (water) 82% for $MAPbBr_3$@$Pb(OH)_2$ 50.9% for $MAPbBr_{3-x}Cl_x$@$Pb(OH)_2$ 71.3% for $CsPbBr_3$@$Pb(OH)_2$	[160]
$CsPbBr_3$@Ag_2S	54 (hexane)	Janus NPs 8–10 ($CsPbBr_3$) 2 (Ag_2S)	82	6.3% (PLQY, water, 30 days)	[161]
$CsPbX_3$@ZnS	70.1–75.7 (toluene)	Janus NPs 18 ($CsPbX_3$) 2 (ZnS)	N.P.	60% of original PL intensity (12 storage days under ambient conditions)	[162]
$CsPbBr_3$@CdS	88 (toluene)	22.1 ± 1.5	N.P.	N.P.	[163]
$CsPbBr_3$@Au	2.97 for $CsPbCl_3$@Au 52.07 for $CsPbBr_3$@Au 23.05 for $CsPbI_3$@Au	Janus NPs 8–10 ($CsPbX_3$) <5 (Au)	N.P.	N.P.	[164]
$CsPbBr_3$@Ag	82.5 for $CsPbCl_xBr_{3-x}$@Ag	15–24 nm ($CsPbX_3$) 2–5 nm (Ag)	N.P.	N.P.	[165]
$CsPbX_3$/$CsPb_2Br_5$	78.9 for $CsPb_xX_{3-x}$/ $CsPb_2Br_5$ 77.4 for $CsPbBr_3$/ $CsPb_2Br_5$	~10	N.P.	% original PL intensity (10 days) $CsPbBr_3$/$CsPb_2Br_5$ 93% (UV), 94% (water), 42% (100 °C) $CsPb_xX_{3-x}$/$CsPb_2Br_5$ 90% (UV), 88% (water), 25% (10 days, 100 °C)	[166]
$CsPbBr_3$/$CsPb_2Br_5$	N.P.	~10	N.P.	2 h (ethanol:water, ultrasonication)	[167]
$MAPbBr_3$/ $(OA)_2PbBr_4$	92 (hexane)	~5–12	N.P.	85% of original PL intensity after 1 month (storage under ambient conditions, 60% RH)	[15, 168]
Polymeric coatings					
$MAPbX_3$@ (PS-b-P2VP) diblock copolymer	63 for $MAPbBr_3$ 55 for $MAPbI_3$ (toluene)	11–27	N.P.	$MAPbBr_3$ 30% of original PL intensity after 30 days (film, water)	[169]
$APbX_3$@ (PS-b-P2VP) diblock copolymer	N.P.	5.16 ± 3 ($MAPbBr_3$) From 7.92 ± 0.78 to 65.4 ± 6.2 ($MAPbI_3$) 7.35 ± 1.2 ($FAPbI_3$)	N.P.	$MAPbBr_3$ 58% of original PL intensity after 8 weeks (storage, ambient conditions)	[170]
$CsPbBr_3$@ (PS-b-P2VP) diblock copolymer	51% (toluene)	20	N.P.	80% of original PL intensity after 15 h (water) 100% of original PL intensity after 1000 h (isopropanol)	[171]
$CsPbX_3$@PHEMA-g- (PAA-b-cPS)	N.P.	$CsPbBr_3$ 21.2 ± 1.8	N.P.	% original PL intensity (toluene) $CsPbBr_3$ 85% (35 h, UV-illumination) 90% (1-month, storage at 60% RH) 88% (2 h, 80° C) 84% (6 h, toluene:water, (1:10))	[172]
$MAPbBr_3$@ polystyrene-b-poly(ethyl oxide)	56 (toluene)	25.8–104	43 (vesicles) 29 (NCs)	% original PL intensity (water) 33% (PLQY, 7 months, water)	[173]
$CsPbBr_3$@polymer/SiO_2	88 (toluene)	22.8–27.6	N.P.	80% of its original PL intensity after 14 days (films under 80% RH)	[174]

(*continued on next page*)

Table 2 (*continued*)

Modification or replacement of the native ligand					
LHP/shell	PLQY (%)	Particle size (nm)	PLQY (water) (%)	Stability	Refs.
$CsPbBr_3$@mPEG-NH_2	N.P.	40–80	41	% original PL intensity (water) 130% (1 week), 80% (100° C)	[175]
$CsPbBr_3$@polyimide	88.1 (toluene)	135.2	N.P.	% original PL intensity (toluene) 90% (40 days, ambient conditions) 80% (60 min, water:toluene)	[176]
Top-down NCs synthesis					
2D-$CsPbBr_3$ nanosheets	N.P.	Nanosheets (1 μm × 1 μm) 8 nm-thicked	82.3%	% original PL intensity 87% (168 h, water) 85% (2 h, UV illumination, water)	[177]
$MAPbX_3$	67 ($MAPbBr_3$) 22 ($MAPbBr_xI_{1-x})_3$) 6 ($MAPbI_3$)	$MAPbBr_3$ (4.4 ± 0.9) $MAPbBr_xI_{1-x})_3$ (8.1 ± 1) $MAPbX_3$ (6 ± 1)	N.P.	N.P.	[72]
$CsPbBr_3$ Nanowires	60 (ciclohexane)	2.1 nm-thicked	N.P.	80% of original PL intensity (120 min, water:ciclohexane)	[178]
$CsPb_2Br_5$@SiO_2	90 (toluene)	36.1 ± 4.5	5	100% of original PL intensity (3 days, water)	[179]

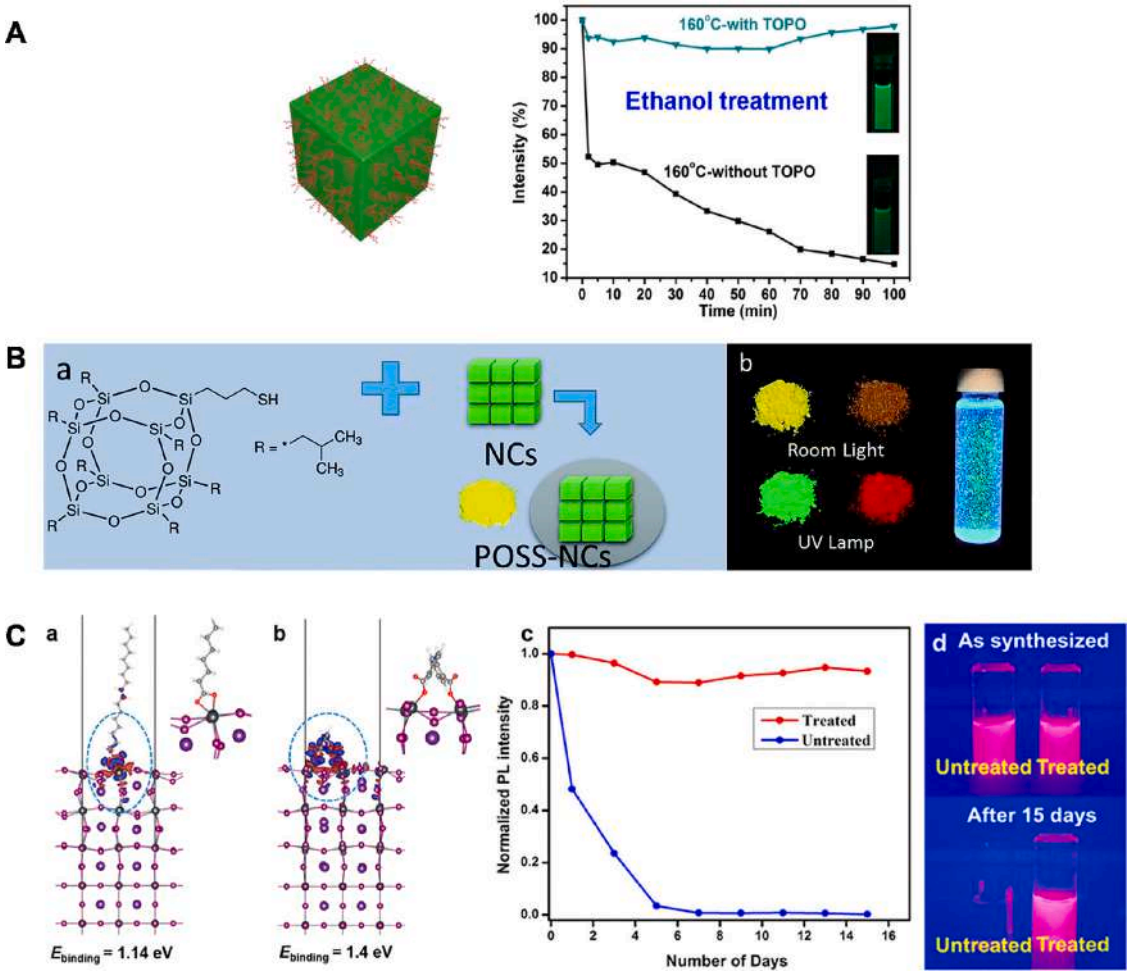

Fig. 11. Stabilization strategies *via* surface modifications or the replacement of the native ligand. A) $CsPbBr_3$ NCs stabilized in ethanol solvent *via* post-synthetic treatment with trioctylphosphine oxide ligand (Adapted from Ref. [135] Copyright 2017 American Chemical Society) B) Multicolored and water-resistant $CsPbX_3$ powders obtained after NCs coating with polyhedral oligomeric silsesquioxan (POSS). Reproduced from Ref [137]. with permission from the Royal Society of Chemistry and C) phase-stable cubic $CsPbI_3$ NCs obtained by post-synthetic passivation with bidentate 2,2′-iminodibenzoic acid. (Reprinted from Ref [144]. Copyright 2018 American Chemical Society).

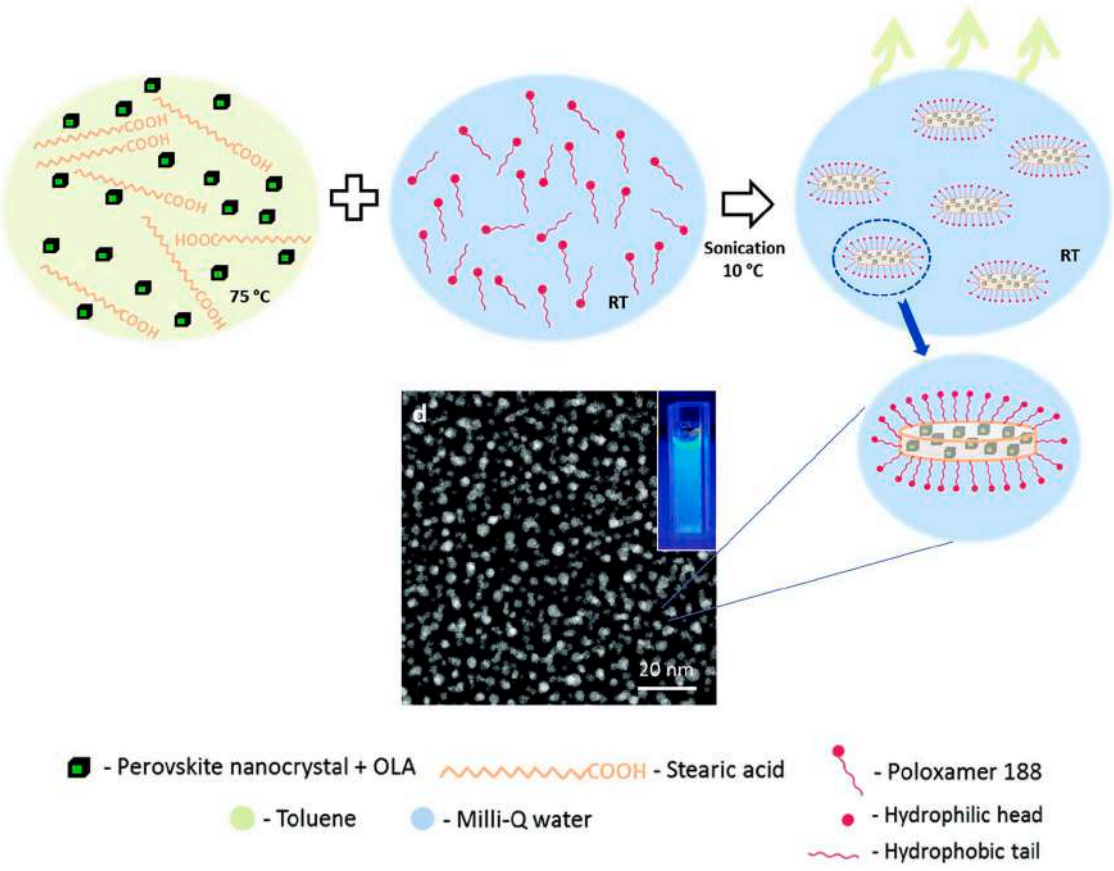

Fig. 12. Scheme procedure for the encapsulation of $CsPbBr_3$ perovskite in a solid lipid matrix of stearic acid micelles. Reproduced from Ref. [145] with permission from the Royal Society of Chemistry.

water resistance properties. These heterostructures can be obtained by finely tuning HI reaction conditions, exhibit good stability with UV exposure and water-immersion for up to 10 days (Fig. 14) [166,167, 184].

4.1.4. Polymeric coatings

The encapsulation of LHP in polymeric shells constitutes a smart and versatile strategy because it allows shells to be designed with devised functionality through the synthetic control and chemical derivatization of "puzzle pieces": monomers. In this way, several reports have described efficient coatings for metal and semiconductor NCs by means of amphiphilic polymers, which contain hydrophobic groups that interact with the original ligand and hydrophilic groups to allow the dispersion of NCs in water. This strategy has enabled the development of commercial NPs of a variety of materials stabilized in aqueous media without altering their optical properties [185,186].

With this strategy in mind, several works have used the rational design of polymeric micelles, which act as nanoreactors that assist crystal growth, which occurs inside their cores and protects them from water decomposition or sintering processes. For example, several works have proposed employing preformed polystyrene-poly(2-vinylpyridine) (PS-b-P2VP) diblock copolymer core-shell micelles in toluene with the P2VP part forming the core and the PS part forming the shell for the controlled synthesis of $MAPbX_3$ NCs. In short, perovskite precursor salts added to the micelle dispersion in toluene accumulate in the cores of micelles due to diffusion. Therefore, the solubility product changes and precursors crystallize to form perovskite, an entropically driven process. In this way, the core confines perovskite formation, whereas the shell separates individual reservoirs. This process has been demonstrated to be highly reproducible and results in monodisperse luminescent NCs with sizes that are tunable through the core polymer block length, and provides perovskite NCs encapsulated in polymer shells, which display strong stability against moisture and halide ion migration [169–171]. (Fig. 15)

The amphiphilic block copolymer nanoreactor strategy can afford stable perovskite NCs with controlled compositions and surface chemistry. Thus it has been extended to other block copolymer compositions, such as poly(2-hydroxyethyl methacrylate)-graft-(poly(acrylic acid) block-partially cross-linked polystyrene[172] and polystyrene-b-poly (ethyl oxide) [173].

In a smart approach, He et al. construct a tri-block polymeric nanoreactor that starts from cyclodextrin structures. The judiciously design of copolymer hydrophilic/hydrophobic features renders dual-shelled $CsPbBr_3$@polymer/SiO_2 NPs with a controlled, yet tunable, perovskite core diameter, SiO_2 shell thickness, and surface chemistry [174]. These NPs exhibit stability at 80% RH, but quickly degrade in water media.

Another interesting approach to the synthesis of LHP polymeric core-shell NPs is the replacement of synthetic precursors with polymer ligands. For example, using methoxypolyethylene glycol amine as a synthetic precursor of LARP methodologies leads to the formation of $CsPbBr_3$/mPEG-NH_2 NPs, which preserve their structural stability and exhibit superior water solubility. It is worth noting that although these NPs preserve their luminescence for over 1 week, they eventually evolve to dendritic structures of sizes up to several microns [175]. Furthermore, the introduction of polyimide into LARP can effectively improve LHP stability against harsh environments, such as moisture, heat, oxygen and light [176].

The encapsulation of perovskite NCs inside polymeric shells seems effective for preparing more resistant NPs, which are stable in water

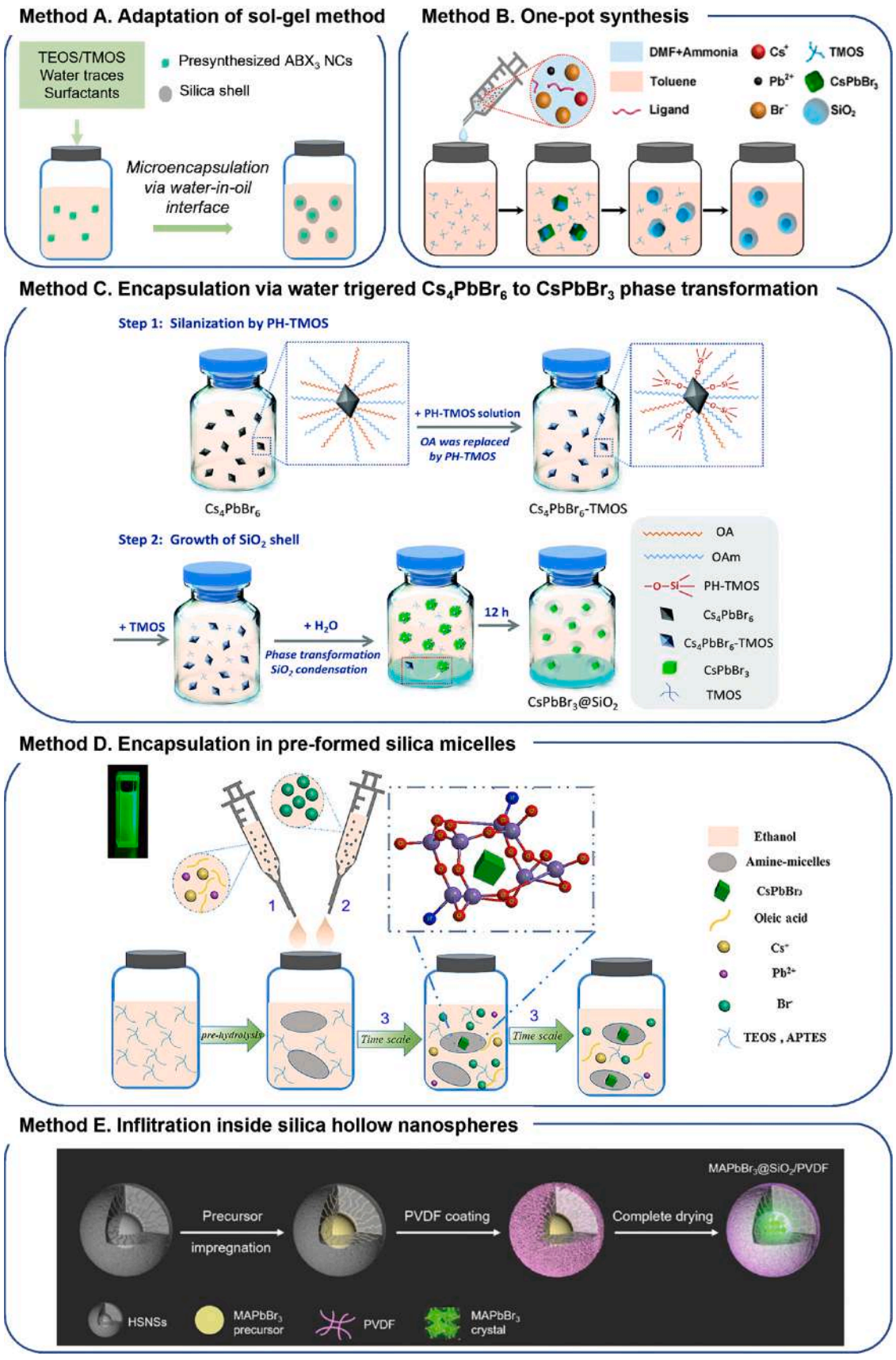

Fig. 13. Schematic representation of the more representative procedures for the encapsulation of LHP NCs on silica shells. The figure is adapted from Ref [123,146, 148,155]. Copyright 2016, 2018 and 2020 American Chemical Society. Copyright 2021 Royal Society of Chemistry.

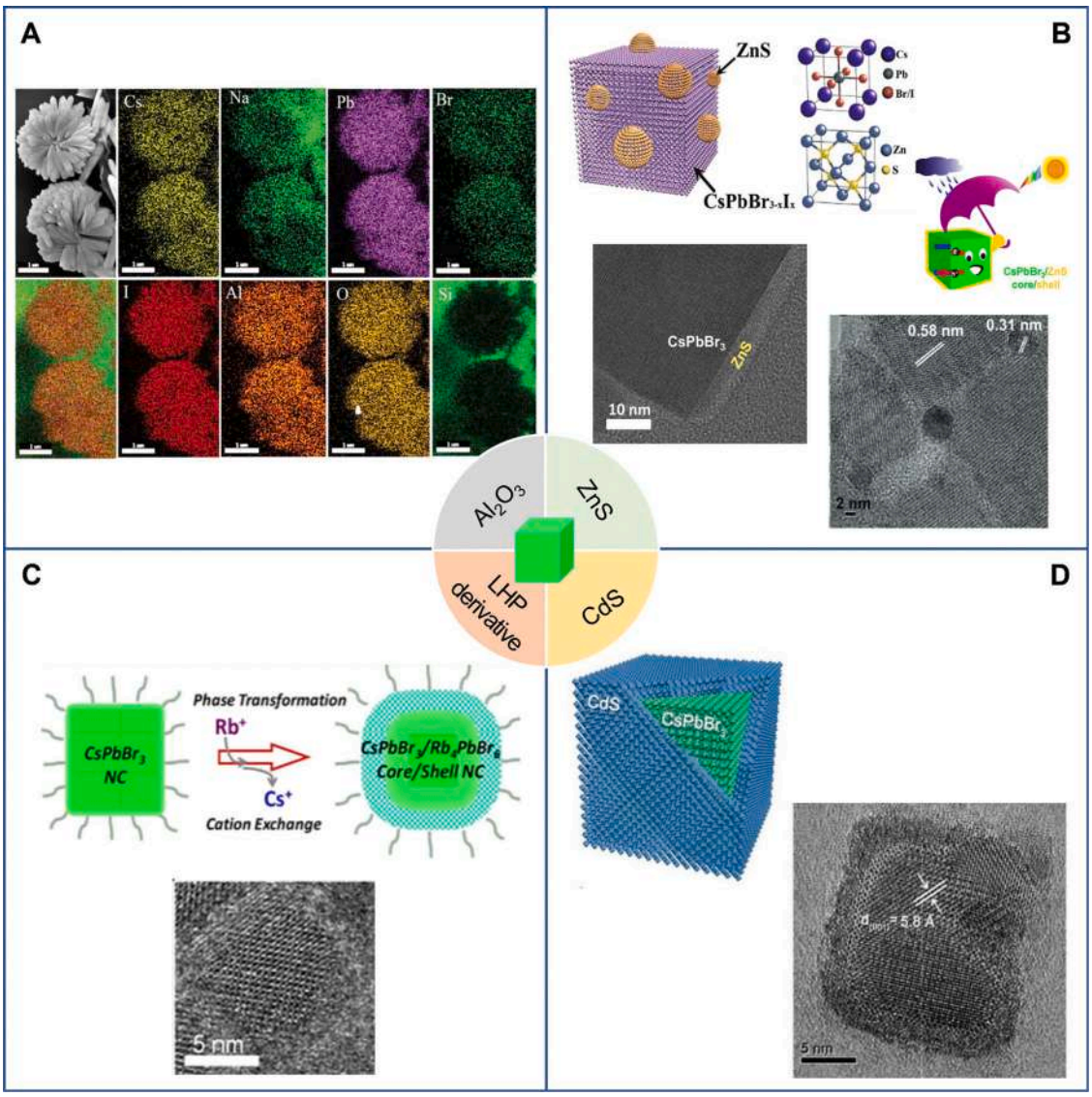

Fig. 14. Schematic diagram of LHP NCs encapsulated in different inorganic shells. (A) SEM image and elemental mapping of $CsPbX_3$@Al_2O_3 microstructures. Reproduced from Ref. [156] with permission from the Royal Society of Chemistry. (B) $CsPbX_3$ decorated with the ZnS overcoating. Reprinted from Ref. [162,181] Copyright 2017 Wiley-VCH. Copyright 2020 American Chemical Society. (C) Schematic illustration and TEM image showing $MAPbBr_3$ coated with a Rb_4PbBr_6 perovskite-related structure. Reprinted from Ref [184]. Copyright 2018 American Chemical Society D) $CsPbBr_3$@CdS core-shell NPs. Reproduced from Ref [183]. Copyright 2019 Wiley-VCH.

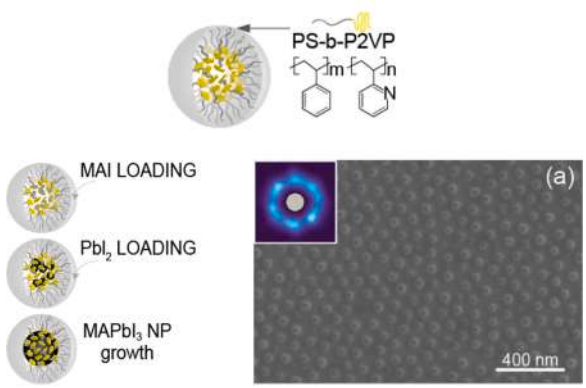

Fig. 15. Schematic illustration and SEM micrograph of the $MAPbI_3$ nanoparticles that form in the diblock copolymer polystyrene-b-poly(2-vinyl pyridine) copolymer shell. Adapted from Ref [170]. Copyright 2019 American Chemical Society.

over longer periods. They also present the ability to functionalize polymeric coatings with multiple different functional groups, which facilitates the processing of the final NPs. Therefore, this approach presents a very high potential for obtaining colloidal aqueous suspensions of LHP. Nevertheless, most of the described polymeric coated NPs present poor chemical and structural stability in water. Thus further ligand design research is mandatory. In addition, some disadvantages of these strategies still need to be solved, such as substantially increased diameters, which hinders their application in biosensing and imaging applications, and obtaining shells which prevents aggregation phenomena.

Top-down nanoparticle synthesis. Nanomaterial synthesis approaches can be broadly divided into two categories: "top-down" and "bottom-up". The "top-down" approach often uses lithographic, mechanical or chemical techniques (i.e. laser-beam, grinding, polishing of chemical etching) as tools for cutting, milling and processing small NCs by starting from bigger ones or composites. Conversely, "bottom-up" approaches exploit the chemical properties of molecules for the assembly of core-

shell NPs. Although bottom-up strategies seem more suitable for developing LHP NCs because they well control the process and can produce much smaller sized and highly monodispersed nanoparticles, it is worth mentioning that there have recently been some works that describe LHP NCs synthesis *via* top-down methods.

Accordingly, ultrahigh intrinsically water-stable all-inorganic 2D $CsPbBr_3$ (1 μm × 1 μm) nanosheets are obtained *via* the aqueous phase exfoliation method of larger Cs_4PbBr_6 NCs. Compared to conventional perovskite NCs, these unique quasi-2D $CsPbBr_3$ nanosheets present water stability after 168 h [177]. In a similar approach, Jana et al. have reported a top–down aqueous synthesis of α-$FAPbI_3$ NCs from bulk δ-$FAPbI_3$, which remained stable under ambient conditions for more than 6 months. In addition, as-synthesized α-$FAPbI_3$ exhibits dual emission in yellow and red regions, which indicates the formation of the self-trapped emissive excited state [187].

In a two-step consecutive processes, ultrathin $CsPbBr_3$ nanowires have been obtained by the transformation of $CsPbBr_3$ nanocubes into Cs_4PbBr_6 smaller NCs in the presence of thiourea, cysteine or thioacetamide, followed by further rearrangement into NWs. The resulting materials obtained a large PLQY (up to 60%). They also displayed good resistance to water treatment, whichwas attributed to surface passivation by thiourea [178].

$MAPb(X)_3$ colloidal NCs have also been successfully synthesized by laser irradiation (532 nm) of bulk crystals [72,188]. (Fig. 16A). Finally, this group has described monodispersed and water-resistant blue luminescent $CsPb_2Br_5$@SiO_2 core-shell NPs, which were synthesized by the top-down formation of $CsPb_2Br_5$ from larger $CsPbBr_3$ NCs, followed by their encapsulation in silica shells (Fig. 16B) [179].

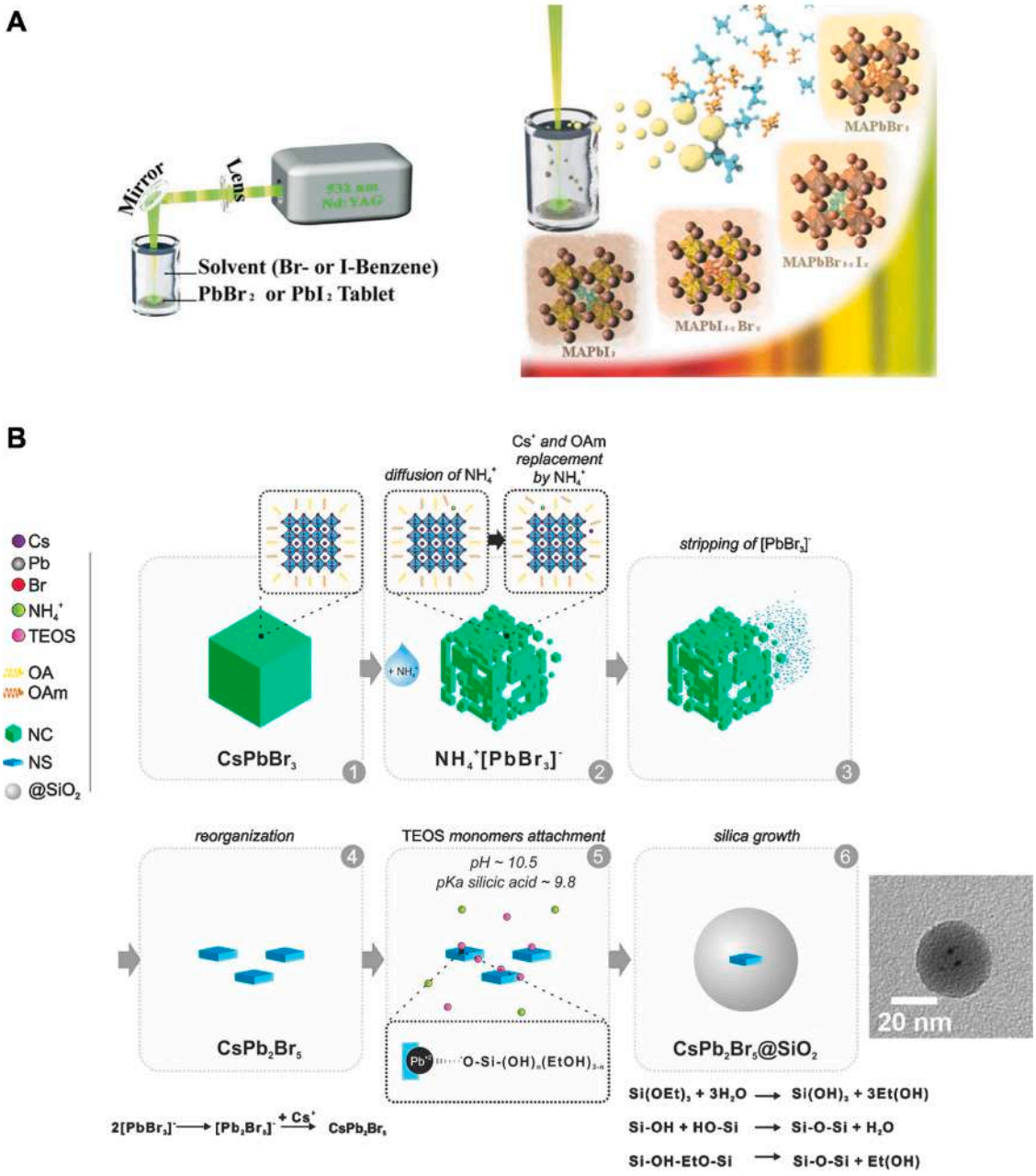

Fig. 16. A) Schematic description of the laser ablation synthesis setup for the top-down preparation of ligand free LHP inks. Adapted from Ref [188]. Copyright 2017 Wiley-VCH. (B) Schematic representation of the top-down formation mechanism of $CsPb_2Br_5$ silica-coated core-shell NPs from $CsPbBr_3$ NCs. Reprinted from Ref [179]. Copyright 2021 American Chemical Society.

4.2. LHP composites

The previous section summarizes recent developments related to obtaining LHP and core-shell nanomaterials with improved water resistance at a single particle level. However, ever since the investigation of LHP NCs began, several methodologies have been reported to improve the stability of LHP NCs by embedding them in other materials' matrices, such as different types of polymers, silica, alumina, among others. Although particles singularity is lost in these approaches, the developed perovskite nanocomposites can be processed in different shapes and morphologies, such as film, gels, fibers, or even small NCs, with a myriad of applications, some of which have already been proven; e.g. backlight displays, photovoltaic devices, light-emitting diodes. Others are still to be exploited; e.g., biosensing gratings, anti-counterfitting, scintillators or planar waveguides. We now move on to introduce and discuss different strategies, which have been identified in the literature, to prepare LHP composites by either *in situ* crystal growth or post-synthetic encapsulation in host matrices (Fig. 17).

4.2.1. Polymeric composites

A straightforward route that enables the successful encapsulation of LHP NCs on the macroscale is performed by the dynamic swelling-deswelling process of polymer materials. Typically, by mixing perovskite precursors or directly presynthesized NCs and hydrophilic polymers, when the solvent evaporates, polymers deswell, shrink back and form a robust hydrophobic matrix around LHP. In addition, by selecting polymers with an adequate functional group, they can act as multidentate ligands that attach intimately to NCs surface to result in well dispersed PS NCs that are very efficient against water, oxygen or heat. LHP microencapsulation by the swelling-deswelling process has been described for a wide variety of polymers, including PMMA [189], polycarbonate (PC), acrylonitrile butadiene styrene (ABS), cellulose, polyvinyl chloride (PVC) and S4-vinylbenzyl-dimethyloctadecylammonium chloride (V18), and some diblock copolymers [190–192]., ethyl-envinylacetate (EVA) [193], polyvinylidene(difluoride) [194] or poly (styrene-ethylene-butylene-styrene)[195] (Fig. 18 (A–C)).

Another universal strategy to obtain highly stable luminescent perovskite-polymer composites for most commercially available monomers and polymers is that performed by thermal or UV-photoinitiated polymerization [196,197]. Pan *et al.* introduce a facile and effective strategy to prepare solution processable $CsPbX_3$ NC-polymer inks by mixing LHP NCs prepassivated with methacrylic acid (MA) ligands with hydrophobic methyl methacrylate and methacrylisobutyl POSS monomers. The resulting inks can be processed in different configurations and, with the UV-curing process, this can render nanocomposites with remarkable chemical stability to water and much enhanced thermal stability [198] (Fig. 18 (D-E)). In a similar methodology, perovskite-organogels with record-high stability (> 110 days immersed in water with different pH and temperature values) and tunable mechanical properties were prepared by *in situ* producing and embedding perovskite NCs in the hydrophobic polyacrylate matrix [199].

In another work, Carrillo-Carrión *et al.* propose employing amphiphilic polymer poly-(isobutylene-alt-maleic anhydride)-graft-dodecyl (PMA), which has been widely used to provide NPs with colloidal stability in aqueous media. In these methods, aliphatic chains assemble in native olefin ligands, while maleic anhydride enables NP water dispersion after their hydrolysis in aqueous media. By this method, 1–2 fine μm-sized nanopowders dispersed in water with LHP NCs homogeneously dispersed inside are described (Fig. 18 (F–I)). [200]

4.2.2. Liquid atomization methods

The liquid-atomization, solvent-removal or spray-assisted methods are common terms used to refer to such approaches [201,202]. The main principle consists of the atomization of a liquid solution into fine droplets, followed by a fast solvent evaporation process, which generates an already dried product with micro- or nano-sized particles. This is, in fact, the main advantage of atomization-based approaches. No further drying steps are needed, which makes the whole process cheaper and shorter. Electrospraying, electrospinning, spray-drying and spray-pyrolysis are examples of the techniques in this category. [203, 204]

By liquid atomization methods, Yang et al. [205] prepared stable $CsPbBr_3$@polystyrene microspheres (of around 4–5 μm and 10 μm, respectively). This results from electrospraying LHP NCs synthesized by

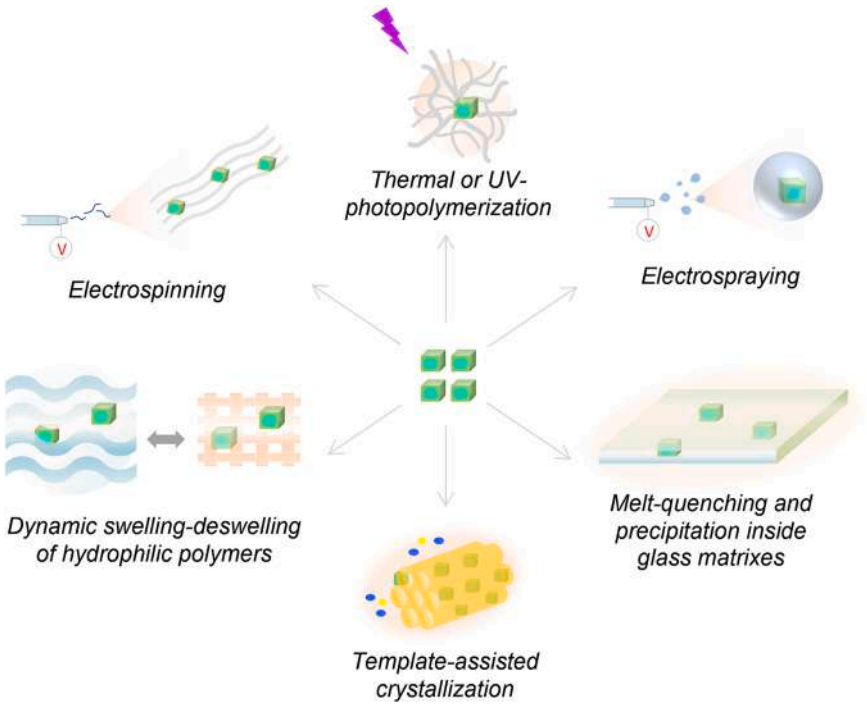

Fig. 17. Main strategies for obtaining LHP composites: a schematic overview.

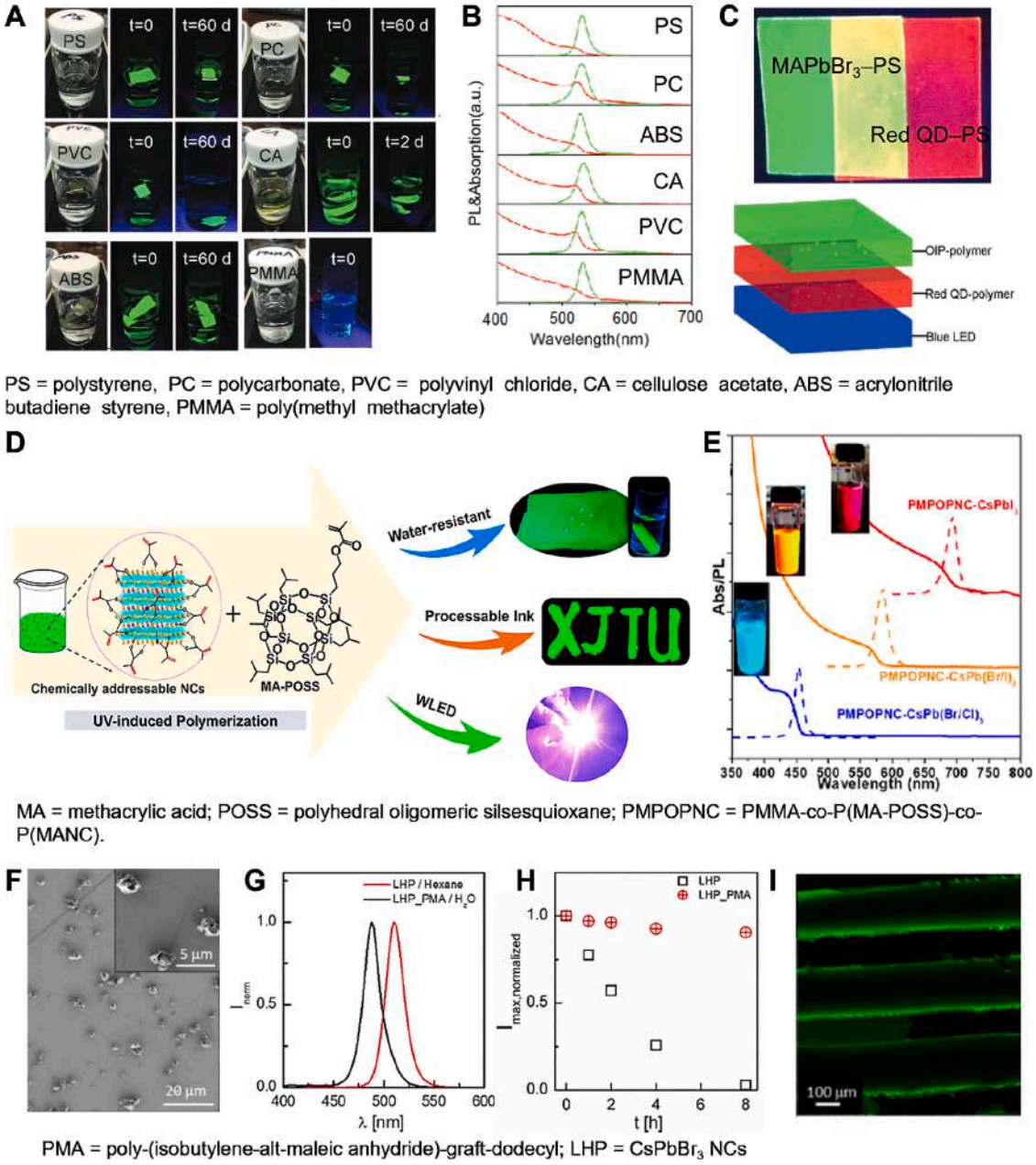

Fig. 18. Perovskite–polymer composites: (A) water-stability and (B) optical properties of several $MAPbBr_3$–polymer films obtained by the swelling-deswelling method; (C) photograph of red QD–polystyrene (QD-PS) and $MAPbBr_3$–polystyrene composite films under UV illumination and a scheme of white light generation by integrating composite films with the blue light-emitting diode. (D) Obtaining a processable ink and the WLED device based on $CsPbX_3$ NCs–polymer composites by means of UV-photoinitiated polymerization; (E) optical properties of different $CsPbX_3$ NCs–polymer composites. (F) SEM image of the LHP NCs embedded in the amphiphilic polymeric matrix of PMA; (G) PL spectra and (H) thermal stability at 60 °C of LHP NCs in hexane and LHP-PMA composite in water; (I) confocal image (green channel) of HP-PMA grating after being immersed in water for 1 h. (A-C) Adapted from Ref [190]. Copyright 2016 WILEY-VCH. (D,E) Reproduced from Ref [198]. Copyright 2018 American Chemical Society. (f-i) Adapted from Ref [200]. Copyright 2019 Elsevier Ltd.

the LARP methodology with polystyrene polymer. (Fig. 19 (A-D)).

Wang et al. embedded $CsPbBr_3$ NCs in poly-vinylidene fluoride (PVDF). The resulting NPs exhibit an average size of ca. 600 nm and stability in an aqueous solution of several buffers. In addition, their potential as luminescence probes for cell membrane imaging in MCF-7 cells was proven [206].

By adjusting procedure conditions, such as voltage, flow rate, distance, environmental conditions, electrical conductivity and other rheological properties of the solution, the kind of produced particle can evolve from spherical-like particles by electrospraying to fibers by electrospinning. Fiber manufacturing has awakened special interests in producing white light-emitting diodes (WLEDs) [207–209] (Fig. 19 (E–J). By employing the coaxial electrospinning process, where LHP and polymeric solutions are injected from separate needles, Jiang et al. [210] prepared multicolored fibers in red and green, respectively, which produced white light when irradiated by a blue LED.

Apart from LEDs applications, others have made their way to the biosensing field. Considering $CsPbBr_3$ perovskites' excellent optical properties and the high surface-to-volume ratio of as-prepared electrospun polymer-based nanofibers [211], fluorescence resonance energy transfer (FRET) based on detection fibers has been developed to identify the presence of ultralow concentrations of Rhodamine 6 G (R6G),

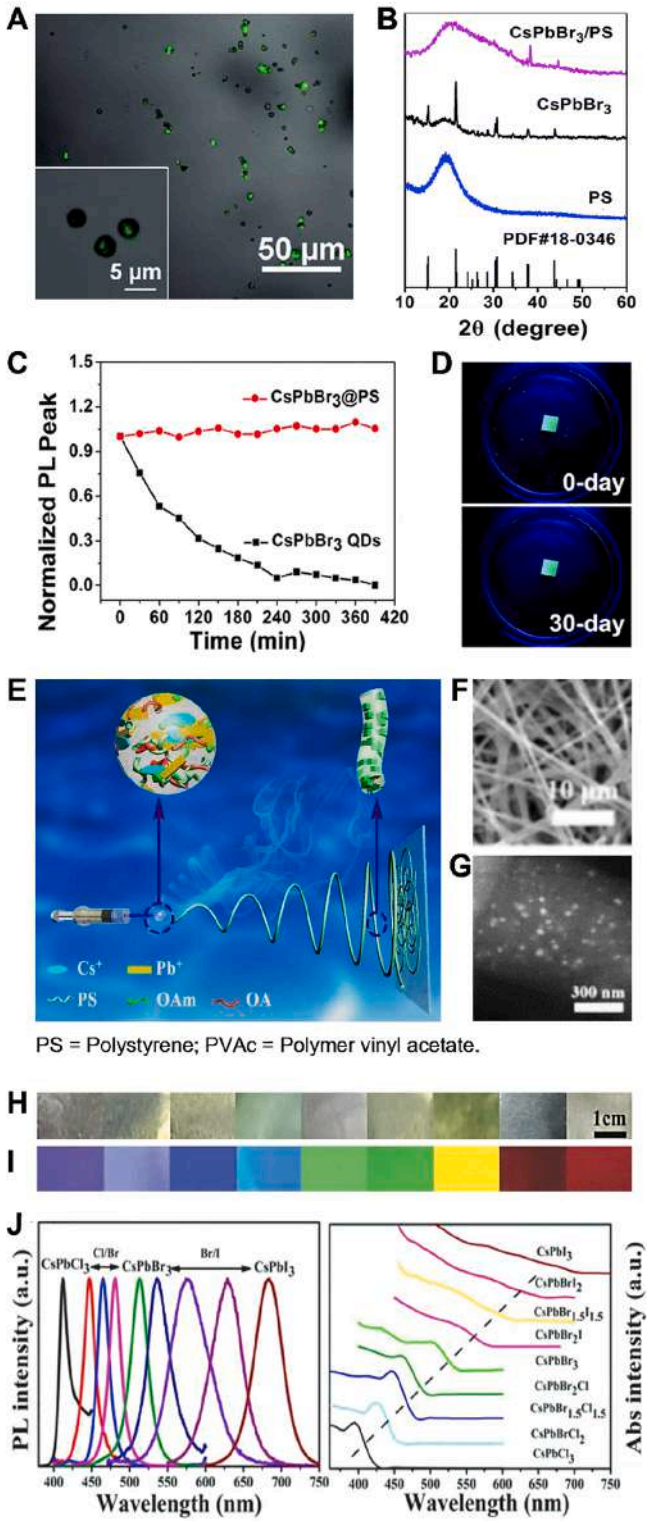

Fig. 19. LHP composites obtained by liquid atomization methods: A) confocal laser scanning microscopy image of $CsPbBr_3$-PS microspheres; (B) XRD patterns of PS, pure $CsPbBr_3$ NCs and $CsPbBr_3$@PS microspheres; (C) stability of $CsPbBr_3$ NCs and $CsPbBr_3$@PS in water:toluene 1:1; (D) images of $CsPbBr_3$@PS electrosprayed on Al foil in water and 30 days later under UV light irradiation (365 nm). (E) schematic image of the obtained $CsPbBr_3$@PS fibers; (F) secondary electron and (G) backscattered electron SEM images of $CsPbBr_3$@PS fibers; (H) ambient light and (I) UV-light images of $CsPbX_3$@PVAc fibers with tailored compositions and (J) their optical properties. (A-D) Adapted from Ref [205]. with permission from the Royal Society of Chemistry. (E-J) Adapted from Ref [207]. Copyright 2018 WILEY-VCH.

trypsin, Cu^{+2} and pH [212].

To date, this cost-effective technique has been successfully used on the laboratory scale, and the biggest challenge is only scaling-up for industrial purposes. One way to increase production would be to use several spraying nozzles or increase the number of spraying equipments. [213]

4.2.3. *Perovskite glasses*

As an alternative, inorganic oxide glass is believed to be a robust host for protecting perovskite NCs. By making good use of stability, applications of NCs embedded glasses on nonlinear optical devices [214, 215], emitting devices [216–218], and signal amplification in the fiber-optic communication system [219], have been explored.

Within this framework, by designing appropriate glass composition, microencapsulation inside glass can be done by conventional melting-quenching and a subsequent heat treatment technique. As halide is highly volatile at a high temperature, the glasses chosen to precipitate $CsPbX_3$ NCs should have a low melting point (<1300 °C), such as borosilicates [220–222], phosphosilicate [223–225], tellurium-based [226] and germinate glasses [218,227] (Fig. 20).

To benefit from outstanding PL and stability, glasses with halide perovskite NCs are quite suitable for light sources and photonic devices, and most reported perovskite glasses nanocomposites have been employed as light converters. For example, by precipitating $CsPbBr_3$ in a glass slice and coupling it with a GaN blue LED, green light-emitting device with a luminous efficiency of 118 lm W^{-1} and an external quantum efficiency of 28.14% has been described. With $CsPbBr_3$ and $CsPbBrI_2$ nanocrystal–embedded glass slices as light converters, white light with a luminous efficiency of 50–60 lm W^{-1} and an external efficiency of 20–25% can be achieved.

Regarding stability, glass is a proven excellent candidate to provide protection from harsh environments. Liu et al. [221] obtained $CsPbBrI_2$ NCs in borosilicate glass, which maintained 95.8% of their initial luminescence intensity under accelerated aging conditions (85% RH, 85 ºC) for 500 h. Yuan et al. [226] also successfully synthesized $CsPbBr_3$ NCs in tellurite-based glass, and showed improved water stability because 60% of the emission intensity was maintained after immersing NCs-embedded glass in water for up to 45 days. $CsPbBr_3$ NCs were also successfully precipitated in boro-germanate glass ($CsPbBr_3$ NCs@glass) with well-designed compositions, and not only retained a large PLQY (of 43% upon 450 nm excitation) and a narrow bandwidth (fwhm of 22 nm), but also showed significantly enhanced stability in relation to water, heat and UV/blue irradiation [227].

Although LHP's instability problems can be well solved by embedding $CsPbX_3$ (X = Cl, Br, I) NCs in these glasses, some urgent drawbacks still need to be overcome. For instance, the high melting temperature of silicate-based glasses results in the remarkable volatilization of Br sources and reduces the amount of crystallized perovskite in glass. In addition, challenges still remain as to the high costs incurred from using expensive GeO_2, while phosphate and tellurite glasses also exhibit poor chemical/mechanical stabilities.

4.2.4. *Template-assisted methods*

This approach adopts some ordered media, such as mesoporous silica, as a template for allowing the growth of LHP NCs in their pore structure. By this method, LHP crystal sizes and emission properties can be tuned by adjusting template pore dimensions. It makes this strategy especially appealing for the synthesis of small-sized LHP NCs, which are difficult to synthesize by wet methods given the instability problem caused by size effect (smaller than 7-8 nm). In addition, the template can act as a physical barrier that prevents LHP coming into contact with water and can improve their stability.

The template is usually added to a solution containing perovskite precursors with low pressure in a flask. Then precursors enter template pores due to pressure differentiation. Finally, by moderate heat treatment, LHP NCs form inside template pores. Several works have recently

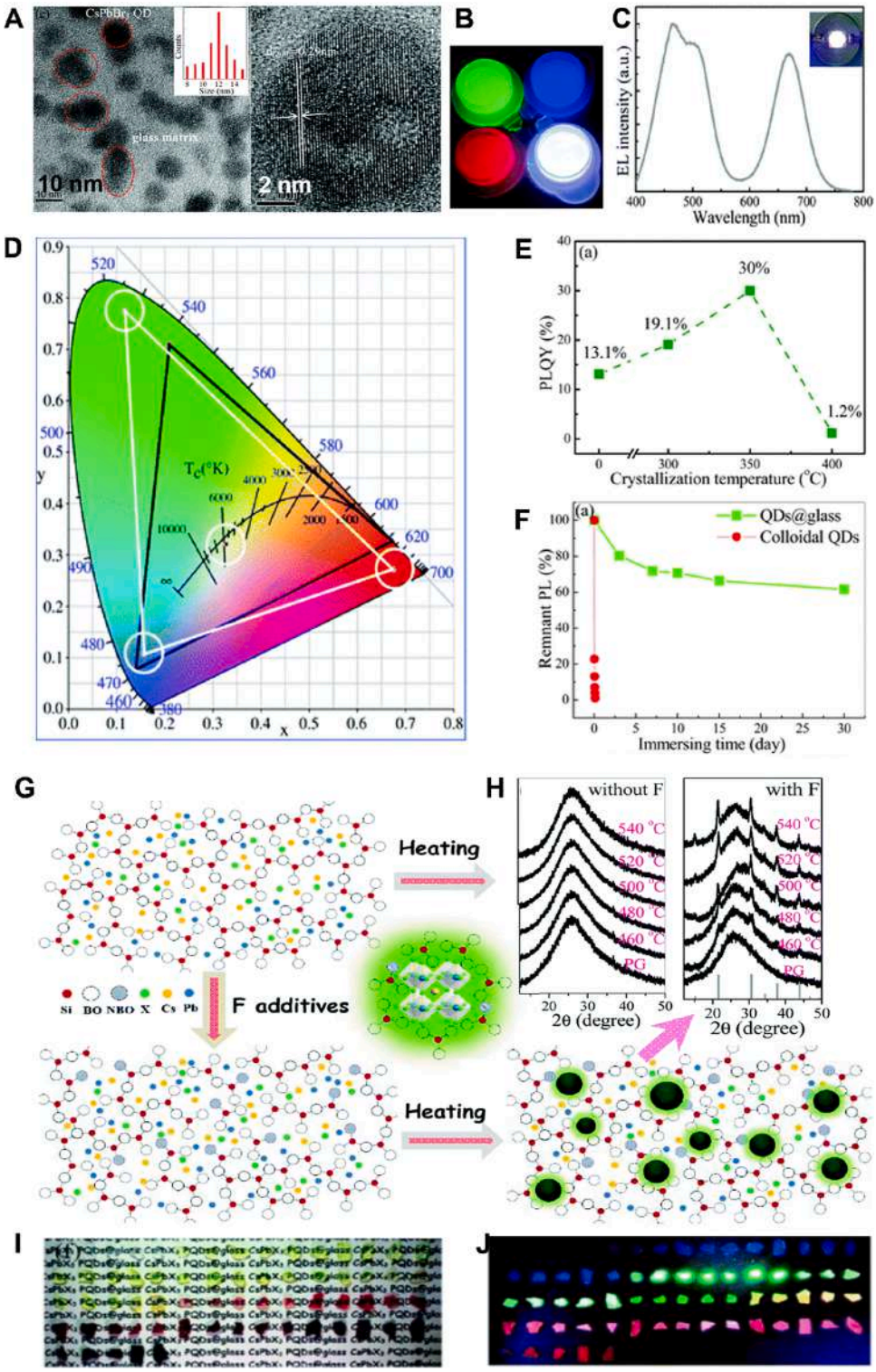

Fig. 20. Perovskite glasses: (A) TEM image of a low-melting (700 °C) phosphosilicate glass embedded with $CsPbBr_3$ NCs and the HRTEM micrograph of an individual $CsPbBr_3$ NP. (B) Luminescent images of different Zn–P–B–Sb based oxide glass powders embedded with LHP NCs dispersed in silicone gel: blue-emitting ($CsPbBrCl_2$), green-emitting ($CsPbBr_3$), red-emitting ($CsPbBr_{0.5}I_{2.5}$) and their white-emitting mixture. (C) Electroluminescence spectrum of a LED device recorded by coupling the mixture of blue, green and red glass powders with a UV chip; the inset is the corresponding device driven by an operation current of 20 mA. D) CIE chromaticity coordinates of the LED devices in operation and the NTSC TV color standard (black triangle). E) PLQY values of the $CsPbBr_3$ NCs@glass samples obtained by glass crystallization at different temperatures and F) their stability in aqueous solution. G) Schematic diagram of the obtained fluoride-doped $CsPbX_3$@oxyhalide borosilicate glasses and H) the XRD patterns of glass samples heated at several temperatures for 2 h. (I, J) Series of $CsPbX_3$ @glass monoliths under daylight irradiation and 365 nm UV light, respectively. (A, B-F) Reproduced from Ref [224,225]. with permission from the Royal Society of Chemistry (G-J) Reproduced from Ref [222]. with permission from the Royal Society of Chemistry.

demonstrated that perovskite NCs of different halide and A-cation compositions can be controllably formed in a variety of porous matrices, including MSU-H and MCM-48 [154], MCM-41 and SBA-15 [228,229], KIT-6 [230] and Zeolite-Y [231] (Fig. 21). In addition, templated-synthesized PS NCs exhibit pore size-dependent PL spectra and good stability with no noticeable drop in brightness, not even after a few days. For instance, LHPs nanowires confined inside anodic alumina oxide substrates in combination with PMMA sealing exhibit highly stable emission intensity that degrades only 19% after continuous 250 h of UV excitation and degrades 30% after three months when stored in air at 50% humidity [232] The main shortcoming of this strategy is the small PLQY reported for these nanocomposites regarding the NCs synthesized by ligand-assisted methodologies.

APbX3 NCs have been successfully infiltrated and grown inside film mesoporous host matrices, such as HKUST-1[233], Au-PDMS [234], SiO_2 nanowires [235] and electrochemical etched electrodes [236].

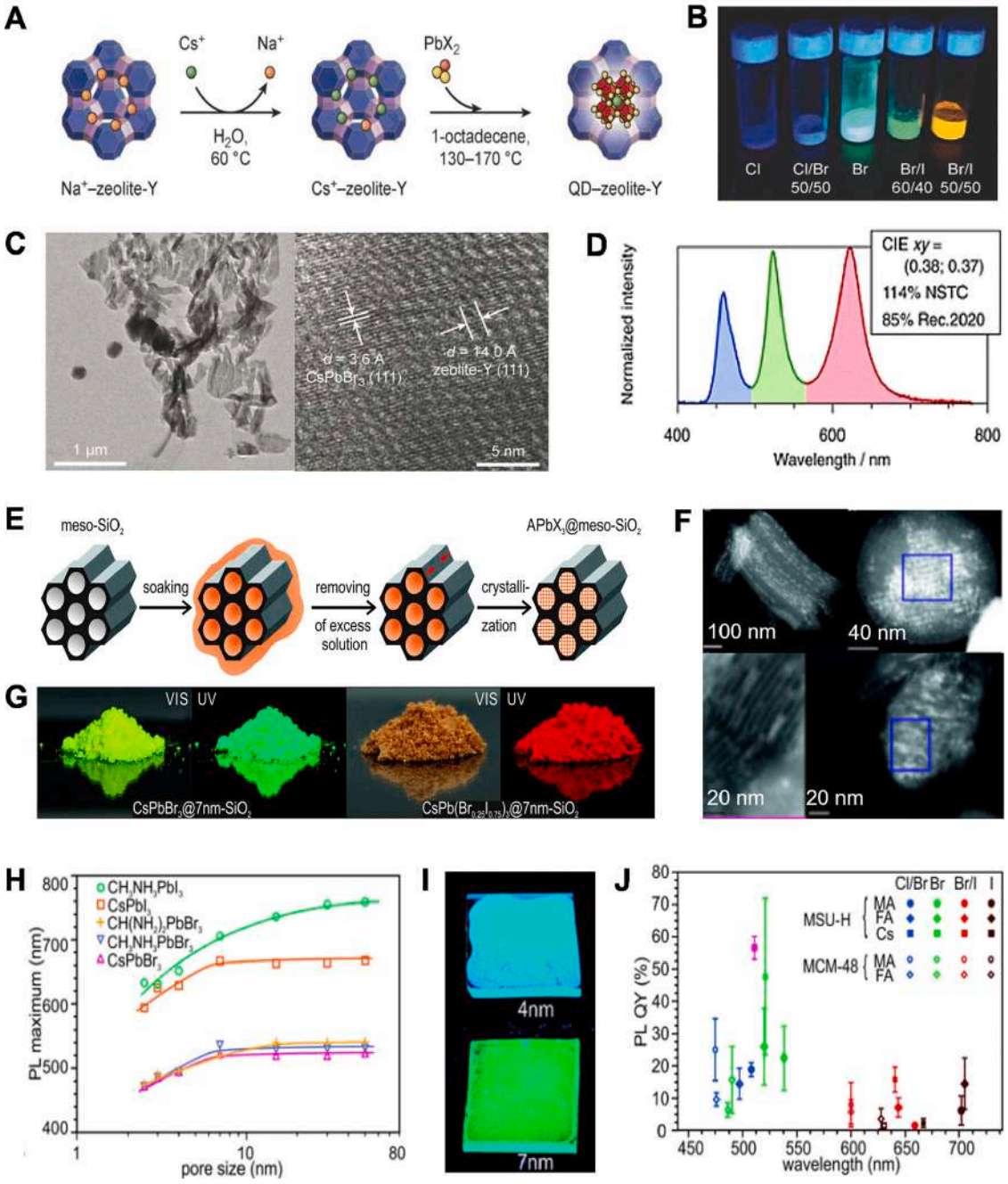

Fig. 21. Obtaining template-assisted LHP composites: (A) Scheme of the two-step synthesis of $CsPbX_3$–zeolite-Y composites; (B) TEM and HRTEM images of composite particles; (C) photograph of composites with several halide compositions subjected to UV excitation at 365 nm; (D) the output spectrum of a working WLED. It consists of an InGaN chip driven at 20 mA, a $CsPbBr_3$–zeolite-Y green phosphor and a $CsPb(Br_{0.4},I_{0.6})_3$ QD red phosphor; (E) thermal stability of $CsPbBr_3$–xeolite-Y composites. (F) Scheme showing the template-assisted synthesis of $APbX_3$ NCs in mesoporous silica pores. (G) HAADF-STEM images of a different SiO_2 sample (MSU-H, SBA-15, MCM-41) partially filled with $CsPbI_3$ NCs. (H) Photograph of composites LHP@SiO_2 under ambient light and UV-light. (I) PL maximum as a function of the template pore size for several $APbX_3$ perovskite NCs grown in meso-SiO_2. (J) UV-light (365 nm) photographs of films prepared from suspensions of the $CsPbBr_3$@SiO_2 composites stabilized with bis(2-ethylhexyl) sulfosuccinate. (K) PLQY for several lead halide perovskite NCs synthesized in 7 nm-SiO_2 (MSU-H) and 3 nm-SiO_2 (MCM-48). (A–E) Reproduced from Ref [231]. Copyright 2017 WILEY-VCH. Reproduced from Ref [154]. Copyright 2016 American Chemical Society.

5. Applications

5.1. Imaging and biosensing applications of LHP NCs

LHP NCs are a new class of luminescent materials with the potential to surpass the performance of inorganic (gold, silver, CdSe, CdS nanoparticles, etc.) and organic fluorophore predecessors in sensitivity terms in the imaging nanodiagnostics and biosensing field [16,237]. LHP offer unique properties that make them ideal as luminescent contrast agents, such as their small particle size, composition and size-tunable optical properties, wide color gamut, high PLQY, the simplicity of their synthesis methods, together with the low cost of starting materials, the simultaneous excitation of multiple fluorescence colors and multiplex capabilities [6,45].

Besides all the above advantages, one of the most appealing properties for their use as biological label lies in their nonlinear optics.

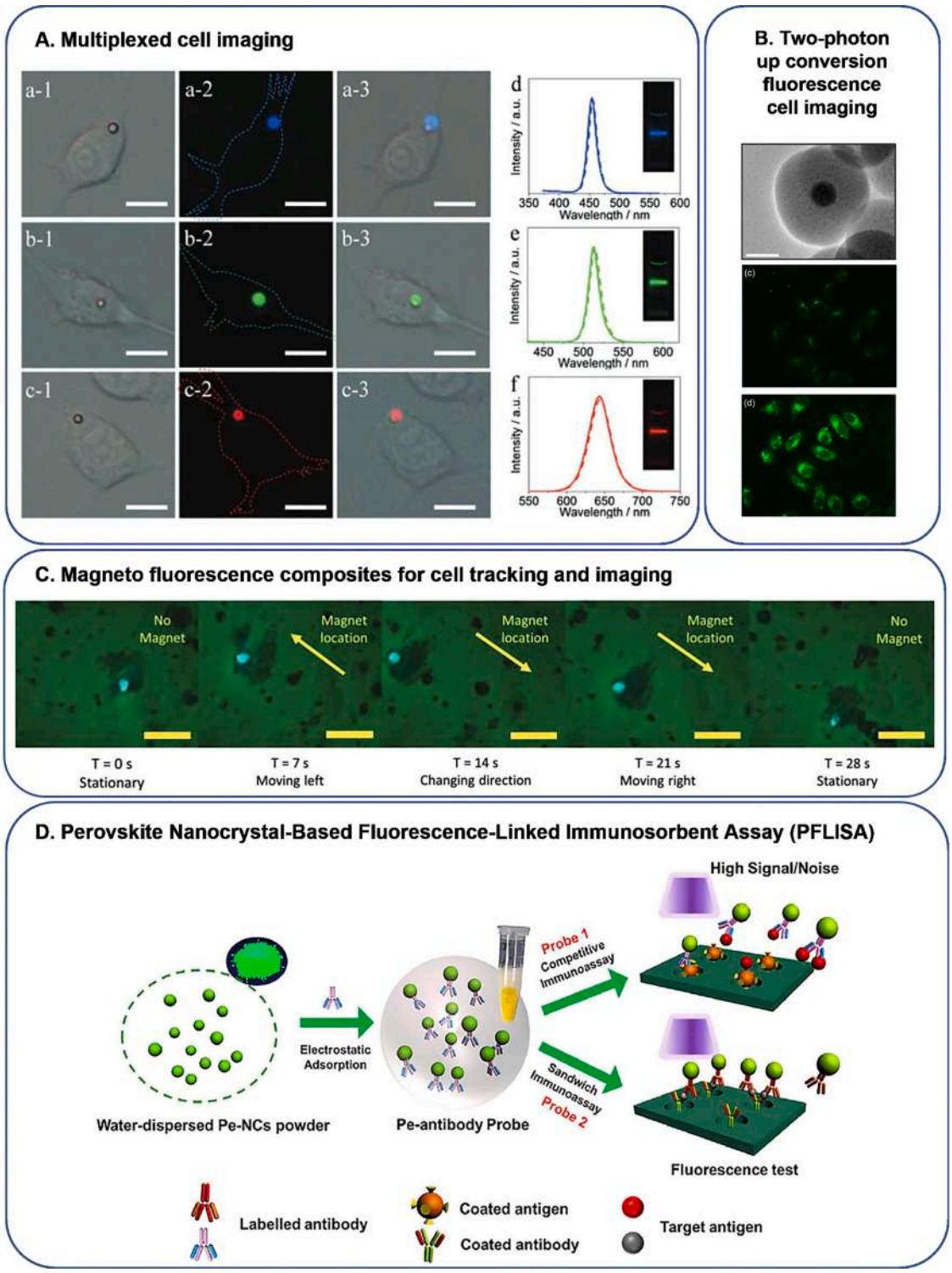

Fig. 22. Schematic representation of the most representative strategies of LHP NCs fluorescent labels for biosensing and bioimaging. A) Bright-field and fluorescence images of live cells incubated with mixed LHP NCs embedded in polystyrene beads. Reprinted with permission of Ref [16]. Copyright 2017 WILEY-VCH. B) Two-photon up conversion imaging of HepG2 carcinoma cells cultured with $CsPbBr_3$@SiO_2 core-shell nanoparticles. Adapted from Ref [246]. Copyright 2022 Elsevier Ltd. C) Directed motion MDA-MB-231 breast cancer stem cells tagged with magneto-fluorescent particle perovskite nanoparticles under the magnetic field effect. Reproduced from Ref [245]. Copyright 2019 WILEY-VCH D) Scheme of the Perovskite Nanocrystal-Based Fluorescence-Linked Immunosorbent Assay (PFLISA) for Aflatoxin detection. Reprinted from Ref [247]. Copyright 2020 Elsevier Ltd.

Several studies reveal multiphoton absorption cross-sections (up to five photons) processes from an infrared light source and the subsequent emission of a photon of higher energy [61,238,239]. The high degree of nonlinear absorption offers significant advantages, such as increased spatial confinement, reduced background autofluorescence, improved sensitivity of several orders of magnitude and, above all, little biological damage to the studied sample [240,241]. Therefore, despite remaining in very early scientific and technical development stages, MHPs have demonstrated ideal optical properties that make them a promising luminophore with a bright future in many areas of biology, such as

labels and contrast agents for *in vitro* bioimaging and biosensing (i.e. inmunostaining, DNA and protein microarraying, flow-cytometry based diagnosis) and for the super-resolution imaging applications that go beyond optical diffraction limits [242]. The most representative works of LHP NCs in the imaging and biosensing field are summarized in Fig. 22.

However, their implementation as luminescent probes involves developing protective shells which, on the one hand, prevent their degradation in aqueous biological media and, on the other hand, endow their chemical functionalization with biocompatible functional groups. Within this framework, Luo et al. makes the most of the zwitterionic nature of peptide biomolecules to prepare protein-passivated $CH_3NH_3PbBr_3$ NCs with a large product yield (44%) and with potential optical biosensing and imaging applications [243]. In a parallel work, Zhang et al. demonstrated macrophage internalization and multiplexed cell imaging for the first time by embedding polyvinyl pyrrolidone-capped $CsPbX_3$ perovskite in polystyrene beads (particle size ~ 3–5 μm). They claim that using seven-colored LHP NCs showing nonoverlapping spectra will make it possible to individually tag about 10 million cells [16]. This pioneer research work triggers the study of cell imaging capabilities for perovskite nanocomposites. However, most of them involve the important issue of working with a large particle size, which is frequently larger than the average size of a cell or the biological system under study, which hinders its practical applications.

At this point it is worth citing the studies of Zhaoyan et al. because they make relevant progress by significantly reducing NP size to 50 nm and demonstrate the specific tracking of tumor cells [244]. Their work describes multicolor cell imaging and the specific detection of folate receptors overexpression in tumor cells by introducing phospholipidic capped-LHP NCs stabilized in buffer media and derivatized with a specific folate-targeting ligand. A smart alternative approach is the development a new perovskite-based magneto-fluorescent nanocomposite that allows the *in situ* real-time optical visualization of magnetically induced cellular movements, and with a potential application in magnetically driven drug delivery and hyperthermia treatment [245]. In a recent study, Zhong et al. described the two-photon up-conversion imaging of HepG2 carcinoma cells cultured with $CsPbBr_3@SiO_2$ core-shell NPs [246]. This study paves the way toward exploiting LHP NCs as future NIR imaging labels with a high signal-to-noise ratio (elimination of biological autofluorescence), a profound light penetration depth, and reduced cell photodamage.

Apart from cell imaging studies, LHP also present appealing features to be used as luminescent labels for the *in vitro* optical biosensing and bioanalytical system (fluorescent immunosensing, DNA and protein microarrays, etc.). This line has been less explored because of the difficulties with developing perovskite NCs stabilized in aqueous media whose single particle nature remains intact, and because their surface chemistry is still not yet well-understood and effective surface functionalization strategies are lacking.

Dong et al. developed an NP fluorescence-linked immunosorbent assay methodology based on LHP NCs encapsulated in olefin shell and functionalized with hydroxyl groups for Aflatoxin detection purposes [247]. As part of this approach, it is worth mentioning a recent work of this group, which describes luminescent labels $LHP@SiO_2$ core-shell NPs for specific protein detection [179].

Further to their use as luminescent labels, LHP NCs and nanocomposites can also be employed in biosensing. For instance, Chaomin developed a paper-based test for microRNAs detection based on Electroluminiscence Resonance Energy Transfer (ERET) between electroluminescent phosphour nanosheets and gold NPs, which uses a LHP solar cell as a power source to provide constant voltage at detection limits of 0.1 pM [248]. In addition, several works describe photoelectrochemical biosensors for the detection of targets of interest based on perovskite electrodes. Along these lines, Qin et al. demonstrated the photoelectrochemical detection of oncogenic alpha-glycoprotein with 0.08 $ngmL^{-1}$ sensitivity by means of $CsPbCl_3$ perovskite NCs/a TiO_2 inverse opal photonic crystals electrode [248].

One of the major drawbacks of implementing perovskite NCs as an imaging and bioimaging probe is their intrinsic toxicity. Indeed some considerations should take the following into account: (i) the wide variety of *in vitro* applications for biosensing (luminescent microarrays, flow cytometry, paper-based immnoassays, etc.) and bioimaging (inmunostainning, cell histology, *in vitro* cell tracking, etc.); (ii) the NPs that are suitable for biological applications need to be properly encapsulated in protective shells, which preserves their stability in water and simultaneously reduces the release of heavy metals; (iii) due to their high absorption coefficients, together with their large PLQY, they will enable target detection in the presence of a very low concentration of a label. This fact, combined with small NPs sizes, implies a very low lead concentration; iv) according to the International Lead Association, lead (Pb) is one of the most effectively recycled materials in the world and 80% of modern Pb usage is recycled in agreement with well-established protocols[249]; v) in the quest for alternatives, research into Pb-free perovskite NCs with lower toxicity and stabler metals is actively on-going. Recently, perovskite NPs with similar properties to their lead counterparts have been obtained. [75]

5.2. Optoelectronic and photonic applications of LHP NCs

5.2.1. Solar cells

LHP possess intrinsic properties like a wide absorption spectrum, fast charge separation, long transport distance of electrons and holes, a long carrier separation lifetime, simple manufacturing by solution-processed methodologies and more, which make them promising materials for the new generation of cost-competitive high-efficiency solar cells. The vast majority of studies into perovskite solar cells have been done on perovskite polycrystalline films, and not on devices fabricated from NCs. Currently, a 25.2% record photoconversion efficiency is described for an $MAPbBr_3$ thin film device [250].

One of the major drawbacks that makes placing LHP solar cells on the market difficult is $CsPbI_3$ NCs' poor stability, which easily converts into δ-$CsPbI_3$ under ambient conditions. An effective way of stabilizing the α phase is to reduce their dimensions to a nanometer size, which has led research interest in developing NCs-based perovskite solar cells [8]. However, the insulating aliphatic ligands introduced during NCs synthesis severely hamper the separation and transportation of photogenerated-charges, which results in perovskite nanocrystalline solar cells' worse power conversion efficiency (PCE) regarding polycrystalline counterparts. Therefore, reducing their recombination has become a bottleneck to further enhance perovskite nanocrystalline solar cells' PCE, and considerable effort has been made in three directions: surface ligand engineering, film processing conditions and the selection of adequate contacts that maximize energy level alignments.

In 2014, Luther et al. described a $CsPbI_3$ NCs solar cell device with a high open-circuit voltage of 1.23 V (around 85% of the Shockley-Queisser theoretical limit), a short-circuit current (J_{SC}) of 13.4 mA cm^{-2} and final photovoltaic conversion efficiency over 10% [8]. Since then, this group has made the effort to enhance the electrical coupling in LHP NCs and to develop highly efficient perovskite nanocrystalline solar cells through the synthesis of A-site alloyed NCs [251,252], layer–by-layer film processing [253], post-synthetic treatment with halide salts[252] and the incorporation of a conductive polymer-perovskite hybrid layer [254]. To date, the highest PCE achieved is 16.6% [255]. (Fig. 23) In parallel, active investigation into low-toxicity perovskite solar cells has been active, with record efficiency of 12.96 for tin-based perovskite NCs having been recently described [256].

Ligand engineering plays a major role in the future of NCs-based solar cells, and several works highlight how the adequate tuning of both the types and numbers of surface ligands can reduce the defects and enhance the transportation efficiency of photogenerated carriers [9,252,257,258]. In addition, effective encapsulation of solar devices in a

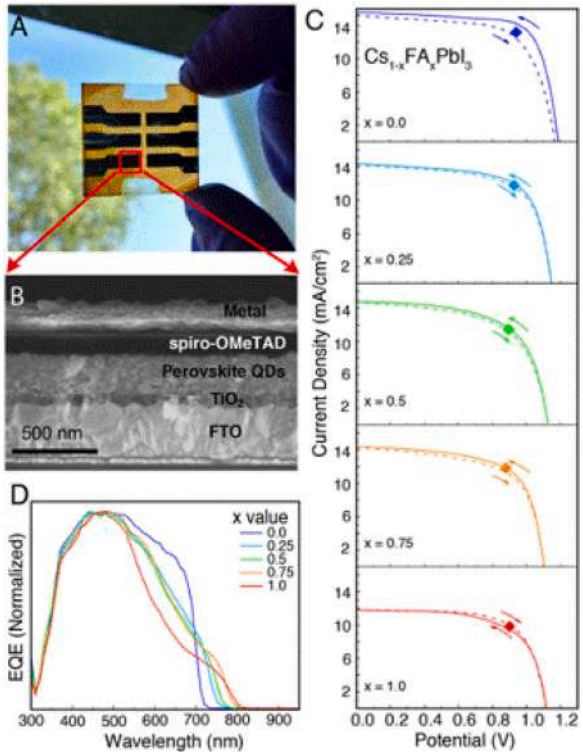

Fig. 23. Device features and the performance of alloyed $Cs_{1-x}FA_xPbI_3$ NCs-based LHP solar cells with power conversion efficiencies of ~10%. Reprinted from Ref [251]. Copyright 2018 American Chemical Society.

robust stable insulator is a requirement to guarantee the device's stable performance. Although a huge gap currently exists with polycrystalline hybrid organic-inorganic perovskite solar cells' PCE, we believe that the vast amount of research conducted in this field will soon make $CsPbX_3$ NCs-based solar cells strong candidates in the photovoltaic area.

5.2.2. LEDs

LHP NCs encompass several attributes that allow their implementation into high-quality next-generation LEDs, such as high color purity, with the full width half maximum of 15–25 nm for electroluminescence spectra and a wide color gamut, high external quantum efficiency (EQE), current efficiency (CE) and a low-temperature solution processing-based fabrication route, which would considerably reduce their manufacturing costs. Current commercial inorganic LEDs are made off rare-earth phosphors and epitaxial III–V semiconductors, which incur high manufacturing costs. Next-generation organic light-emitting diodes (OLEDs) still require vacuum-based sublimation during the deposition of active layers, which is an expensive technique for large-scale fabrication, whereas QDs-based LEDs require high quality QDs, which implies sophisticated synthesis methods to hinder their final commercial implementation. Indeed, LHP possess many appealing features to bypass the above-mentioned issues. In the last four years, LHP LEDs have rapidly progressed in EQEs by going from below 0.1% to over 20%. This has been encouraged by unprecedented rapid improvements [259], and because more researchers have focused on this research and produced many hopeful results.

While most earlier reports have focused on film-processed bulk perovskite emitters rather than on presynthesized NCs, it was soon realized that perovskite NCs offer several advantages for LEDs fabrication. For instance, small size and dimensionality increase exciton binding energy and cut diffusion length to, thus, prevent current leakage in LEDs, and not in bulk perovskite counterparts [260]. Besides, perovskite NCs also offer advantages for adjusting their semiconductor properties

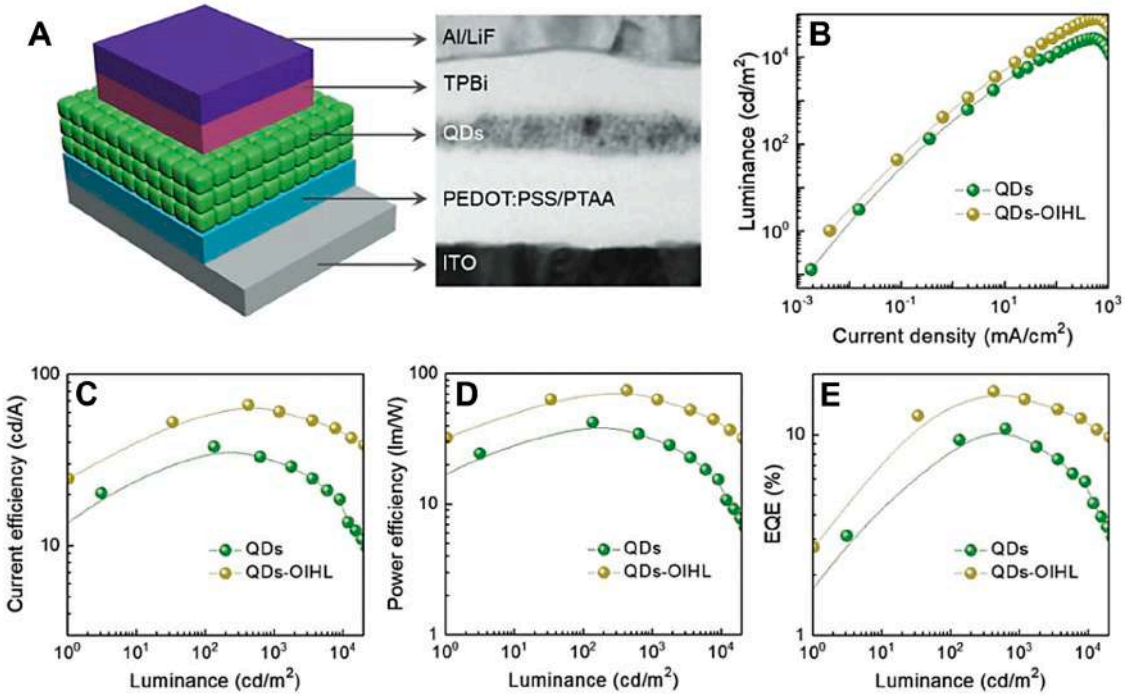

Fig. 24. Device architecture and performance features of NCs-based LEDs LHP prepared form dual passivated (DDAB ligands and metal bromide salts) $CsPbBr_3$ NCs. A) Left: the illustration of the device architecture; right; a cross-sectional TEM image showing the device's multiple layers. B) Luminance of devices as a function of current density. C) Current efficiency; D) power efficiency; E) EQE of devices as a function of luminance. LHP LEDs exhibit an EQE maximum peak of 16.48%. Reproduced from Ref [265]. Copyright 2018 Wiley-VCH.

by their interfacial engineering due to their high surface-to-volume ratio [261].

The utilization of colloidal LHP NCs in LEDs was first described by Song et al. [262]. Despite their large PLQY, the obtained LEDs showed EQE and maximum luminance values less than 0.2% and 1000 cd m^{-2}, respectively. This poor efficiency is attributed mainly to the presence of insulating long-chain aliphatic molecule, which make charge carrier injection and transport difficult.

To circumvent these issues and to improve overall EQE, tremendous efforts are being made. For instance, Li *et al.* achieved a 50-fold improvement in EQE with values of 6.27% for $CsPbBr_3$ LEDs by controlling surface ligand density [263]. Chiba et al. exchanged native organic ligands, such as oleylamine and OA, with DDAB to obtain LEDs with a current efficiency of 18.8 cd A^{-1} and an EQE of 8.73% [264].

In another study, Song et al. [265]. reported an organic-inorganic hybrid ligand strategy to passivate perovskite NCs. They reported about LEDs that exhibit a maximum EQE peak of 16.48% (Fig. 24).

Until the present-day, the most efficient LED, with a EQE peak of 21.3%, has been reported by Kido et al. They reported highly efficient light-emitting devices fabricated by an anion exchange from pristine $CsPbBr_3$ using halide-anion-containing alkyl ammonium and aryl ammonium salts [266].

Although LHP LEDs are considered for next-generation LEDs, there is still a number of drawbacks to be addressed before their commercial implementation. The first challenge is related to poor intrinsic perovskite stability. Although many works have proposed plenty of synthetic approaches to stabilize halide perovskite materials with considerable improvement, they still do not meet the criteria for practical devices (operational stability $>$ 20 000 h) [267]. The stability of NC-based LHP LEDs could be further enhanced by combining them with moisture-resisting materials, such as fluorinated polymers.

Besides, further research is mandatory to develop large-scale production techniques that are compatible for industrialization *via* low-cost solution processing. Finally, the toxicity of Pb cations, which can be easily released to the environment, is a major obstacle that needs to be overcome. Toward this goal, several reports demonstrate that Pb-free perovskites can function well as emissive layers in LHP LEDs [268–270].

5.2.3. Displays and light converters

The optical and electrical features of LHP also make them suitable for displays and white light emission [271,272]. Generally, white light generation through LEDs consists in combining a blue LED device with a color conversion layer composed of inorganic phosphor (pigment) particles, such as oxide and nitride derivatives [273,274]. In these systems, the blue emission promotes the excitation of yellow phosphor (cerium-doped yttrium aluminum garnet, YAG:Ce^{3+}). White light is generated when the original blue light is combined with the emitted yellow light. However, this technology still has some issues as regards the color quality, scalability, cost, stability and availability of rare earths elements, and different luminescent materials need to be employed as an alternative to phosphors. [271,275]

More recently, colloidal CdSe/ZnS and InP/ZnS QDs have been incorporated into LEDs by replacing conventional phosphors to fine tune the emission spectrum [276], and have become a current choice technology for liquid crystal displays (LCDs) televisions. Similarly to QD-LED technology, LHP NCs present appealing features to be exploited as color converters in full-color displays, such as high color purity, wide color gamut coverage, a near-unity PLQY and low cost [166,277,278] (Fig. 25A).

Classic YAG:Ce^{3+} yellow phosphor integrated into a blue LED chip component results in a typical color rendering index (CRI) of ≈80 or below, whereas hybrid LHP/phosphors hybrid LEDs, which incorporate a complementary red component from $CsPbI_3$, renders efficient emission with a high CRI above 90 and enables good power efficiency over 70 lm W^{-1} [279–281].

In another scenario, several works have reported color converters made solely of LHP as a color conversion layer in a commercial UV (365 nm) LED. However, these systems have a lower CRI compared to the hybrid one due to the narrow band emission of perovskite NCs, and they need another color component to broaden the emission spectra [282, 283].

Unlike the fabrication of LEDs, using LHP color converters presents many advantages in stability terms. In principle, they do not need to be electrically contacted and all the considerations concerning electrical features, charge carrier transport and injection can be neglected. Most LHP color converter devices are processed, such a film of pre-synthesized colloidal NCs dispersed in an insulating polymeric or inorganic matrix and deposited on top of blue LED by wet methods (spin-coating or dip coating) [281,284]. They are generally processed as monochromatic optical filters (Red, Green, Blue, RGB) to avoid ion migration concerns, although several examples report multicolor films (with a tunable emission spectrum between 450 and 550 nm) fabricated by adjusting the LHP ratio with a different halide composition [282, 283].

Alternatively, the exclusion of toxic Pb- and heavy lanthanide-based phosphors in white LEDs would be a bright prospect for lighting applications. Along these lines, many lead-free LHP NCs based down converters[269,285] with good operating qualities are reported. For instance, Luo et al. fabricated dual perovskite $Cs_2AgInCl_6$ down shifters that exhibit superior performance as phosphor in white LED because of their broad band emission, and have a superior operation lifetime of over 10 000 h under continuous UV illumination under ambient conditions [285].

In addition, Bakr et al. pointed out the potentiality of LHP NCs for wireless communication technology, which uses light to transmit data between devices (Light Fidelity, Li-Fi) [11] (Fig. 25B). Similarly to the way that Wi-Fi uses radio frequency to induce voltage in an antenna to transmit data, Li-Fi employes the modulation of light intensity to transmit data. In their work, they fabricated a $CsPbBr_3$ NC red phosphor white light converter, which exhibited an unprecedented modulation bandwidth of 491 MHz, which is ~40-fold higher than that of conventional phosphors, with the capability of transmitting a high data rate of up to 2 Gbit/s. Moreover, this perovskite-enhanced white light source exhibits a high color rendering index of 89 and a correlated color temperature to, therefore, enable dual visible light communication and solid-state lighting functionalities [11,286].

5.2.4. Lasers

Recently, Pb halide perovskites have come over as an excellent class of optical gain media for lasers. This addresses their large PLQY, which reduces nonradiative losses, and will contribute to lower threshold pumping, high absorption coefficients and a slow Auger recombination, which are beneficial for achieving low-threshold and ultrastable room temperature-stimulated emissions in an atmospheric environment. In addition, the high optical gain coefficients of MHPs are comparable to those of the industry reference materials, such as gallium arsenide [287]. Apart from their ideal optical properties, one of the most fascinating features for using MHPs as gain media is their tailorable bandgaps, which offer the possibility of tuning spectral emission regions from visible to near-infrared (350–700 nm). As they also possess excellent processability properties. MHPs may not only be fabricated as diverse optical microcavities, but may also be integrated with several commercial optical cavities to construct laser devices [288,289].

In the past 5 years, more progress has been made in investigating LHP laser devices, which comprise a microstructure and composition investigation [288,290–292]. Fig. 26 summarizes some representative works of LHP microstructuring procedures for lasing applications. By engineering the composition and structure of MHPs, considerable progress has been made to improve performance and to extend the functionalities of perovskite lasers, such as lowering the lasing threshold down to hundreds of nJ cm^{-2} [293,294], broadening the wavelength spectral emission [295], improving spectral purity (single-mode output)

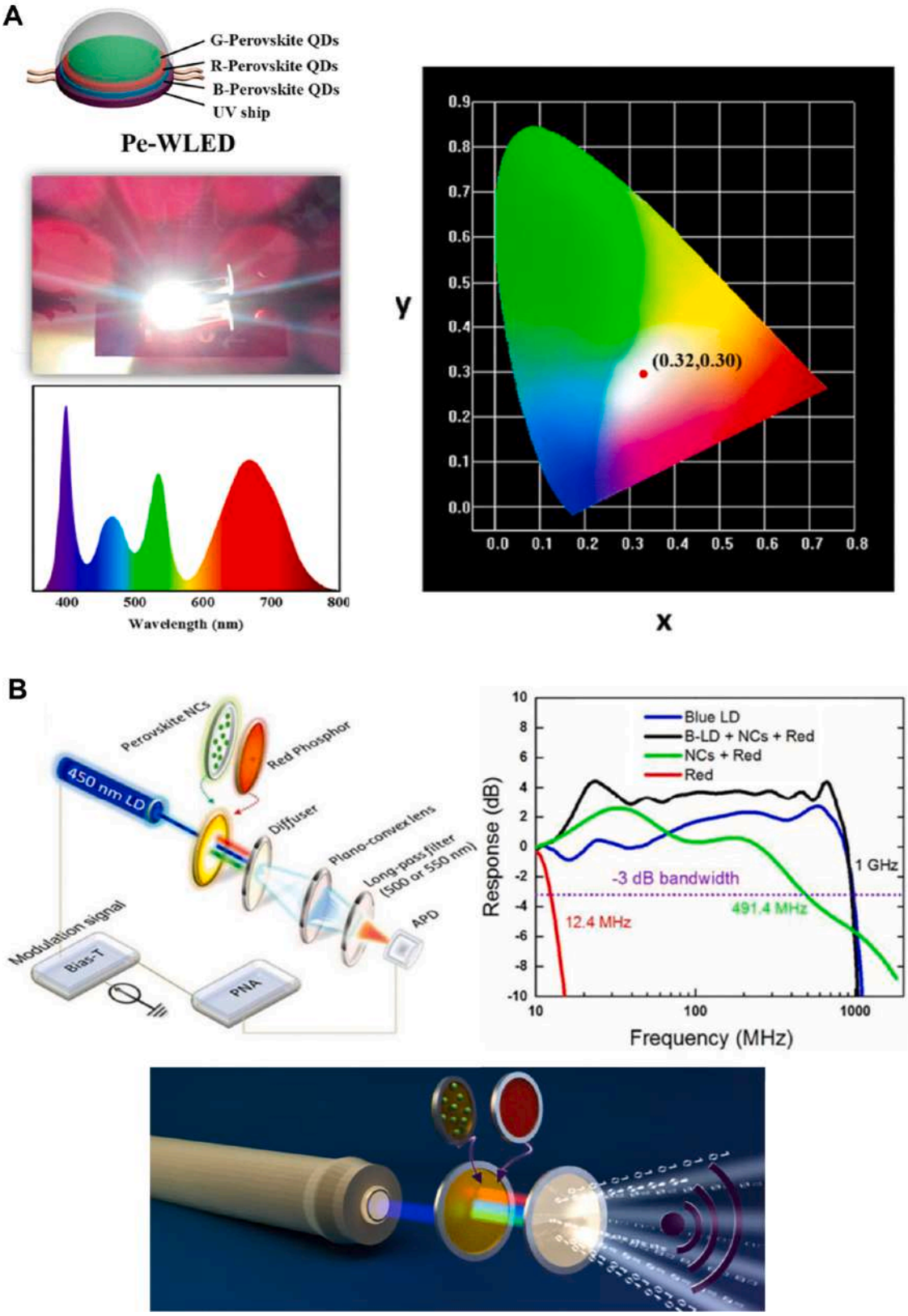

Fig. 25. A) Schematic description of white-LED based on halide perovskites assembled on a UV LED chip, which results in white light generation. Reproduced from Ref [282]. Copyright 2017 American Chemical Society. (B) Schematic drawing of a setup for modulation bandwidth and data transmission measurements using perovskite NCs and the measured frequency results for different device configurations. Reproduced from Ref [11]. Copyright 2016 American Chemical Society.

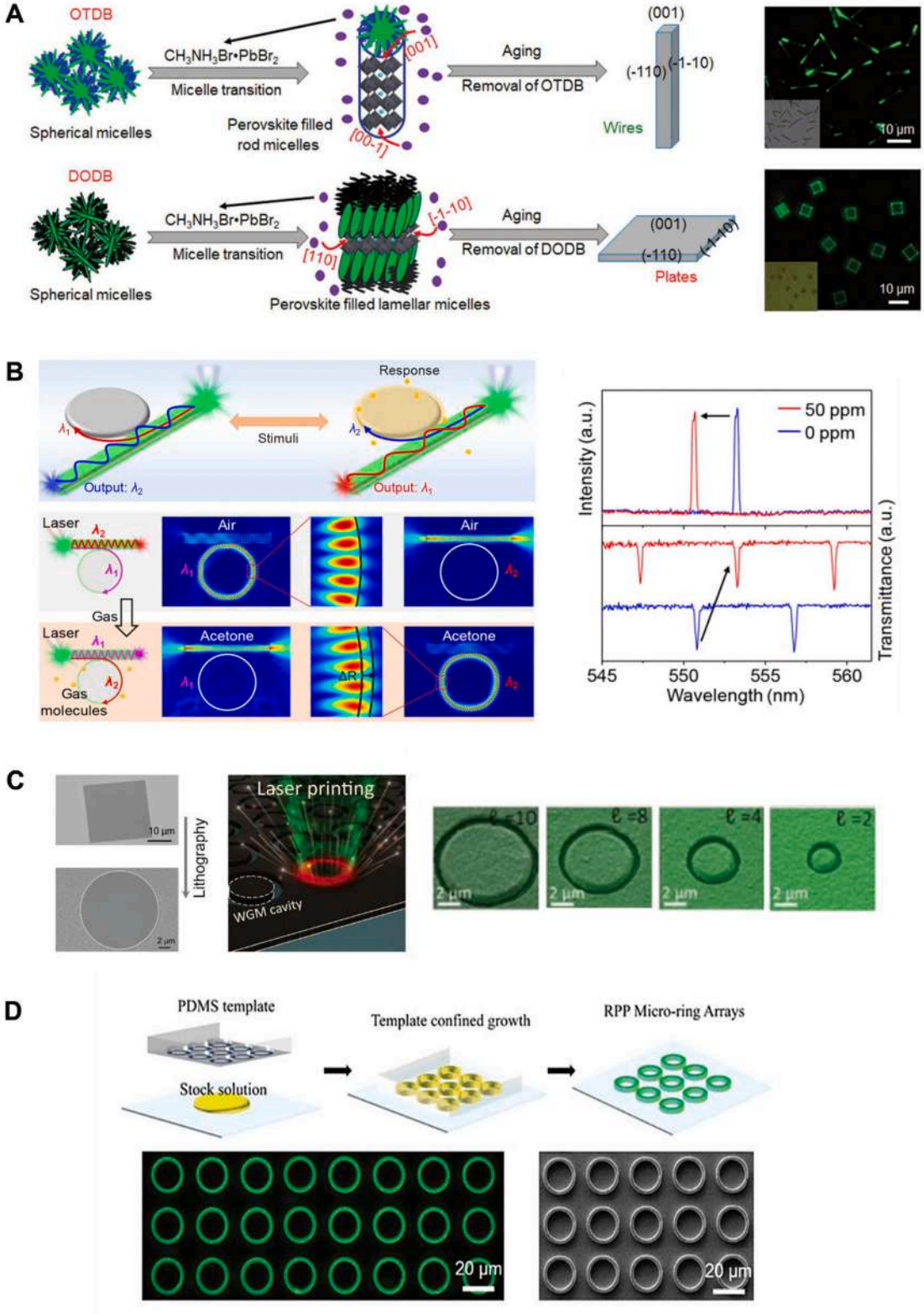

Fig. 26. Controllable synthesis of perovskite microcrystals and processed microcavities of particular interest in laser technologies. (A) Schematic illustration showing the surfactant-assisted self-assembly mechanism formation of $MAPbBr_3$ wires and plates and photoluminescence images. (B) Scheme showing the design principle of modulated lasing set up from a responsive organic microdisk-coupled perovskite wire. Numerically simulated electric field distributions of two lasing modes. Wavelength switching behavior of the lasing spectra (top) and transmittance spectra (bottom) of the coupled microstructure before and after being exposed to stimuli. (C) Schematic illustration showing the fabrication of perovskite microdisks through laser ablation with a donut-shaped femtosecond laser beam and (D) template-induced solution growth of perovskite microring cavities. (A and D) Reproduced from Ref [290,291]. Copyright 2017 WILEY-VCH. (B and C) Reproduced from Ref [292,293]. Copyright 2016 American Chemical Society.

and temporal coherence (linewidth narrowing down to ~0.09) [296], reducing the device dimension down to subwavelength scales [297], and prolonging the device's lifetime up to dozens of hours of continuous operation [298–300].

However, there are many challenges that still need to be addressed to acquire electrically pumped perovskite lasers. The first one is that continuous-wave lasing in perovskites only operates at cryogenic temperatures, and further research is mandatory to unveil the lasing death mechanism and to provide guidance for designing perovskites toward room-temperature continuous-wave lasing. The second challenge is heat management in perovskite laser devices, which is one to two orders lower than conventional inorganic semiconductors [301–303], which can induce device degradation. Hence device architecture optimization is imperative for mitigating heat accumulation in the perovskite gain layer toward electrically injected perovskite lasers. The third challenge is about the lasing threshold of MHPs, which still needs to be further lowered to be competitive with established technologies [304,305]. Besides, MHPs possess poor stability[306] because they degrade when exposed to moisture.

Thus interface engineering and the development of encapsulation strategies play an important role to overcome some of the aforementioned drawbacks. From the stability point of view, several reports indicate how to enhance stability through protection with polymers, boron nitride films and DBR cavities [307,308]. In an alternative approach, the encapsulation of perovskite lasers with high thermal-conductivity boron nitride films can accelerate thermal dissipation and improve overall device stability [309].

Regarding toxicity issues, and despite increasing advancements made in LHP for lasing purposes, Pb-free perovskites are still not widely implemented in lasing systems. Xing et al. described a tin-based perovskite laser, which surprisingly possesses good optical gain properties in the near-infrared region [310]. However, tin perovskites have poor stability and optoelectronic properties compared to Pb perovskites.

5.3. Other applications

Given their excellent optoelectronic properties, perovskite NCs are found in a number of interesting applications beyond the aforementioned imaging and optoelectronic devices, such as photodetectors [311], X-Ray imaging [312–314], anti-counterfeiting [315], sensing [316] or photocatalysis [317] (Fig. 27).

For instance, LHP NCs are promising candidates for use in photodetectors for their optical and electronic properties, such as high extinction coefficients, long carrier diffusion and carrier mobilities, plus

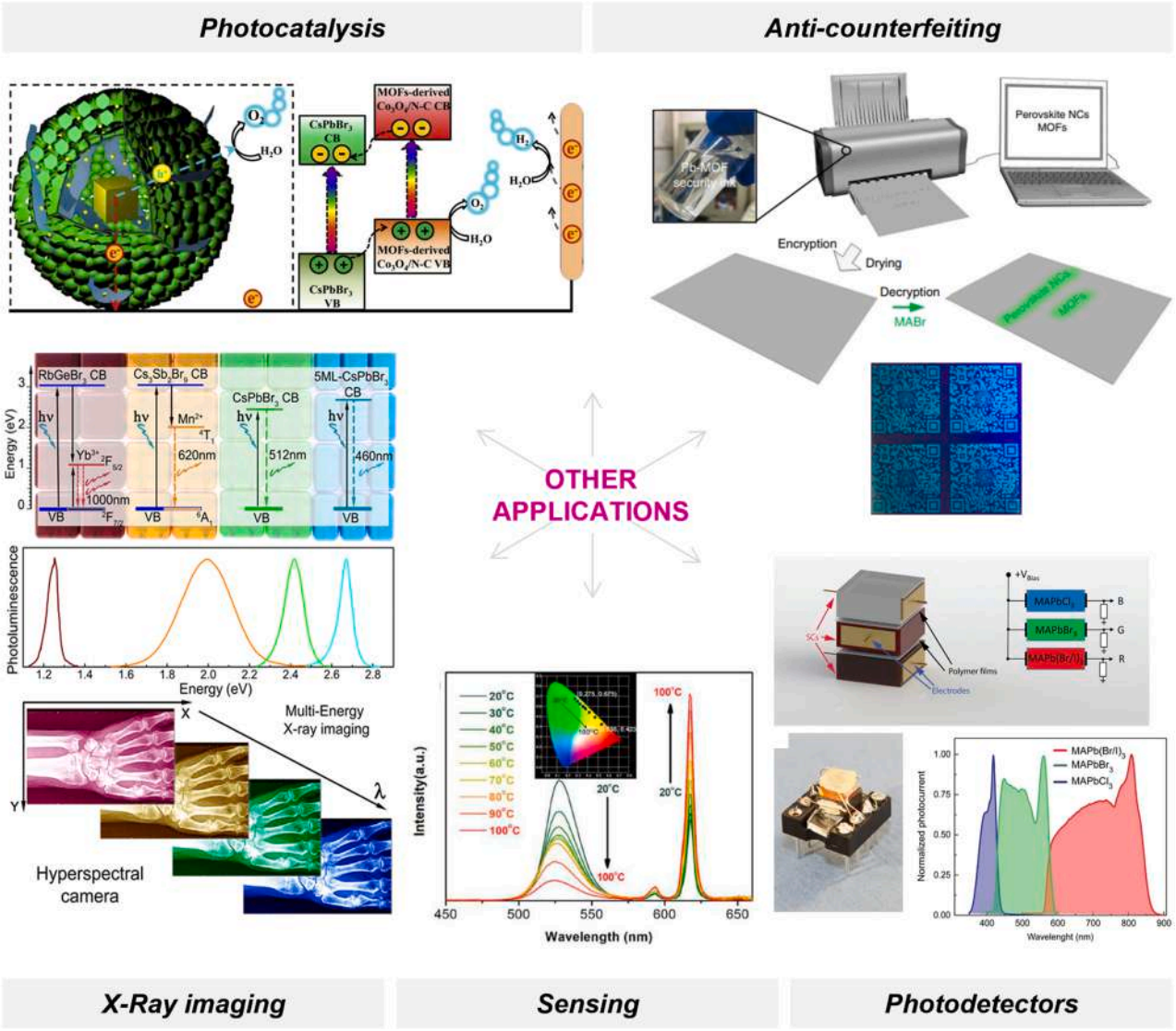

Fig. 27. Schematic showing the other LHP application. The images used to illustrate properties and applications were adapted from Ref [311,312,315–317]. Copyright 2017. Springer Nature Ltd. Copyright 2019 AIP Publishing. Copyright 2020 American Chemical Society. Copyright 2020 Elsevier Ltd.

the possibility of covering a broad light range (including visible and NIR spectra) with a good sensitive response, and so on.

To date, there have been fabricated perovskite-based photodetectors with high responsivity exceeding 10^4 AW^{-1} [318,319], detectivity approaching 10^{14} Jones [320,321], small noise equivalent power (NEP $<$ 50 fW $Hz^{-1/2}$) [322,323], a wide linear dynamic range of 150 dB [319,324], and a short response time <1 ns [313,325], by optimizing chemical composition and structure, cell architecture and interfacial engineering. Therefore, LHP-based photodetector devices can compete with avalanche photodiodes, such as GaAs and Si, and offer the advantages of a low-cost solution process. In commercialization terms, perovskite will face many of the same challenges as perovskite solar cells; i.e. stability, toxicity issues, and competition from more mature technologies. Concerning toxicity issues, recent work demonstrated direct integration of lead-free halide perovskite with mature silicon industry paving the way to fabricate monolithically integrated and high-performance photodetectors [326].

Another particular application of LHP NCs is for X-ray imaging for medical diagnosis purposes. Computed Radiography (CR) evolution and the replacement of current radiographic films with new digital detector arrays (DDA) present some unique advantages, such as a potential reduction of the X-Ray dose, the possibility of post-processing and data storage, higher image quality, faster results, among others.

Current solid-state technology presents two available X-ray imaging approaches by means of flat panel detectors. The first is based on indirect conversion and combines the use of scintillators and semiconductor photodetector to detect the light emitted by the scintillator. The second approach comprises the direct conversion of X-ray photons into electrical current. The latter approach is reported to provide higher resolution and sensitive photoconduction [327], and is observable in several crystalline inorganic semiconductors under X-ray illumination, including amorphous Se, crystalline Si and CdTe. However, most of these devices present poor absorptivity problems for X-rays [328]. Recently, methylammonium lead iodide perovskite was demonstrated to possess an appealing combination of a fast photoresponse and a high absorption cross-section for X-rays owing to heavy Pb and I atoms, and solution-processed perovskite detectors, which give high values for both X-ray sensitivity (up to 25 μC mGyair $^{-1}$ cm^{-3}) and responsivity (1.9×10^4 carriers/photon), the latter of which was one order of magnitude higher than that achieved with Tl-doped CsI-based indirect detectors and amorphous Se-based direct detectors [313]. This result has triggered a commercial interest in perovskite absorbers and X-ray and γ-ray detectors [329].

6. Conclusions and future perspectives

This review covers many aspects concerning strategies for preparing stable and water dispersible LHPs, and composites with enhanced stability against moisture. Although active research on this topic has been carried out in recent years, there are still several open issues which require further development, and are discussed below. Also, some promising future research directions from the chemical perspective are remarked.

Surface Chemistry and Interface Engineering

Despite the significant progress made in recent years to study LHP surface chemistry and the ligand interface binding motif, they are still not fully understood. In surface chemistry terms, standard $CsPbBr_3$ NCs have been widely studied and it has been established that NCs are bound mainly to oleylamine *via* A-site vacancy, and present a high ligand shell dynamic nature, which brings about the rapid loss of colloidal features. Several works tackle this issue by replacement or the post-synthetic exchange of olefin native ligands with strong binding ones, such as TOP or TOPO, or by employing ligands with higher steric hindrance, such as oligomeric silsesquioxane or 2-adamantylammonium bromide. However, further research and the comprehensive study of the role of the binding group in surface trap passivation and their influence on the stability of NCs are still necessary.

It is also important to establish analytical protocols for the accurate and reliable determination of surface features and ligand densities by complementary techniques, including high-resolution microscopy, FTIR, 2D H—NMR, ICP-MS and XPS coupled with theoretical computations. Their combinations will address open questions associated with ligand binding mechanisms, post-synthesis treatments and degradation mechanisms. It will be also relevant for determining what density of ligands is required on the NC surface to promote phase stability of iodide-based perovskites.

Understandably, to date most studies have focused on unraveling the surface-ligand binding nature, and future research should address interfacial engineering and attempt to obtain NCs with devised functionality and processability according to the ultimate purpose, such as electronic wired-NCs, hydrophilic terminations for water dispersible NCs or the tuning of surface hydrophobicity and charge density to promote NP interfacial assembly in 2D or 3D architectures.

In addition, most works in the literature have focused on the surface chemistry of standard $CsPbBr_3$. However, LHP surface chemistry very much relies on halide composition. Thus, elucidating ligand perovskite surface interactions should be extended to different halide compositions.

LHP Encapsulation at a Single Particle Level

Obtaining water dispersible perovskite NCs is a challenging task due to the thermodynamically favorable decomposition in the presence of water, which requires robust and cross-linked networks that hinder water molecules entering LHP NCs cores. Of the different studied strategies, replacing native ligands or their post-synthetic modification by stronger binding, or one with higher steric hindrance, confers colloidal preservation and phase stability. However, it does not address the moisture and chemical stability issues at a single particle level and, thus, more robust coatings which hamper water diffusion to perovskite cores are required.

Employing inorganic shells seems a promising route for the rational design of robust and efficient core-shell NPs. Most efforts made in this line have centered on encapsulation in well-established silica shells by softening sol-gel methodologies. By this approach, a variety of perovskite-core shell NCs dispersed in water or protic solvent with a size range of 20–200 nm and a PLQY∼80% are described. However, softening under processing conditions renders amorphous shell materials that are not, thus, dense enough to protect perovskite cores under humid conditions. An alternative to surpass harsh silica shell growth conditions is to exploit phase transformative features 0D (Cs_4PbX_6) →3D ($CsPbX_3$) combined with sol-gel methods. Although, these methods render lower PLQY than their hot injection counterparts, they enable to obtain more robust shells towards water degradation. To date, few works have reported LHP@SiO_2 core-shell nanoparticles stable in water and smaller than 50 nm, and most of them are focused on pure green-emitting NCs and exhibit negligible PLQY. Thus, there is much room for improvement in synthesizing high luminescent, multicolor NPs stable in water media.

Apart from silica, several works, have tackled encapsulation in other inorganic materials, such as metal oxide frameworks, chalcogenides, metal particles and perovskite related-structures. However, most of them have centered on developing hybrid NCs with dual functionality, such as plasmon-induced light harvesting improvement, enhancing absorption cross-sections or photocatalysis, but almost none of these works has described fully encapsulated core-shell NPs or water-compatible ones. Thus, the development of core shell NPs in alternative inorganic shells is an almost unexplored field.

Polymer coatings also offer a smart approach for developing core-shell NPs. The use of polymer coating presents the advantage gained from the hydrophobicity nature of polymeric materials, plus the versatility of polymer chemistry by adjusting monomer moieties and the number of monomers. In this context, several polymeric nanocapsules that act as a nanoreactor and assist inward crystal growth have been designed. In addition, replacing olefin native olefin ligands with polymeric ones or using solvent-antisolvent methods has rendered different

polymer core-shell NPs with enhanced stability in water.

According to these authors opinion, polymer coating is a solid alternative to design a future synthetic approach to obtain colloidal aqueous suspensions of LHP. Nevertheless, some disadvantages of these strategies still need to be solved, such as requiring complex interface engineering with a dual-shelled coating (i.e. hydrophobic nature that preserves am unaltered LHP core and hydrophilic termination that enables dispersion in protic media) and substantially increased diameters compared to those coated with simple organic ligands.

It is worth mentioning that, whatever the encapsulation strategy, most works report emission in mixtures of water and aprotic solvent and carry out structural characterization in an aprotic solvent. Hence, a structural description of NCs dispersed in protic media, and a comprehensive study of structural stability on the water should be addressed. In addition, most of the research on this topic has been devoted to standard $CsPbBr_3$ NCs, pointing to the need to obtain multicolor core-shell NPs that cover visible range.

Finally, the encapsulation of LHP in a crystalline and stable shell that is still conductive is desirable, albeit challenging. Unfortunately, replacing long-chain aliphatic molecules with shorter ligands affects their structural and moisture stability. Several works have taken post-processing ligand exchange and passivation steps to address this issue with LHP thin films. In line with this, research into thin-film processed self-assembled NCs and film ligand replacement will be relevant to implement electrically wired LHP NCs integrated into optoelectronic devices.

LHP Composites

The encapsulation of LHP in different host matrices renders water-stable composites and opens up manufacturing possibilities (i.e. fibers, films, gratings, etc.) with a myriad of applications, such as light converters, displays, LEDs, scintillators, X-Ray detectors, and others still to explore like planar waveguide, anticounterfiting or biosensing gratings.

In this context, polymer materials are the most widely investigated matrices for embedding LHP NCs. LHP@polymer composites are fabricated mainly in two ways: (i) *in situ* preparation of LHP NCs polymer composites; (ii) the post-encapsulation of LHP NCs into polymers. Thus different strategies like cutting across polymer swelling-deswelling, thermal or photoinduced polymerization or liquid atomization methods, such as electrospraying and electrospinning, have been described.

An alternative strategy for stabilizing LHP NCs is template-assisted methods. Typically, these methods adopt some ordered structures to promote *in situ* controlled growth inside their pores. Thus it does not require the use of colloidal stabilization ligands and LHP optical features can be tuned by adjusting the pore size of the matrix. However, further efforts are necessary to improve not only NCs loading into pores, but also the nanocomposite PLQY.

Perovskite glass has also demonstrated as a robust host to protect LHP, but some challenges still remain to use low-melting point glasses because they are expensive or offer poor mechano-chemical stability.

In summary, almost all LHP composites have better thermal, photo, air and humidity stability than standard NCs, as well as bright PL, and they still need to overcome several drawbacks, such as the homogeneous NCs dispersion in host materials and long-term stability under harsh conditions (e.g., high temperatures, acid media) and scaling up manufacturing methods.

Applications

The final application will dictate the election of a strategy for designing stable LHP NCs. For instance, on the one hand, the integration of NCs in an electrically driven optical device will require "wired-nanocrystals" and an accurate design of ligand shell at a single particle level. On the other hand, the uses of LHP NCs as color converters or displays enable the use of protective insulating materials, such as polymers, and their manufacture as composites and much effort is focused on improving the dispersion of NCs in hosting materials and scaling up the methodologies. Notwithstanding, in general terms, the implementation of LHP as luminescent probes, whatever the field of application, still needs to address their long-term stability while retaining emission properties, according to the International Commission on Illumination (CIE). Especially for blue-emitting NCs that still exhibit lower PLQY and red-emitting, which present a strong tendency to undergo phase transition into the non-emitting "yellow phase." Additionally, the demands for environmentally friendly metal-halide perovskites and the fundamental research of alternative classes of materials that replicate the exceptional features of LHP have encouraged the scientific community to undertake extensive theoretical and experimental studies for designing lead-free metal halide perovskites, which enable practical and safe applications of perovskites.

More specifically, although it is a scarcely explored area, metal halide perovskite nanocrystals are highly luminescent materials with excellent features to be exploited as luminescent labels in immunochemistry and biosensing. Compared with organic dyes, the most extended labels, possess a broad absorption that gradually increases toward shorter wavelengths (below the first excitonic absorption band) and a narrow emission band of a mostly symmetric shape. Due to these properties, a single light source can be used multicolor to excite multicolor perovskite NCs simultaneously and track different analytes without signal overlap. Their high PLQY (~100%) and large Stokes shifts reduce autofluorescence, increasing sensitivity. Unlike other extended inorganic NCs such as chalcogenide quantum dots, LHP NCs exhibit milder and cheaper synthesis protocols. Their emission properties can be tuned according to their composition, covering a wider color gamut. They also show giant multiphoton absorption, even five-photons, making them promising for NIR-label biosensing and for super-resolution imaging applications beyond the optical diffraction limits. Thus, we envision that soon, perovskite NCs will enable the manufacture of high-throughput analytical platforms for the simultaneous and sensitive detection of multiple analytes, reducing the costs of the current detection kits.

Despite the advantages, several challenges still need to be addressed for their practical use. First, the production of monodisperse NCs with small sizes (down to 30 nm) is particularly important to achieve good sensitivity on biosensing protocols. Also, most of the described methodologies use green NCs, $CsPbBr_3$, making it necessary to expand these methods to other halide compositions to obtain multicolor labels and develop multiplexed assays. Finally, the resulting NCs are often stable in nonpolar solvents or ethanol. Thus shells should be further strengthened to obtain water-dispersible nanoparticles. Besides that, the description of biomolecule-NC conjugation protocols and the analysis of the long-term stability of resulting nanoparticles in water or biological fluids is still pending.

To integrate LHP in electrically connected devices such as solar cells, LEDs, or lasers, future work should be focused on ligand engineering and the development of self-assembled processed thin films and post-synthetic ligand removal or exchange. It will enable the processing of photoconductive films with reduced charge carrier losses and situate LHP NCs-based optoelectronic devices as a strong candidate with superior phase stability and emitting properties and overall performance than their bulk counterparts.

Along these lines, perovskite-based solar cells have achieved photoconversion efficiencies of up to 16%, representing the highest efficiencies for any QD-based solar cell. Unlike bulk perovskite counterparts, using NCs offers the advantage of stabilizing metastable phases. Currently, the research on solar cells is focused on achieving stability and high efficiency simultaneously. Toward this goal, there is an active study on NCs interface engineering to establish the density of ligands to promote phase stability and maximize charge transport across the films. It is known that the commercial success of LHP solar cells is limited because of the Pb toxic nature, and current lead-free solar devices need to achieve the performance and operational stability of lead-containing ones. In light of this concern, research on alternative perovskite-inspired materials should be kept forward until commercial

lead-free perovskite solar cell is achieved.

In the field of lasing, perovskite NCs has emerged as a new class of cost-effective and wavelength-tunable lasing materials. Although tremendous progress has been made in developing perovskite-based lasers, there remain challenges that hamper practical and commercially available lasers utilizing the perovskite NCs. First, perovskite NCs are severely affected by chemical and environmental factors (i.e., oxygen, moisture, heat, and continuous light illumination instabilities). Although several works described encapsulation strategies that addressed these issues, they only apply to green-emitting $CsPbBr_3$ NCs. At the same time, the stability of blue-emitting and red-emitting perovskite NCs needs to catch up. Finally, until now, only optically pumped lasing has been demonstrated in perovskite NCs, whereas electrical pumping is more practically desired. As the organic ligands used for the passivation of perovskite NC surfaces generally exhibit poor electrical conductivity, hampering the carrier injection and transport, it is imperative to design NCs interfaces and film architectures which enable efficient injection of charge carriers into the perovskite NC layer.

Concerning LHP LED technology, incredible progress over the past few years has been achieved, and devices with excellent features, including highly efficient light emission, high-color purity, ultrawide color gamut, low cost of raw materials and fabrication methods, as well as good compatibility with existing technologies, are described. However, before evolving into practical products, LHP-LEDs need to overcome some critical bottlenecks. First, the manufacture of large-scale panels which maintain their optical performance. Second, concerning the toxicity of lead atoms, the lead-free perovskite-inspired materials' performance has lagged behind their lead-based counterparts, and further research on perovskite-inspired materials is still necessary. Finally, the operational stability of LHP-LEDs still needs to be addressed.

As detailed above, the potential of perovskite materials is overwhelming, and perovskite materials will not be fully exploited until surface chemistry and stability be better understood and controlled.

Declaration of Competing Interest

The authors declare that they have no known competing financial interests or personal relationships that could have appeared to influence the work reported in this paper.

Data availability

No data was used for the research described in the article.

Acknowledgments

This work was financially supported by EU FEDER Project ADBIHOL /AEI/10.13039/501100011033 from MCIN/AEI and PROMETEO/ 2020/094 from the Generalitat Valenciana. C.C. thanks the Spanish Ministry of Economy and Competitiveness for her predoctoral contract (FPI/17 Scholarship). W.T acknowledges financial support for Ph.D studies (FPI-UPV 2019 grants).

References

[1] L.N. Quan, B.P. Rand, R.H. Friend, S.G. Mhaisalkar, T.W. Lee, E.H. Sargent, Perovskites for next-generation optical sources, Chem. Rev. 119 (2019) 7444–7477, https://doi.org/10.1021/acs.chemrev.9b00107.

[2] A.K. Jena, A. Kulkarni, T. Miyasaka, Halide perovskite photovoltaics: background, status, and future prospects, Chem. Rev. 119 (2019) 3036–3103, https://doi.org/10.1021/acs.chemrev.8b00539.

[3] H. Huang, M.I. Bodnarchuk, S.V. Kershaw, M.V. Kovalenko, A.L. Rogach, Lead halide perovskite nanocrystals in the research spotlight: stability and defect tolerance, ACS Energy Lett. 2 (2017) 2071–2083, https://doi.org/10.1021/acsenergylett.7b00547.

[4] J. Kim, S.H. Lee, J.H. Lee, K.H. Hong, The role of intrinsic defects in methylammonium lead iodide perovskite, J. Phys. Chem. Lett. 5 (2014) 1312–1317, https://doi.org/10.1021/jz500370k.

[5] D.W. de Quilettes, S.M. Vorpahl, S.D. Stranks, H. Nagaoka, G.E. Eperon, M. E. Ziffer, H.J. Snaith, D.S. Ginger, Impact of microstructure on local carrier lifetime in perovskite solar cells, Science 348 (2015) 683–686, https://doi.org/10.1126/science.aaa5333 (80-.).

[6] L. Protesescu, S. Yakunin, M.I. Bodnarchuk, F. Krieg, R. Caputo, C.H. Hendon, R. X. Yang, A. Walsh, M.V. Kovalenko, Nanocrystals of cesium lead halide perovskites (CsPbX3, X = Cl, Br, and I): novel optoelectronic materials showing bright emission with wide color gamut, Nano Lett. 15 (2015) 3692–3696, https://doi.org/10.1021/nl5048779.

[7] J. Shamsi, A.S. Urban, M. Imran, L. De Trizio, L. Manna, Metal halide perovskite nanocrystals: synthesis, post-synthesis modifications, and their optical properties, Chem. Rev. 119 (2019) 3296–3348, https://doi.org/10.1021/acs.chemrev.8b00644.

[8] A. Swarnkar, A.R. Marshall, E.M. Sanehira, B.D. Chernomordik, D.T. Moore, J. A. Christians, T. Chakrabarti, J.M. Luther, Quantum dot-induced phase stabilization of α-CsPbI3 perovskite for high-efficiency photovoltaics, Science 354 (2016) 92–95, https://doi.org/10.1126/science.aag2700 (80-.).

[9] Q.A. Akkerman, M. Gandini, F. Di Stasio, P. Rastogi, F. Palazon, G. Bertoni, J. M. Ball, M. Prato, A. Petrozza, L. Manna, Strongly emissive perovskite nanocrystal inks for high-voltage solar cells, Nat. Energy 2 (2017) 16194, https://doi.org/10.1038/nenergy.2016.194.

[10] F. Meinardi, Q.A. Akkerman, F. Bruni, S. Park, M. Mauri, Z. Dang, L. Manna, S. Brovelli, Doped halide perovskite nanocrystals for reabsorption-free luminescent solar concentrators, ACS Energy Lett. 2 (2017) 2368–2377, https://doi.org/10.1021/acsenergylett.7b00701.

[11] I. Dursun, C. Shen, M.R. Parida, J. Pan, S.P. Sarmah, D. Priante, N. Alyami, J. Liu, M.I. Saidaminov, M.S. Alias, A.L. Abdelhady, T.K. Ng, O.F. Mohammed, B.S. Ooi, O.M. Bakr, Perovskite nanocrystals as a color converter for visible light communication, ACS Photonics 3 (2016) 1150–1156, https://doi.org/10.1021/acsphotonics.6b00187.

[12] D.N. Congreve, M.C. Weidman, M. Seitz, W. Paritmongkol, N.S. Dahod, W. A. Tisdale, Tunable light-emitting diodes utilizing quantum-confined layered perovskite emitters, ACS Photonics 4 (2017) 476–481, https://doi.org/10.1021/acsphotonics.6b00963.

[13] J. Zhang, Q. Wang, X. Zhang, J. Jiang, Z. Gao, Z. Jin, S. Liu, High-performance transparent ultraviolet photodetectors based on inorganic perovskite CsPbCl3 nanocrystals, RSC Adv. 7 (2017) 36722–36727, https://doi.org/10.1039/c7ra06597c.

[14] G. Gao, Q. Xi, H. Zhou, Y. Zhao, C. Wu, L. Wang, P. Guo, J. Xu, Novel inorganic perovskite quantum dots for photocatalysis, Nanoscale 9 (2017) 12032–12038, https://doi.org/10.1039/c7nr04421f.

[15] W. Chen, S. Bhaumik, S.A. Veldhuis, G. Xing, Q. Xu, M. Grätzel, S. Mhaisalkar, N. Mathews, T.C. Sum, Giant five-photon absorption from multidimensional core-shell halide perovskite colloidal nanocrystals, Nat. Commun. 8 (2017) 15198, https://doi.org/10.1038/ncomms15198.

[16] H. Zhang, X. Wang, Q. Liao, Z. Xu, H. Li, L. Zheng, H. Fu, Embedding perovskite nanocrystals into a polymer matrix for tunable luminescence probes in cell imaging, Adv. Funct. Mater. 27 (2017), https://doi.org/10.1002/adfm.201604382.

[17] Z. Yang, J. Xu, S. Zong, S. Xu, D. Zhu, Y. Zhang, C. Chen, C. Wang, Z. Wang, Y. Cui, Lead halide perovskite nanocrystals-phospholipid micelles and their biological applications: multiplex cellular imaging and *in vitro* tumor targeting, ACS Appl. Mater. Interfaces 11 (2019) 47671–47679, https://doi.org/10.1021/acsami.9b12924.

[18] J.H. Yu, S.H. Kwon, Z. Petrášek, O.K. Park, S.W. Jun, K. Shin, M. Choi, Y. Il Park, K. Park, H. Bin Na, N. Lee, D.W. Lee, J.H. Kim, P. Schwille, T. Hyeon, High-resolution three-photon biomedical imaging using doped ZnS nanocrystals, Nat. Mater. 12 (2013) 359–366, https://doi.org/10.1038/nmat3565.

[19] L.E. Brus, Electron-electron and electron-hole interactions in small semiconductor crystallites: the size dependence of the lowest excited electronic state, J. Chem. Phys. 80 (1984) 4403–4409, https://doi.org/10.1063/1.447218.

[20] J.M. Pietryga, Y.S. Park, J. Lim, A.F. Fidler, W.K. Bae, S. Brovelli, V.I. Klimov, Spectroscopic and device aspects of nanocrystal quantum dots, Chem. Rev. 116 (2016) 10513–10622, https://doi.org/10.1021/acs.chemrev.6b00169.

[21] B.A. Kairdolf, A.M. Smith, T.H. Stokes, M.D. Wang, A.N. Young, S. Nie, Semiconductor quantum dots for bioimaging and biodiagnostic applications, Annu. Rev. Anal. Chem 6 (2013) 143–162, https://doi.org/10.1146/annurev-anchem-060908-155136.

[22] L.C. Schmidt, A. Pertegás, S. González-Carrero, O. Malinkiewicz, S. Agouram, G. Mínguez Espallargas, H.J. Bolink, R.E. Galian, J. Pérez-Prieto, Nontemplate synthesis of CH3NH3PbBr3 perovskite nanoparticles, J. Am. Chem. Soc. 136 (2014) 850–853, https://doi.org/10.1021/ja4109209.

[23] F. Zhang, H. Zhong, C. Chen, X.G. Wu, X. Hu, H. Huang, J. Han, B. Zou, Y. Dong, Brightly luminescent and color-tunable colloidal CH3NH3PbX3 (X = Br, I, Cl) quantum dots: potential alternatives for display technology, ACS Nano 9 (2015) 4533–4542, https://doi.org/10.1021/acsnano.5b01154.

[24] D. Aldakov, P. Reiss, Safer-by-design fluorescent nanocrystals: metal halide perovskites vs semiconductor quantum dots, J. Phys. Chem. C 123 (2019) 12527–12541, https://doi.org/10.1021/acs.jpcc.8b12228.

[25] B. Saparov, D.B. Mitzi, Organic-inorganic perovskites: structural versatility for functional materials design, Chem. Rev. 116 (2016) 4558–4596, https://doi.org/10.1021/acs.chemrev.5b00715.

[26] W. Travis, E.N.K. Glover, H. Bronstein, D.O. Scanlon, R.G. Palgrave, On the application of the tolerance factor to inorganic and hybrid halide perovskites: a revised system, Chem. Sci. 7 (2016) 4548–4556, https://doi.org/10.1039/c5sc04845a.

[27] L. Protesescu, S. Yakunin, S. Kumar, J. Bär, F. Bertolotti, N. Masciocchi, A. Guagliardi, M. Grotevent, I. Shorubalko, M.I. Bodnarchuk, C.J. Shih, M. V. Kovalenko, Dismantling the "red wall" of colloidal perovskites: highly luminescent formamidinium and formamidinium-cesium lead iodide nanocrystals, ACS Nano 11 (2017) 3119–3134, https://doi.org/10.1021/acsnano.7b00116.

[28] Q. Li, L. Zhang, Z. Chen, Z. Quan, Metal halide perovskites under compression, J. Mater. Chem. A 7 (2019) 16089–16108, https://doi.org/10.1039/C9TA04930D.

[29] R.E. Brandt, V. Stevanović, D.S. Ginley, T. Buonassisi, Identifying defect-tolerant semiconductors with high minority carrier lifetimes: beyond hybrid lead halide perovskites, MRS Commun. 5 (2015) 265–275, https://doi.org/10.1557/mrc.2015.26.

[30] J. Kang, L.W. Wang, High defect tolerance in lead halide perovskite CsPbBr3, J. Phys. Chem. Lett. 8 (2017) 489–493, https://doi.org/10.1021/acs.jpclett.6b02800.

[31] A. Buin, P. Pietsch, J. Xu, O. Voznyy, A.H. Ip, R. Comin, E.H. Sargent, Materials processing routes to trap-free halide perovskites, Nano Lett. 14 (2014) 6281–6286, https://doi.org/10.1021/nl502612m.

[32] W.J. Yin, T. Shi, Y. Yan, Unusual defect physics in CH3NH3PbI3 perovskite solar cell absorber, Appl. Phys. Lett. 104 (2014), 063903, https://doi.org/10.1063/1.4864778.

[33] H.P. Wang, S. Li, X. Liu, Z. Shi, X. Fang, J.H. He, Low-dimensional metal halide perovskite photodetectors, Adv. Mater. 33 (2021), https://doi.org/10.1002/ADMA.202003309.

[34] M. Palummo, E. Berrios, D. Varsano, G. Giorgi, Optical properties of lead-free double perovskites by *ab initio* excited-state methods, ACS Energy Lett. 2020 (2020) 457–463, https://doi.org/10.1021/ACSENERGYLETT.9B02593/ASSET/IMAGES/LARGE/NZ9B02593_0004.JPEG.

[35] S. Meloni, G. Palermo, N. Ashari-Astani, M. Grätzel, U. Rothlisberger, Valence and conduction band tuning in halide perovskites for solar cell applications, J. Mater. Chem. A 4 (2016) 15997–16002, https://doi.org/10.1039/c6ta04949d.

[36] S. Gholipour, M. Saliba, Bandgap tuning and compositional exchange for lead halide perovskite materials, Charact. Tech. Perovskite Sol. Cell Mater. (2020) 1–22, https://doi.org/10.1016/b978-0-12-814727-6.00001-3. Elsevier.

[37] I. Levchuk, A. Osvet, X. Tang, M. Brandl, J.D. Perea, F. Hoegl, G.J. Matt, R. Hock, M. Batentschuk, C.J. Brabec, Brightly luminescent and color-tunable formamidinium lead halide perovskite FAPbX3 (X = Cl, Br, I) colloidal nanocrystals, Nano Lett. 17 (2017) 2765–2770, https://doi.org/10.1021/acs.nanolett.6b04781.

[38] J.A. Castañeda, G. Nagamine, E. Yassitepe, L.G. Bonato, O. Voznyy, S. Hoogland, A.F. Nogueira, E.H. Sargent, C.H.B. Cruz, L.A. Padilha, Efficient biexciton interaction in perovskite quantum dots under weak and strong confinement, ACS Nano 10 (2016) 8603–8609, https://doi.org/10.1021/acsnano.6b03908.

[39] L. Protesescu, S. Yakunin, M.I. Bodnarchuk, F. Bertolotti, N. Masciocchi, A. Guagliardi, M.V. Kovalenko, Monodisperse formamidinium lead bromide nanocrystals with bright and stable green photoluminescence, J. Am. Chem. Soc. 138 (2016) 14202–14205, https://doi.org/10.1021/jacs.6b08900.

[40] K. Hills-Kimball, Y. Nagaoka, C. Cao, E. Chaykovsky, O. Chen, Synthesis of formamidinium lead halide perovskite nanocrystals through solid–liquid–solid cation exchange, J. Mater. Chem. C 5 (2017) 5680–5684, https://doi.org/10.1039/C7TC00598A.

[41] T.C. Jellicoe, J.M. Richter, H.F.J. Glass, M. Tabachnyk, R. Brady, S.E. Dutton, A. Rao, R.H. Friend, D. Credgington, N.C. Greenham, M.L. Böhm, Synthesis and optical properties of lead-free cesium tin halide perovskite nanocrystals, J. Am. Chem. Soc. 138 (2016) 2941–2944, https://doi.org/10.1021/jacs.5b13470.

[42] P.P. Sun, Q.S. Li, L.N. Yang, Z.S. Li, Theoretical insights into a potential lead-free hybrid perovskite: substituting Pb2+ with Ge2+, Nanoscale 8 (2016) 1503–1512, https://doi.org/10.1039/c5nr05337d.

[43] S. Chatterjee, A.J. Pal, Influence of metal substitution on hybrid halide perovskites: towards lead-free perovskite solar cells, J. Mater. Chem. A 6 (2018) 3793–3823, https://doi.org/10.1039/c7ta09943f.

[44] X. Wu, W. Song, Q. Li, X. Zhao, D. He, Z. Quan, Synthesis of lead-free $CsGeI_3$ perovskite colloidal nanocrystals and electron beam-induced transformations, Chem. Asian J. 13 (2018) 1654–1659, https://doi.org/10.1002/asia.201800573.

[45] S. Gonzalez-Carrero, L. Francés-Soriano, M. González-Béjar, S. Agouram, R. E. Galian, J. Pérez-Prieto, The luminescence of $CH_3NH_3PbBr_3$ perovskite nanoparticles crests the summit and their photostability under wet conditions is enhanced, Small 12 (2016) 5245–5250, https://doi.org/10.1002/smll.201600209.

[46] F. Liu, Y. Zhang, C. Ding, S. Kobayashi, T. Izuishi, N. Nakazawa, T. Toyoda, T. Ohta, S. Hayase, T. Minemoto, K. Yoshino, S. Dai, Q. Shen, Highly luminescent phase-stable CsPbI3 perovskite quantum dots achieving near 100% absolute photoluminescence quantum yield, ACS Nano 11 (2017) 10373–10383, https://doi.org/10.1021/acsnano.7b05442.

[47] Y. Tong, E. Bladt, M.F. Aygüler, A. Manzi, K.Z. Milowska, V.A. Hintermayr, P. Docampo, S. Bals, A.S. Urban, L. Polavarapu, J. Feldmann, Highly luminescent cesium lead halide perovskite nanocrystals with tunable composition and thickness by ultrasonication, Angew. Chem. Int. Ed. 55 (2016) 13887–13892, https://doi.org/10.1002/anie.201605909.

[48] K. Tanaka, T. Takahashi, T. Ban, T. Kondo, K. Uchida, N. Miura, Comparative study on the excitons in lead-halide-based perovskite-type crystals CH3NH3PbBr3 CH3NH 3PbI3, Solid State Commun. 127 (2003) 619–623, https://doi.org/10.1016/S0038-1098(03)00566-0.

[49] W. Van der Stam, J.J. Geuchies, T. Altantzis, K.H.W. Van Den Bos, J.D. Meeldijk, S. Van Aert, S. Bals, D. Vanmaekelbergh, C. De Mello Donega, Highly emissive divalent-ion-doped colloidal CsPb1-xMxBr3 perovskite nanocrystals through cation exchange, J. Am. Chem. Soc. 139 (2017) 4087–4097, https://doi.org/10.1021/jacs.6b13079.

[50] J.A. Sichert, Y. Tong, N. Mutz, M. Vollmer, S. Fischer, K.Z. Milowska, R. G. Cortadella, B. Nickel, C. Cardenas-Daw, J.K. Stolarczyk, A.S. Urban, J. Feldmann, Quantum size effect in organometal halide perovskite nanoplatelets, Nano Lett. 15 (2015) 6521–6527, https://doi.org/10.1021/acs.nanolett.5b02985.

[51] J. Shamsi, Z. Dang, P. Bianchini, C. Canale, F. Di Stasio, R. Brescia, M. Prato, L. Manna, Colloidal synthesis of quantum confined single crystal CsPbBr3 nanosheets with lateral size control up to the micrometer range, J. Am. Chem. Soc. 138 (2016) 7240–7243, https://doi.org/10.1021/jacs.6b03166.

[52] Z. Li, E. Hong, X. Zhang, M. Deng, X. Fang, Perovskite-type 2D materials for high-performance photodetectors, J. Phys. Chem. Lett. 13 (2022) 1215–1225, https://doi.org/10.1021/ACS.JPCLETT.1C04225/ASSET/IMAGES/LARGE/JZ1C04225_0005.JPEG.

[53] A.B. Wong, Y. Bekenstein, J. Kang, C.S. Kley, D. Kim, N.A. Gibson, D. Zhang, Y. Yu, S.R. Leone, L.W. Wang, A.P. Alivisatos, P. Yang, Strongly quantum confined colloidal cesium tin iodide perovskite nanoplates: lessons for reducing defect density and improving stability, Nano Lett. 18 (2018) 2060–2066, https://doi.org/10.1021/acs.nanolett.8b00077.

[54] Q.A. Akkerman, S.G. Motti, A.R. Srimath Kandada, E. Mosconi, V. D'Innocenzo, G. Bertoni, S. Marras, B.A. Kamino, L. Miranda, F. De Angelis, A. Petrozza, M. Prato, L. Manna, Solution synthesis approach to colloidal cesium lead halide perovskite nanoplatelets with monolayer-level thickness control, J. Am. Chem. Soc. 138 (2016) 1010–1016, https://doi.org/10.1021/jacs.5b12124.

[55] V.A. Hintermayr, A.F. Richter, F. Ehrat, M. Döblinger, W. Vanderlinden, J. A. Sichert, Y. Tong, L. Polavarapu, J. Feldmann, A.S. Urban, Tuning the optical properties of perovskite nanoplatelets through composition and thickness by ligand-assisted exfoliation, Adv. Mater. 28 (2016) 9478–9485, https://doi.org/10.1002/adma.201602897.

[56] M.C. Weidman, M. Seitz, S.D. Stranks, W.A. Tisdale, Highly tunable colloidal perovskite nanoplatelets through variable cation, metal, and halide composition, ACS Nano 10 (2016) 7830–7839, https://doi.org/10.1021/acsnano.6b03496.

[57] M.C. Brennan, J.E. Herr, T.S. Nguyen-Beck, J. Zinna, S. Draguta, S. Rouvimov, J. Parkhill, M. Kuno, Origin of the size-dependent stokes shift in cspbbr3 perovskite nanocrystals, J. Am. Chem. Soc. 139 (2017) 12201–12208, https://doi.org/10.1021/jacs.7b05683.

[58] F. Li, Z. Xia, Y. Gong, L. Gu, Q. Liu, Optical properties of Mn2+ doped cesium lead halide perovskite nanocrystals: via a cation-anion co-substitution exchange reaction, J. Mater. Chem. C 5 (2017) 9281–9287, https://doi.org/10.1039/c7tc03575f.

[59] W. Liu, Q. Lin, H. Li, K. Wu, I. Robel, J.M. Pietryga, V.I. Klimov, Mn2+-doped lead halide perovskite nanocrystals with dual-color emission controlled by halide content, J. Am. Chem. Soc. 138 (2016) 14954–14961, https://doi.org/10.1021/jacs.6b08085.

[60] S. Ten Brinck, I. Infante, Surface termination, morphology, and bright photoluminescence of cesium lead halide perovskite nanocrystals, ACS Energy Lett. 1 (2016) 1266–1272, https://doi.org/10.1021/acsenergylett.6b00595.

[61] Y. Wang, X. Li, X. Zhao, L. Xiao, H. Zeng, H. Sun, Nonlinear absorption and low-threshold multiphoton pumped stimulated emission from all-inorganic perovskite nanocrystals, Nano Lett. 16 (2016) 448–453, https://doi.org/10.1021/acs.nanolett.5b04110.

[62] T.J. Milstein, D.M. Kroupa, D.R. Gamelin, Picosecond quantum cutting generates photoluminescence quantum yields over 100% in ytterbium-doped CsPbCl3 nanocrystals, Nano Lett. 18 (2018) 3792–3799, https://doi.org/10.1021/acs.nanolett.8b01066.

[63] S. Yakunin, L. Protesescu, F. Krieg, M.I. Bodnarchuk, G. Nedelcu, M. Humer, G. De Luca, M. Fiebig, W. Heiss, M.V. Kovalenko, Low-threshold amplified spontaneous emission and lasing from colloidal nanocrystals of caesium lead halide perovskites, Nat. Commun. 6 (2015) 8056, https://doi.org/10.1038/ncomms9056.

[64] N.S. Makarov, S. Guo, O. Isaienko, W. Liu, I. Robel, V.I. Klimov, Spectral and dynamical properties of single excitons, biexcitons, and trions in cesium-lead-halide perovskite quantum dots, Nano Lett. 16 (2016) 2349–2362, https://doi.org/10.1021/ACS.NANOLETT.5B05077/ASSET/IMAGES/LARGE/NL-2015-05077P_0009.JPEG.

[65] A. Balena, A. Perulli, M. Fernandez, M.L. De Giorgi, G. Nedelcu, M.V. Kovalenko, M. Anni, Temperature dependence of the amplified spontaneous emission from CsPbBr3 nanocrystal thin films, J. Phys. Chem. C 122 (2018) 5813–5819, https://doi.org/10.1021/ACS.JPCC.8B01419/ASSET/IMAGES/LARGE/JP-2018-01419E_0001.JPEG.

[66] R.K. Singh, N. Jain, P. Singh, R. Kumar, J. Singh, S. Dutta, T.M. Chen, S. Som, H. C. Swart, Development in the innovation of lead halide-based perovskite quantum dots from rare earth-doped garnet-based phosphors for light-emitting diodes. Spectroscopy Lanthan Doped Oxide Materials, Elsevier Inc., 2019, pp. 21–56, https://doi.org/10.1016/B978-0-08-102935-0.00002-2.

[67] X. Li, Y. Wu, S. Zhang, B. Cai, Y. Gu, J. Song, H. Zeng, CsPbX3 quantum dots for lighting and displays: roomerature synthesis, photoluminescence superiorities, underlying origins and white light-emitting diodes, Adv. Funct. Mater. 26 (2016) 2435–2445, https://doi.org/10.1002/adfm.201600109.

[68] O. Vybornyi, S. Yakunin, M.V. Kovalenko, Polar-solvent-free colloidal synthesis of highly luminescent alkylammonium lead halide perovskite nanocrystals, Nanoscale 8 (2016) 6278–6283, https://doi.org/10.1039/c5nr06890h.

[69] M.R. Ahmadian-Yazdi, M. Eslamian, Fabrication of semiconducting methylammonium lead halide perovskite particles by spray technology,

Nanoscale Res. Lett. 13 (2018) 4–11, https://doi.org/10.1186/s11671-017-2430-0.
[70] S. Yun, A. Kirakosyan, S.G. Yoon, J. Choi, Scalable synthesis of exfoliated organometal halide perovskite nanocrystals by ligand-assisted ball milling, ACS Sustain. Chem. Eng. 6 (2018) 3733–3738, https://doi.org/10.1021/acssuschemeng.7b04092.
[71] L. Protesescu, S. Yakunin, O. Nazarenko, D.N. Dirin, M.V. Kovalenko, Low-cost synthesis of highly luminescent colloidal lead halide perovskite nanocrystals by wet ball milling, ACS Appl. Nano Mater. 1 (2018) 1300–1308, https://doi.org/10.1021/acsanm.8b00038.
[72] I. Rosa-Pardo, M. Rando-Brotons, S. Pocoví-Martínez, R.E. Galian, J. PérezPrieto, Laser ablation of hybrid perovskite bulks into nanoparticles: adamantylammonium halides as ligands and halide sources, ChemNanoMat 5 (2019) 328–333, https://doi.org/10.1002/cnma.201800621.
[73] A. Pan, B. He, X. Fan, Z. Liu, J.J. Urban, A.P. Alivisatos, L. He, Y. Liu, Insight into the ligand-mediated synthesis of colloidal CsPbBr3 perovskite nanocrystals: the role of organic acid, base, and cesium precursors, ACS Nano 10 (2016) 7943–7954, https://doi.org/10.1021/ACSNANO.6B03863/ASSET/IMAGES/LARGE/NN-2016-03863G_0009.JPEG.
[74] Z. Yi, N.H. Ladi, X. Shai, H. Li, Y. Shen, M. Wang, Will organic-inorganic hybrid halide lead perovskites be eliminated from optoelectronic applications? Nanoscale Adv. 1 (2019) 1276–1289, https://doi.org/10.1039/c8na00416a.
[75] Q. Fan, G.V. Biesold-McGee, J. Ma, Q. Xu, S. Pan, J. Peng, Z. Lin, Lead-Free Halide Perovskite Nanocrystals: crystal Structures, Synthesis, Stabilities, and Optical Properties, Angew. Chem. Int. Ed. 59 (2020) 1030–1046, https://doi.org/10.1002/anie.201904862.
[76] T. Miyasaka, A. Kulkarni, G.M. Kim, S. Öz, A.K. Jena, Perovskite solar cells: can we go organic-free, lead-free, and dopant-free? Adv. Energy Mater. 10 (2020), 1902500 https://doi.org/10.1002/aenm.201902500.
[77] S. Attique, N. Ali, S. Ali, R. Khatoon, N. Li, A. Khesro, S. Rauf, S. Yang, H. Wu, A potential checkmate to lead: bismuth in organometal halide perovskites, structure, properties, and applications, Adv. Sci. 7 (2020), 1903143, https://doi.org/10.1002/advs.201903143.
[78] Y. Wang, R. Wen, Y. Liu, L. Bi, M. Yang, H. Sun, Y. Zheng, G. Zhang, Z. Gao, Rigid amine-induced pseudo-3 d lead-free bismuth halide perovskite with an improved band edge for visible-light absorption, ChemSusChem 13 (2020) 2753–2760, https://doi.org/10.1002/cssc.202000282.
[79] B.J. Moon, S.J. Kim, S. Lee, A. Lee, H. Lee, D.S. Lee, T. Kim, S. Lee, S. Bae, S. H. Lee, Rare-earth-element-ytterbium-substituted lead-free inorganic perovskite nanocrystals for optoelectronic applications, Adv. Mater. 31 (2019), 1901716, https://doi.org/10.1002/adma.201901716.
[80] Z. Zeng, Y. Xu, Z. Zhang, Z. Gao, M. Luo, Z. Yin, C. Zhang, J. Xu, B. Huang, F. Luo, Y. Du, C. Yan, Rare-earth-containing perovskite nanomaterials: design, synthesis, properties and applications, Chem. Soc. Rev. 49 (2020) 1109–1143, https://doi.org/10.1039/c9cs00330d.
[81] G.P. Nagabhushana, R. Shivaramaiah, A. Navrotsky, Direct calorimetric verification of thermodynamic instability of lead halide hybrid perovskites, Proc. Natl. Acad. Sci. U. S. A. 113 (2016) 7717–7721, https://doi.org/10.1073/pnas.1607850113.
[82] Y.Y. Zhang, S. Chen, P. Xu, H. Xiang, X.G. Gong, A. Walsh, S.H. Wei, Intrinsic instability of the hybrid halide perovskite semiconductor CH3NH3PbI3 *, Chin. Phys. Lett. 35 (2018), 036104, https://doi.org/10.1088/0256-307X/35/3/036104.
[83] C. Yi, J. Luo, S. Meloni, A. Boziki, N. Ashari-Astani, C. Grätzel, S.M. Zakeeruddin, U. Röthlisberger, M. Grätzel, Entropic stabilization of mixed A-cation ABX3 metal halide perovskites for high performance perovskite solar cells, Energy Environ. Sci. 9 (2016) 656–662, https://doi.org/10.1039/c5ee03255e.
[84] M.G. Ju, M. Chen, Y. Zhou, J. Dai, L. Ma, N.P. Padture, X.C. Zeng, Toward eco-friendly and stable perovskite materials for photovoltaics, Joule 2 (2018) 1231–1241, https://doi.org/10.1016/j.joule.2018.04.026.
[85] B. Conings, J. Drijkoningen, N. Gauquelin, A. Babayigit, J. D'Haen, L. D'Olieslaeger, A. Ethirajan, J. Verbeeck, J. Manca, E. Mosconi, F. De Angelis, H.-.G. Boyen, Intrinsic thermal instability of methylammonium lead trihalide perovskite, Adv. Energy Mater. 5 (2015), 1500477, https://doi.org/10.1002/aenm.201500477.
[86] Z. Li, M. Yang, J.S. Park, S.H. Wei, J.J. Berry, K. Zhu, Stabilizing perovskite structures by tuning tolerance factor: formation of formamidinium and cesium lead iodide solid-state alloys, Chem. Mater. 28 (2016) 284–292, https://doi.org/10.1021/acs.chemmater.5b04107.
[87] M. Saliba, T. Matsui, J.Y. Seo, K. Domanski, J.P. Correa-Baena, M.K. Nazeeruddin, S.M. Zakeeruddin, W. Tress, A. Abate, A. Hagfeldt, M. Grätzel, Cesium-containing triple cation perovskite solar cells: improved stability, reproducibility and high efficiency, Energy Environ. Sci. 9 (2016) 1989–1997, https://doi.org/10.1039/c5ee03874j.
[88] D.M. Trots, S.V. Myagkota, High-temperature structural evolution of caesium and rubidium triiodoplumbates, J. Phys. Chem. Solids 69 (2008) 2520–2526, https://doi.org/10.1016/j.jpcs.2008.05.007.
[89] C.C. Stoumpos, C.D. Malliakas, M.G. Kanatzidis, Semiconducting tin and lead iodide perovskites with organic cations: phase transitions, high mobilities, and near-infrared photoluminescent properties, Inorg. Chem. 52 (2013) 9019–9038, https://doi.org/10.1021/ic401215x.
[90] Q. Han, S.H. Bae, P. Sun, Y.T. Hsieh, Y.M. Yang, Y.S. Rim, H. Zhao, Q. Chen, W. Shi, G. Li, Y. Yang, Single crystal formamidinium lead iodide ($FAPbI_3$): insight into the structural, optical, and electrical properties, Adv. Mater. 28 (2016) 2253–2258, https://doi.org/10.1002/adma.201505002.
[91] M.I. Saidaminov, A.L. Abdelhady, B. Murali, E. Alarousu, V.M. Burlakov, W. Peng, I. Dursun, L. Wang, Y. He, G. MacUlan, A. Goriely, T. Wu, O.F. Mohammed, O. M. Bakr, High-quality bulk hybrid perovskite single crystals within minutes by inverse temperature crystallization, Nat. Commun. 6 (2015) 1–6, https://doi.org/10.1038/ncomms8586.
[92] M.I. Saidaminov, A.L. Abdelhady, G. Maculan, O.M. Bakr, Retrograde solubility of formamidinium and methylammonium lead halide perovskites enabling rapid single crystal growth, Chem. Commun. 51 (2015) 17658–17661, https://doi.org/10.1039/c5cc06916e.
[93] T. Leijtens, K. Bush, R. Cheacharoen, R. Beal, A. Bowring, M.D. McGehee, Towards enabling stable lead halide perovskite solar cells; interplay between structural, environmental, and thermal stability, J. Mater. Chem. A 5 (2017) 11483–11500, https://doi.org/10.1039/c7ta00434f.
[94] J. De Roo, M. Ibáñez, P. Geiregat, G. Nedelcu, W. Walravens, J. Maes, J. C. Martins, I. Van Driessche, M.V. Kovalenko, Z. Hens, Highly dynamic ligand binding and light absorption coefficient of cesium lead bromide perovskite nanocrystals, ACS Nano 10 (2016) 2071–2081, https://doi.org/10.1021/acsnano.5b06295.
[95] J. Maes, L. Balcaen, E. Drijvers, Q. Zhao, J. De Roo, A. Vantomme, F. Vanhaecke, P. Geiregat, Z. Hens, Light absorption coefficient of CsPbBr3 perovskite nanocrystals, J. Phys. Chem. Lett. 9 (2018) 3093–3097, https://doi.org/10.1021/acs.jpclett.8b01065.
[96] V.K. Ravi, P.K. Santra, N. Joshi, J. Chugh, S.K. Singh, H. Rensmo, P. Ghosh, A. Nag, Origin of the substitution mechanism for the binding of organic ligands on the surface of CsPbBr3 perovskite nanocubes, J. Phys. Chem. Lett. 8 (2017) 4988–4994, https://doi.org/10.1021/acs.jpclett.7b02192.
[97] H. Jin, E. Debroye, M. Keshavarz, I.G. Scheblykin, M.B.J. Roeffaers, J. Hofkens, J. A. Steele, It's a trap! On the nature of localised states and charge trapping in lead halide perovskites, Mater. Horiz. 7 (2020) 397–410, https://doi.org/10.1039/C9MH00500E.
[98] F. Di Stasio, S. Christodoulou, N. Huo, G. Konstantatos, Near-unity photoluminescence quantum yield in CsPbBr3 nanocrystal solid-state films via postsynthesis treatment with lead bromide, Chem. Mater. 29 (2017) 7663–7667, https://doi.org/10.1021/acs.chemmater.7b02834.
[99] B.A. Koscher, J.K. Swabeck, N.D. Bronstein, A.P. Alivisatos, Essentially trap-free CsPbBr3 colloidal nanocrystals by postsynthetic thiocyanate surface treatment, J. Am. Chem. Soc. 139 (2017) 6566–6569, https://doi.org/10.1021/jacs.7b02817.
[100] M.R. Alpert, J.S. Niezgoda, A.Z. Chen, B.J. Foley, S. Cuthriell, L.U. Yoon, J. J. Choi, Colloidal nanocrystals as a platform for rapid screening of charge trap passivating molecules for metal halide perovskite thin films, Chem. Mater. 30 (2018) 4515–4526, https://doi.org/10.1021/acs.chemmater.8b00414.
[101] R. Zhu, H. Liu, L. Shen, D. Sun, X. Li, Modifying CH3NH3PbBr3 nanocrystals with arylamines, J. Phys. Chem. Solids 103 (2017) 164–169, https://doi.org/10.1016/j.jpcs.2016.12.018.
[102] J. Pan, S.P. Sarmah, B. Murali, I. Dursun, W. Peng, M.R. Parida, J. Liu, L. Sinatra, N. Alyami, C. Zhao, E. Alarousu, T.K. Ng, B.S. Ooi, O.M. Bakr, O.F. Mohammed, Air-stable surface-passivated perovskite quantum dots for ultra-robust, single- and two-photon-induced amplified spontaneous emission, J. Phys. Chem. Lett. 6 (2015) 5027–5033, https://doi.org/10.1021/acs.jpclett.5b02460.
[103] N.K. Noel, A. Abate, S.D. Stranks, E.S. Parrott, V.M. Burlakov, A. Goriely, H. J. Snaith, Enhanced photoluminescence and solar cell performance via Lewis base passivation of organic-inorganic lead halide perovskites, ACS Nano 8 (2014) 9815–9821, https://doi.org/10.1021/nn5036476.
[104] R.J. Stewart, C. Grieco, A.V. Larsen, J.J. Maier, J.B. Asbury, Approaching bulk carrier dynamics in organo-halide perovskite nanocrystalline films by surface passivation, J. Phys. Chem. Lett. 7 (2016) 1148–1153, https://doi.org/10.1021/acs.jpclett.6b00366.
[105] X. Li, M.I Dar, C. Yi, J. Luo, M. Tschumi, S.M. Zakeeruddin, M.K. Nazeeruddin, H. Han, M. Grätzel, Improved performance and stability of perovskite solar cells by crystal crosslinking with alkylphosphonic acid ω -ammonium chlorides, Nat. Chem. 7 (2015) 703–711, https://doi.org/10.1038/nchem.2324.
[106] L. Zuo, Q. Chen, N. De Marco, Y.T. Hsieh, H. Chen, P. Sun, S.Y. Chang, H. Zhao, S. Dong, Y. Yang, Tailoring the interfacial chemical interaction for high-efficiency perovskite solar cells, Nano Lett. 17 (2017) 269–275, https://doi.org/10.1021/acs.nanolett.6b04015.
[107] J. Cao, J. Yin, S. Yuan, Y. Zhao, J. Li, N. Zheng, Thiols as interfacial modifiers to enhance the performance and stability of perovskite solar cells, Nanoscale 7 (2015) 9443–9447, https://doi.org/10.1039/c5nr01820j.
[108] E. Yassitepe, Z. Yang, O. Voznyy, Y. Kim, G. Walters, J.A. Castañeda, P. Kanjanaboos, M. Yuan, X. Gong, F. Fan, J. Pan, S. Hoogland, R. Comin, O. M. Bakr, L.A. Padilha, A.F. Nogueira, E.H. Sargent, Amine-free synthesis of cesium lead halide perovskite quantum dots for efficient light-emitting diodes, Adv. Funct. Mater. 26 (2016) 8757–8763, https://doi.org/10.1002/adfm.201604580.
[109] F. Krieg, S.T. Ochsenbein, S. Yakunin, S. Ten Brinck, P. Aellen, A. Süess, B. Clerc, D. Guggisberg, O. Nazarenko, Y. Shynkarenko, S. Kumar, C.J. Shih, I. Infante, M. V. Kovalenko, Colloidal CsPbX3 (X = Cl, Br, I) nanocrystals 2.0: zwitterionic capping ligands for improved durability and stability, ACS Energy Lett. 3 (2018) 641–646, https://doi.org/10.1021/acsenergylett.8b00035.
[110] F. Krieg, Q.K. Ong, M. Burian, G. Rainò, D. Naumenko, H. Amenitsch, A. Süess, M. J. Grotevent, F. Krumeich, M.I. Bodnarchuk, I. Shorubalko, F. Stellacci, M. V. Kovalenko, Stable ultraconcentrated and ultradilute colloids of CsPbX3 (X = Cl, Br) nanocrystals using natural lecithin as a capping ligand, J. Am. Chem. Soc. 141 (2020) 19839–19849, https://doi.org/10.1021/jacs.9b09969.
[111] J. Pan, L.N. Quan, Y. Zhao, W. Peng, B. Murali, S.P. Sarmah, M. Yuan, L. Sinatra, N.M. Alyami, J. Liu, E. Yassitepe, Z. Yang, O. Voznyy, R. Comin, M.N. Hedhili, O.

F. Mohammed, Z.H. Lu, D.H. Kim, E.H. Sargent, O.M. Bakr, Highly efficient perovskite-quantum-dot light-emitting diodes by surface engineering, Adv. Mater. 28 (2016) 8718–8725, https://doi.org/10.1002/adma.201600784.
[112] S. Huang, B. Wang, Q. Zhang, Z. Li, A. Shan, L. Li, Postsynthesis potassium-modification method to improve stability of $CsPbBr_3$ perovskite nanocrystals, Adv. Opt. Mater. 6 (2018), 1701106, https://doi.org/10.1002/adom.201701106.
[113] Y.H. Suh, T. Kim, J.W. Choi, C.L. Lee, J. Park, High-performance CsPbX3 perovskite quantum-dot light-emitting devices via solid-state ligand exchange, ACS Appl. Nano Mater. 1 (2018) 488–496, https://doi.org/10.1021/acsanm.7b00212.
[114] L.M. Wheeler, E.M. Sanehira, A.R. Marshall, P. Schulz, M. Suri, N.C. Anderson, J. A. Christians, D. Nordlund, D. Sokaras, T. Kroll, S.P. Harvey, J.J. Berry, L.Y. Lin, J. M. Luther, Targeted ligand-exchange chemistry on cesium lead halide perovskite quantum dots for high-efficiency photovoltaics, J. Am. Chem. Soc. 140 (2018) 10504–10513, https://doi.org/10.1021/jacs.8b04984.
[115] F. Palazon, G. Almeida, Q.A. Akkerman, L. De Trizio, Z. Dang, M. Prato, L. Manna, Changing the dimensionality of cesium lead bromide nanocrystals by reversible postsynthesis transformations with amines, Chem. Mater. 29 (2017) 4167–4171, https://doi.org/10.1021/acs.chemmater.7b00895.
[116] T. Udayabhaskararao, L. Houben, H. Cohen, M. Menahem, I. Pinkas, L. Avram, T. Wolf, A. Teitelboim, M. Leskes, O. Yaffe, D. Oron, M. Kazes, A mechanistic study of phase transformation in perovskite nanocrystals driven by ligand passivation, Chem. Mater. 30 (2018) 84–93, https://doi.org/10.1021/acs.chemmater.7b02425.
[117] X. Chen, D. Chen, J. Li, G. Fang, H. Sheng, J. Zhong, Tunable CsPbBr3/Cs4PbBr6 phase transformation and their optical spectroscopic properties, Dalton Trans. 47 (2018) 5670–5678, https://doi.org/10.1039/c8dt00430g.
[118] Z. Liu, Y. Bekenstein, X. Ye, S.C. Nguyen, J. Swabeck, D. Zhang, S.T. Lee, P. Yang, W. Ma, A.P. Alivisatos, Ligand mediated transformation of cesium lead bromide perovskite nanocrystals to lead depleted Cs4PbBr6 nanocrystals, J. Am. Chem. Soc. 139 (2017) 5309–5312, https://doi.org/10.1021/jacs.7b01409.
[119] J. Li, H. Zhang, S. Wang, D. Long, M. Li, D. Wang, T. Zhang, Inter-conversion between different compounds of ternary Cs-Pb-Br system, Materials 11 (2018), https://doi.org/10.3390/ma11050717 (Basel).
[120] Q.A. Akkerman, S. Park, E. Radicchi, F. Nunzi, E. Mosconi, F. De Angelis, R. Brescia, P. Rastogi, M. Prato, L. Manna, Nearly monodisperse insulator Cs4PbX6 (X = Cl, Br, I) nanocrystals, their mixed halide compositions, and their transformation into CsPbX3 nanocrystals, Nano Lett. 17 (2017) 1924–1930, https://doi.org/10.1021/acs.nanolett.6b05262.
[121] F. Palazon, C. Urso, L. De Trizio, Q. Akkerman, S. Marras, F. Locardi, I. Nelli, M. Ferretti, M. Prato, L. Manna, Postsynthesis transformation of insulating Cs4PbBr6 nanocrystals into bright perovskite CsPbBr3 through physical and chemical extraction of CsBr, ACS Energy Lett. 2 (2017) 2445–2448, https://doi.org/10.1021/acsenergylett.7b00842.
[122] C. Rossi, R. Scarfiello, R. Brescia, L. Goldoni, G. Caputo, L. Carbone, D. Colombara, L. De Trizio, L. Manna, D. Baranov, Exploiting the transformative features of metal halides for the synthesis of $CsPbBr3@SiO_2$ Core–Shell Nanocrystals, Chem. Mater. 34 (2021) 405–413, https://doi.org/10.1021/ACS.CHEMMATER.1C03749.
[123] M. Li, X. Zhang, P. Yang, Controlling the growth of a SiO2 coating on hydrophobic CsPbBr3 nanocrystals towards aqueous transfer and high luminescence, Nanoscale 13 (2021) 3860–3867, https://doi.org/10.1039/D0NR08325A.
[124] S.K. Balakrishnan, P.V. Kamat, Ligand assisted transformation of cubic cspbbr3 nanocrystals into two-dimensional CsPb2Br5 nanosheets, Chem. Mater. 30 (2018) 74–78, https://doi.org/10.1021/acs.chemmater.7b04142.
[125] G. Li, H. Wang, Z. Zhu, Y. Chang, T. Zhang, Z. Song, Y. Jiang, Shape and phase evolution from CsPbBr3 perovskite nanocubes to tetragonal CsPb2Br5 nanosheets with an indirect bandgap, Chem. Commun. 52 (2016) 11296–11299, https://doi.org/10.1039/c6cc05877a.
[126] F. Palazon, S. Dogan, S. Marras, F. Locardi, I. Nelli, P. Rastogi, M. Ferretti, M. Prato, R. Krahne, L. Manna, From CsPbBr3 nano-inks to sintered CsPbBr3-CsPb2Br5 films via thermal annealing: implications on optoelectronic properties, J. Phys. Chem. C 121 (2017) 11956–11961, https://doi.org/10.1021/acs.jpcc.7b03389.
[127] J. Shamsi, P. Rastogi, V. Caligiuri, A.L. Abdelhady, D. Spirito, L. Manna, R. Krahne, Bright-emitting perovskite films by large-scale synthesis and photoinduced solid-state transformation of CsPbBr3 nanoplatelets, ACS Nano 11 (2017) 10206–10213, https://doi.org/10.1021/acsnano.7b04761.
[128] Y. Wang, X. Li, S. Sreejith, F. Cao, Z. Wang, M.C. Stuparu, H. Zeng, H. Sun, Photon driven transformation of cesium lead halide perovskites from few-monolayer nanoplatelets to bulk phase, Adv. Mater. 28 (2016) 10637–10643, https://doi.org/10.1002/adma.201604110.
[129] W. Shen, L. Ruan, Z. Shen, Z. Deng, Reversible light-mediated compositional and structural transitions between CsPbBr3 and CsPb2Br5 nanosheets, Chem. Commun. 54 (2018) 2804–2807, https://doi.org/10.1039/c8cc00139a.
[130] T. Yin, Y. Fang, W.K. Chong, K.T. Ming, S. Jiang, X. Li, J.L. Kuo, J. Fang, T.C. Sum, T.J. White, J. Yan, Z.X. Shen, High-pressure-induced comminution and recrystallization of $CH_3NH_3PbBr_3$ nanocrystals as large thin nanoplates, Adv. Mater. 30 (2018), 1705017, https://doi.org/10.1002/adma.201705017.
[131] G. Xiao, Y. Cao, G. Qi, L. Wang, C. Liu, Z. Ma, X. Yang, Y. Sui, W. Zheng, B. Zou, Pressure effects on structure and optical properties in cesium lead bromide perovskite nanocrystals, J. Am. Chem. Soc. 139 (2017) 10087–10094, https://doi.org/10.1021/jacs.7b05260.
[132] B. Turedi, K.J. Lee, I. Dursun, B. Alamer, Z. Wu, E. Alarousu, O.F. Mohammed, N. Cho, O.M. Bakr, Water-induced dimensionality reduction in metal-halide perovskites, J. Phys. Chem. C 122 (2018) 14128–14134, https://doi.org/10.1021/acs.jpcc.8b01343.
[133] L. Wu, H. Hu, Y. Xu, S. Jiang, M. Chen, Q. Zhong, D. Yang, Q. Liu, Y. Zhao, B. Sun, Q. Zhang, Y. Yin, From nonluminescent Cs4PbX6 (X = Cl, Br, I) nanocrystals to highly luminescent CsPbX3 nanocrystals: water-triggered transformation through a CsX-stripping mechanism, Nano Lett. 17 (2017) 5799–5804, https://doi.org/10.1021/acs.nanolett.7b02896.
[134] Y. Liu, D. Li, L. Zhang, Y. Chen, C. Geng, S. Shi, Z. Zhang, W. Bi, S. Xu, Amine- and acid-free synthesis of stable CsPbBr3 perovskite nanocrystals, Chem. Mater. 32 (2020) 1904–1913, https://doi.org/10.1021/acs.chemmater.9b04558.
[135] L. Wu, Q. Zhong, D. Yang, M. Chen, H. Hu, Q. Pan, H. Liu, M. Cao, Y. Xu, B. Sun, Q. Zhang, Improving the stability and size tunability of cesium lead halide perovskite nanocrystals using trioctylphosphine oxide as the capping ligand, Langmuir 33 (2017) 12689–12696, https://doi.org/10.1021/acs.langmuir.7b02963.
[136] Y. Li, X. Wang, W. Xue, W. Wang, W. Zhu, L. Zhao, Highly luminescent and stable CsPbBr 3 perovskite quantum dots modified by phosphine ligands, Nano Res. 12 (2019) 785–789, https://doi.org/10.1007/s12274-019-2289-8.
[137] H. Huang, B. Chen, Z. Wang, T.F. Hung, A.S. Susha, H. Zhong, A.L. Rogach, Water resistant CsPbX3 nanocrystals coated with polyhedral oligomeric silsesquioxane and their use as solid state luminophores in all-perovskite white light-emitting devices, Chem. Sci. 7 (2016) 5699–5703, https://doi.org/10.1039/c6sc01758d.
[138] T. Xuan, X. Yang, S. Lou, J. Huang, Y. Liu, J. Yu, H. Li, K.L. Wong, C. Wang, J. Wang, Highly stable CsPbBr3 quantum dots coated with alkyl phosphate for white light-emitting diodes, Nanoscale 9 (2017) 15286–15290, https://doi.org/10.1039/c7nr04179a.
[139] Z. Li, Q. Hu, Z. Tan, Y. Yang, M. Leng, X. Liu, C. Ge, G. Niu, J. Tang, Aqueous synthesis of lead halide perovskite nanocrystals with high water stability and bright photoluminescence, ACS Appl. Mater. Interfaces 10 (2018) 43915–43922, https://doi.org/10.1021/acsami.8b16471.
[140] S. Paul, A. Samanta, N-bromosuccinimide as bromide precursor for direct synthesis of stable and highly luminescent green-emitting perovskite nanocrystals, ACS Energy Lett. 5 (2020) 64–69, https://doi.org/10.1021/acsenergylett.9b02363.
[141] Y. Cao, Z. Zhang, L. Li, J.R. Zhang, J.J. Zhu, An improved strategy for high-quality cesium bismuth bromine perovskite quantum dots with remarkable electrochemiluminescence activities, Anal. Chem. 91 (2019) 8607–8614, https://doi.org/10.1021/acs.analchem.9b01918.
[142] Z. Xue, H. Gao, W. Liu, X. Li, Facile room-temperature synthesis of high-chemical-stability nitrogen-doped graphene quantum Dot/CsPbBr 3 composite, ACS Appl. Electron. Mater. 1 (2019) 2244–2252, https://doi.org/10.1021/acsaelm.9b00460.
[143] C. Wang, A.S.R. Chesman, J.J. Jasieniak, Stabilizing the cubic perovskite phase of CsPbI3 nanocrystals by using an alkyl phosphinic acid, Chem. Commun. 53 (2017) 232–235, https://doi.org/10.1039/c6cc08282c.
[144] J. Pan, Y. Shang, J. Yin, M. De Bastiani, W. Peng, I. Dursun, L. Sinatra, A.M. El-Zohry, M.N. Hedhili, A.H. Emwas, O.F. Mohammed, Z. Ning, O.M. Bakr, Bidentate ligand-passivated CsPbI 3 perovskite nanocrystals for stable near-unity photoluminescence quantum yield and efficient red light-emitting diodes, J. Am. Chem. Soc. 140 (2018) 562–565, https://doi.org/10.1021/jacs.7b10647.
[145] L. Gomez, C. De Weerd, J.L. Hueso, T. Gregorkiewicz, Color-stable water-dispersed cesium lead halide perovskite nanocrystals, Nanoscale 9 (2017) 631–636, https://doi.org/10.1039/c6nr08892a.
[146] J. Cheng, S. Yuan, L. Zhu, L. Chen, C. Liu, H. Tong, H. Zeng, Room-temperature *in situ* synthesis of highly efficient $CsPbBr3/SiO_2$ sol in entirely ethanol solvent by constructing amine-functionalized silica micelles, Langmuir 36 (2020) 3565–3572, https://doi.org/10.1021/acs.langmuir.0c00108.
[147] N. Ding, D. Zhou, X. Sun, W. Xu, H. Xu, G. Pan, D. Li, S. Zhang, B. Dong, H. Song, Highly stable and water-soluble monodisperse $CsPbX3/SiO_2$ nanocomposites for white-LED and cells imaging, Nanotechnology 29 (2018), 345703, https://doi.org/10.1088/1361-6528/AAC84D.
[148] Q. Zhong, M. Cao, H. Hu, D. Yang, M. Chen, P. Li, L. Wu, Q. Zhang, One-pot synthesis of highly stable $CsPbBr3@SiO^2$ core-shell nanoparticles, ACS Nano 12 (2018) 8579–8587, https://doi.org/10.1021/acsnano.8b04209.
[149] H. Hu, L. Wu, Y. Tan, Q. Zhong, M. Chen, Y. Qiu, D. Yang, B. Sun, Q. Zhang, Y. Yin, Interfacial synthesis of highly stable CsPbX3/oxide janus nanoparticles, J. Am. Chem. Soc. 140 (2018) 406–412, https://doi.org/10.1021/jacs.7b11003.
[150] W. Song, Y. Wang, B. Wang, Y. Yao, W. Wang, J. Wu, Q. Shen, W. Luo, Z. Zou, Super stable CsPbBr3@SiO2 tumor imaging reagent by stress-response encapsulation, Nano Res. 13 (2020) 795–801, https://doi.org/10.1007/s12274-020-2697-9.
[151] S. Li, D. Lei, W. Ren, X. Guo, S. Wu, Y. Zhu, A.L. Rogach, M. Chhowalla, A.K. Y. Jen, Water-resistant perovskite nanodots enable robust two-photon lasing in aqueous environment, Nat. Commun. 11 (2020) 1–8, https://doi.org/10.1038/s41467-020-15016-2.
[152] S. Huang, Z. Li, L. Kong, N. Zhu, A. Shan, L. Li, Enhancing the stability of CH3NH3PbBr3 quantum dots by embedding in silica spheres derived from tetramethyl orthosilicate in "waterless" toluene, J. Am. Chem. Soc. 138 (2016) 5749–5752, https://doi.org/10.1021/jacs.5b13101.
[153] Z.J. Li, E. Hofman, J. Li, A.H. Davis, C.H. Tung, L.Z. Wu, W. Zheng, Photoelectrochemically active and environmentally stable $CsPbBr_3/TiO_2$ core/shell nanocrystals, Adv. Funct. Mater. 28 (2018), 1704288, https://doi.org/10.1002/adfm.201704288.
[154] D.N. Dirin, L. Protesescu, D. Trummer, I.V. Kochetygov, S. Yakunin, F. Krumeich, N.P. Stadie, M.V. Kovalenko, Harnessing defect-tolerance at the nanoscale: highly luminescent lead halide perovskite nanocrystals in mesoporous silica matrixes,

Nano Lett. 16 (2016) 5866–5874, https://doi.org/10.1021/acs.nanolett.6b02688.
[155] Y. Huang, F. Li, L. Qiu, F. Lin, Z. Lai, S. Wang, L. Lin, Y. Zhu, Y. Wang, Y. Jiang, X. Chen, Enhancing the stability of CH 3 NH 3 PbBr 3 nanoparticles using double hydrophobic shells of SiO_2 and poly(vinylidene fluoride), ACS Appl. Mater. Interfaces 11 (2019) 26384–26391, https://doi.org/10.1021/acsami.9b07841.
[156] Y. Ji, M. Wang, Z. Yang, H. Qiu, S. Ji, J. Dou, N.V. Gaponenko, Highly stable Na: csPb(Br,I)3@Al_2O_3 nanocomposites prepared by a pre-protection strategy, Nanoscale 12 (2020) 6403–6410, https://doi.org/10.1039/d0nr00069h.
[157] P. Song, B. Qiao, D. Song, J. Cao, Z. Shen, G. Zhang, Z. Xu, S. Zhao, S. Wageh, A. Al-Ghamdi, Enhancing the stability and water resistance of CsPbBr3 perovskite nanocrystals by using tetrafluoride and zinc oxide as protective capsules, J. Mater. Sci. (2020) 1–9, https://doi.org/10.1007/s10853-020-04554-1.
[158] K.K. Liu, Q. Liu, D.W. Yang, Y.C. Liang, L.Z. Sui, J.Y. Wei, G.W. Xue, W.B. Zhao, X. Y. Wu, L. Dong, C.X. Shan, Water-induced MAPbBr3@PbBr(OH) with enhanced luminescence and stability, Light Sci. Appl. 9 (2020) 1–11, https://doi.org/10.1038/s41377-020-0283-2.
[159] Z.Z. Ma, Z.F. Shi, L.T. Wang, F. Zhang, D. Wu, D.W. Yang, X. Chen, Y. Zhang, C. X. Shan, X.J. Li, Water-induced fluorescence enhancement of lead-free cesium bismuth halide quantum dots by 130% for stable white light-emitting devices, Nanoscale 12 (2020) 3637–3645, https://doi.org/10.1039/c9nr10075j.
[160] A. Jana, K.S. Kim, Water-stable, fluorescent organic-inorganic hybrid and fully inorganic perovskites, ACS Energy Lett. 3 (2018) 2120–2126, https://doi.org/10.1021/acsenergylett.8b01394.
[161] K. Fu, Y. He, B. Zhang, X. Gao, G. Zou, Enhanced aqueous stability and radiative-charge-transfer of CsPbBr3/Ag2S perovskite nanocrystal hybrids, J. Electroanal. Chem. 858 (2020), 113835, https://doi.org/10.1016/j.jelechem.2020.113835.
[162] W. Chen, J. Hao, W. Hu, Z. Zang, X. Tang, L. Fang, T. Niu, M. Zhou, Enhanced stability and tunable photoluminescence in perovskite CsPbX3/ZnS quantum dot heterostructure, Small 13 (2017), https://doi.org/10.1002/smll.201604085.
[163] X. Tang, J. Yang, S. Li, W. Chen, Z. Hu, J. Qiu, CsPbBr3/CdS core/shell structure quantum dots for inverted light-emitting diodes application, Front. Chem. 7 (2019) 499, https://doi.org/10.3389/fchem.2019.00499.
[164] F.A. Rodríguez Ortiz, B.J. Roman, J.R. Wen, N. Mireles Villegas, D.F. Dacres, M. T. Sheldon, The role of gold oxidation state in the synthesis of Au-CsPbX3 heterostructure or lead-free Cs2AuIAuIIIX6 perovskite nanoparticles, Nanoscale 11 (2019) 18109–18115, https://doi.org/10.1039/c9nr07222e.
[165] S. Ye, M. Yu, W. Yan, J. Song, J. Qu, Enhanced photoluminescence of CsPbBr3@Ag hybrid perovskite quantum dots, J. Mater. Chem. C 5 (2017) 8187–8193, https://doi.org/10.1039/c7tc01969f.
[166] H.C. Yoon, H. Lee, H. Kang, J.H. Oh, Y.R. Do, Highly efficient wide-color-gamut QD-emissive LCDs using red and green perovskite core/shell QDs, J. Mater. Chem. C 6 (2018) 13023–13033, https://doi.org/10.1039/C8TC04537B.
[167] B. Qiao, P. Song, J. Cao, S. Zhao, Z. Shen, D. Gao, Z. Liang, Z. Xu, D. Song, X. Xu, Water-resistant, monodispersed and stably luminescent CsPbBr3/CsPb2Br5 core–shell-like structure lead halide perovskite nanocrystals, Nanotechnology 28 (2017), 445602, https://doi.org/10.1088/1361-6528/AA892E.
[168] S. Bhaumik, S.A. Veldhuis, Y.F. Ng, M. Li, S.K. Muduli, T.C. Sum, B. Damodaran, S. Mhaisalkar, N. Mathews, Highly stable, luminescent core-shell type methylammonium-octylammonium lead bromide layered perovskite nanoparticles, Chem. Commun. 52 (2016) 7118–7121, https://doi.org/10.1039/c6cc01056c.
[169] V.A. Hintermayr, C. Lampe, M. Löw, J. Roemer, W. Vanderlinden, M. Gramlich, A.X. Böhm, C. Sattler, B. Nickel, T. Lohmüller, A.S. Urban, Polymer nanoreactors shield perovskite nanocrystals from degradation, Nano Lett. 19 (2019) 4928–4933, https://doi.org/10.1021/acs.nanolett.9b00982.
[170] L.S. Hui, C. Beswick, A. Getachew, H. Heilbrunner, K. Liang, G. Hanta, R. Arbi, M. Munir, H. Dawood, N. Isik Goktas, R. Lapierre, M.C. Scharber, N.S. Sariciftci, A. Turak, Reverse micelle templating route to ordered monodispersed spherical organo-lead halide perovskite nanoparticles for light emission, ACS Appl. Nano Mater. 2 (2019) 4121–4132, https://doi.org/10.1021/acsanm.9b00585.
[171] S. Hou, Y. Guo, Y. Tang, Q. Quan, Synthesis and stabilization of colloidal perovskite nanocrystals by multidentate polymer micelles, ACS Appl. Mater. Interfaces 9 (2017) 18417–18422, https://doi.org/10.1021/acsami.7b03445.
[172] Y. Liu, Z. Wang, S. Liang, Z. Li, M. Zhang, H. Li, Z. Lin, Polar organic solvent-tolerant perovskite nanocrystals permanently ligated with polymer hairs via star-like molecular bottlebrush trilobe nanoreactors, Nano Lett. 19 (2019) 9019–9028, https://doi.org/10.1021/acs.nanolett.9b04047.
[173] S. Yang, F. Zhang, J. Tai, Y. Li, Y. Yang, H. Wang, J. Zhang, Z. Xie, B. Xu, H. Zhong, K. Liu, B. Yang, A detour strategy for colloidally stable block-copolymer grafted MAPbBr3 quantum dots in water with long photoluminescence lifetime, Nanoscale 10 (2018) 5820–5826, https://doi.org/10.1039/c8nr01493k.
[174] Y. He, Y.J. Yoon, Y.W. Harn, G.V. Biesold-McGee, S. Liang, C.H. Lin, V. V. Tsukruk, N. Thadhani, Z. Kang, Z. Lin, Unconventional route to dual-shelled organolead halide perovskite nanocrystals with controlled dimensions, surface chemistry, and stabilities, Sci. Adv. 5 (2019), https://doi.org/10.1126/sciadv.aax4424 eaax4424.
[175] Q.B. Yan, N. Bao, S.N. Ding, Thermally stable and hydrophilic CsPbBr3/mPEG-NH2 nanocrystals with enhanced aqueous fluorescence for cell imaging, J. Mater. Chem. B. 7 (2019) 4153–4160, https://doi.org/10.1039/c9tb00568d.
[176] J. Zhang, P. Jiang, Y. Wang, X. Liu, J. Ma, G. Tu, *In situ* synthesis of ultrastable CsPbBr3 perovskite nanocrystals coated with polyimide in a CSTR system, ACS Appl. Mater. Interfaces 12 (2020) 3080–3085, https://doi.org/10.1021/acsami.9b20880.
[177] M. Xie, H. Liu, F. Chun, W. Deng, C. Luo, Z. Zhu, M. Yang, Y. Li, W. Li, W. Yan, W. Yang, Aqueous phase exfoliating quasi-2D $CsPbBr_3$ nanosheets with ultrahigh intrinsic water stability, Small 15 (2019), 1901994, https://doi.org/10.1002/smll.201901994.
[178] P. Li, D. Yang, Y. Tan, M. Cao, Q. Zhong, M. Chen, H. Hu, B. Sun, Y. Xu, Q. Zhang, Consecutive interfacial transformation of cesium lead halide nanocubes to ultrathin nanowires with improved stability, ACS Appl. Mater. Interfaces 11 (2019) 3351–3359, https://doi.org/10.1021/acsami.8b19219.
[179] C. Collantes, V.G. Pedro, M.J. Bañuls, Á. Maquieira, Monodispersed CsPb2Br5@SiO_2core-shell nanoparticles as luminescent labels for biosensing, ACS Appl. Nano Mater. 4 (2021) 2011–2018, https://doi.org/10.1021/acsanm.0c03340.
[180] B. Wang, S. Zhang, B. Liu, J. Li, B. Cao, Z. Liu, Stable CsPbBr 3 :sn@SiO_2 and Cs 4 PbBr 6 :sn@SiO_2 core–shell quantum dots with tunable color emission for light-emitting diodes, ACS Appl. Nano Mater. 3 (2020) 3019–3027, https://doi.org/10.1021/acsanm.0c00299.
[181] V.K. Ravi, S. Saikia, S. Yadav, V.V. Nawale, A. Nag, CsPbBr3/ZnS core/shell type nanocrystals for enhancing luminescence lifetime and water stability, ACS Energy Lett. 5 (2020) 1794–1796, https://doi.org/10.1021/ACSENERGYLETT.0C00858/SUPPL_FILE/NZ0C00858_SI_001.PDF.
[182] X. Liu, X. Zhang, L. Li, J. Xu, S. Yu, X. Gong, J. Zhang, H. Yin, Stable luminescence of CsPbBr3/nCdS core/shell perovskite quantum dots with al self-passivation layer modification, ACS Appl. Mater. Interfaces 11 (2019) 40923–40931, https://doi.org/10.1021/ACSAMI.9B14967/SUPPL_FILE/AM9B14967_SI_001.PDF.
[183] X. Tang, J. Yang, S. Li, Z. Liu, Z. Hu, J. Hao, J. Du, Y. Leng, H. Qin, X. Lin, Y. Lin, Y. Tian, M. Zhou, Q. Xiong, X. Tang, J. Yang, S. Li, Z. Hu, J. Hao, M. Zhou, Z. Liu, J. Du, Y. Leng, H. Qin, X. Lin, Y. Lin, Y. Tian, Single halide perovskite/semiconductor core/shell quantum dots with ultrastability and nonblinking properties, Adv. Sci. 6 (2019), 1900412, https://doi.org/10.1002/ADVS.201900412.
[184] B. Wang, C. Zhang, S. Huang, Z. Li, L. Kong, L. Jin, J. Wang, K. Wu, L. Li, Postsynthesis phase transformation for CsPbBr3/Rb4PbBr6 core/shell nanocrystals with exceptional photostability, ACS Appl. Mater. Interfaces 10 (2018) 23303–23310, https://doi.org/10.1021/ACSAMI.8B04198/SUPPL_FILE/AM8B04198_SI_001.PDF.
[185] N. Tomczak, R. Liu, J.G. Vancso, Polymer-coated quantum dots, Nanoscale 5 (2013) 12018–12032, https://doi.org/10.1039/c3nr03949h.
[186] G. Palui, F. Aldeek, W. Wang, H. Mattoussi, Strategies for interfacing inorganic nanocrystals with biological systems based on polymer-coating, Chem. Soc. Rev. 44 (2015) 193–227, https://doi.org/10.1039/c4cs00124a.
[187] A. Jana, Q. Ba, A.S. Nissimagoudar, K.S. Kim, Formation of a photoactive quasi-2D formamidinium lead iodide perovskite in water, J. Mater. Chem. A 7 (2019) 25785–25790, https://doi.org/10.1039/c9ta09631k.
[188] F. Lamberti, L. Litti, M. De Bastiani, R. Sorrentino, M. Gandini, M. Meneghetti, A. Petrozza, F. Lamberti, M. De Bastiani, R. Sorrentino, M. Gandini, A. Petrozza, L. Litti, M. Meneghetti, High-quality, ligands-free, mixed-halide perovskite nanocrystals inks for optoelectronic applications, Adv. Energy Mater. 7 (2017), 1601703, https://doi.org/10.1002/AENM.201601703.
[189] J.C. Yu, A.Y. Lee, D. Bin Kim, E.D. Jung, D.W. Kim, M.H. Song, Enhancing the performance and stability of perovskite nanocrystal light-emitting diodes with a polymer matrix, Adv. Mater. Technol. 2 (2017), 1700003, https://doi.org/10.1002/admt.201700003.
[190] Y. Wang, J. He, H. Chen, J. Chen, R. Zhu, P. Ma, A. Towers, Y. Lin, A.J. Gesquiere, S.T. Wu, Y. Dong, Ultrastable, highly luminescent organic-inorganic perovskite-polymer composite films, Adv. Mater. 28 (2016) 10710–10717, https://doi.org/10.1002/adma.201603964.
[191] G. Rainò, A. Landuyt, F. Krieg, C. Bernasconi, S.T. Ochsenbein, D.N. Dirin, M. I. Bodnarchuk, M.V. Kovalenko, Underestimated effect of a polymer matrix on the light emission of single CsPbBr3 nanocrystals, Nano Lett. 19 (2019) 3648–3653, https://doi.org/10.1021/acs.nanolett.9b00689.
[192] J. Zhu, Z. Xie, X. Sun, S. Zhang, G. Pan, Y. Zhu, B. Dong, X. Bai, H. Zhang, H. Song, Highly efficient and stable inorganic perovskite quantum dots by embedding into a polymer matrix, ChemNanoMat 5 (2019) 346–351, https://doi.org/10.1002/cnma.201800357.
[193] Y. Li, Y. Lv, Z. Guo, L. Dong, J. Zheng, C. Chai, N. Chen, Y. Lu, C. Chen, One-step preparation of long-term stable and flexible CsPbBr3 perovskite quantum dots/ethylene vinyl acetate copolymer composite films for white light-emitting diodes, ACS Appl. Mater. Interfaces 10 (2018) 15888–15894, https://doi.org/10.1021/acsami.8b02857.
[194] P. Liang, P. Zhang, A. Pan, K. Yan, Y. Zhu, M. Yang, L. He, Unusual stability and temperature-dependent properties of highly emissive CsPbBr3 perovskite nanocrystals obtained from in situ crystallization in poly(vinylidene difluoride), ACS Appl. Mater. Interfaces 11 (2019) 22786–22793, https://doi.org/10.1021/acsami.9b06811.
[195] S.N. Raja, Y. Bekenstein, M.A. Koc, S. Fischer, D. Zhang, L. Lin, R.O. Ritchie, P. Yang, A.P. Alivisatos, Encapsulation of perovskite nanocrystals into macroscale polymer matrices: enhanced stability and polarization, ACS Appl. Mater. Interfaces 8 (2016) 35523–35533, https://doi.org/10.1021/acsami.6b09443.
[196] Y. Xin, H. Zhao, J. Zhang, Highly stable and luminescent perovskite-polymer composites from a convenient and universal strategy, ACS Appl. Mater. Interfaces 10 (2018) 4971–4980, https://doi.org/10.1021/acsami.7b16442.
[197] J. Ren, X. Dong, G. Zhang, T. Li, Y. Wang, Air-stable and water-resistant all-inorganic perovskite quantum dot films for white-light-emitting applications, New J. Chem. 41 (2017) 13961–13967, https://doi.org/10.1039/c7nj03017g.
[198] A. Pan, J. Wang, M.J. Jurow, M. Jia, Y. Liu, Y. Wu, Y. Zhang, L. He, Y. Liu, General strategy for the preparation of stable luminous nanocomposite inks using chemically addressable CsPbX3 peroskite nanocrystals, Chem. Mater. 30 (2018) 2771–2780, https://doi.org/10.1021/acs.chemmater.8b00587.

[199] Y. Zhang, Y. Zhao, D. Wu, J. Xue, Y. Qiu, M. Liao, Q. Pei, M.S. Goorsky, X. He, Homogeneous freestanding luminescent perovskite organogel with superior water stability, Adv. Mater. 31 (2019), 1902928, https://doi.org/10.1002/adma.201902928.
[200] C. Carrillo-Carrión, P. del Pino, B. Pelaz, Aqueous stable luminescent perovskite-polymer composites, Appl. Mater. Today 15 (2019) 562–569, https://doi.org/10.1016/j.apmt.2019.04.002.
[201] R. Al-Kassas, M. Bansal, J. Shaw, Nanosizing techniques for improving bioavailability of drugs, J. Control. Release 260 (2017) 202–212, https://doi.org/10.1016/j.jconrel.2017.06.003.
[202] M. Malamatari, K.M.G. Taylor, S. Malamataris, D. Douroumis, K. Kachrimanis, Pharmaceutical nanocrystals: production by wet milling and applications, Drug Discov. Today 23 (2018) 534–547, https://doi.org/10.1016/j.drudis.2018.01.016.
[203] M. Eslamian, M. Ahmed, N. Ashgriz, Modelling of nanoparticle formation during spray pyrolysis, Nanotechnology 17 (2006) 1674–1685, https://doi.org/10.1088/0957-4484/17/6/023.
[204] H. Chan, P. Chi, L. Kwok, Production methods for nanodrug particles using the bottom-up approach ☆, Adv. Drug Deliv. Rev. 63 (2011) 406–416, https://doi.org/10.1016/j.addr.2011.03.011.
[205] X. Yang, T. Xu, Y. Zhu, J. Cai, K. Gu, J. Zhu, Y. Wang, J. Shen, C. Li, Preparation of CsPbBr3@PS composite microspheres with high stability by electrospraying, J. Mater. Chem. C 6 (2018) 7971–7975, https://doi.org/10.1039/c8tc01408f.
[206] F. Wang, H. Wang, A. Ali, Y. Zhang, X. Cui, Y. Liu, In-situ one-step electrospray fabrication of polyvinylidene fluoride encapsulated CsPbBr3 spheres with high stability and cell imaging application, Inorg. Chem. Commun. 106 (2019) 99–103, https://doi.org/10.1016/j.inoche.2019.05.032.
[207] H. Liao, S. Guo, S. Cao, L. Wang, F. Gao, Z. Yang, J. Zheng, W. Yang, A general strategy for in situ growth of all-inorganic $CsPbX_3$ (X = Br, I, and Cl) perovskite nanocrystals in polymer fibers toward significantly enhanced water/thermal stabilities, Adv. Opt. Mater. 6 (2018), 1800346, https://doi.org/10.1002/adom.201800346.
[208] C.C. Lin, D.H. Jiang, C.C. Kuo, C.J. Cho, Y.H. Tsai, T. Satoh, C. Su, Water-resistant efficient stretchable perovskite-embedded fiber membranes for light-emitting diodes, ACS Appl. Mater. Interfaces 10 (2018) 2210–2215, https://doi.org/10.1021/acsami.7b15989.
[209] P.C. Tsai, J.Y. Chen, E. Ercan, C.C. Chueh, S.H. Tung, W.C. Chen, Uniform luminous perovskite nanofibers with color-tunability and improved stability prepared by one-step core/shell electrospinning, Small 14 (2018) 1–9, https://doi.org/10.1002/smll.201704379.
[210] D.H. Jiang, Y.H. Tsai, L. Veeramuthu, F.C. Liang, L.C. Chen, C.C. Lin, T. Satoh, S. H. Tung, C.C. Kuo, Novel ultra-stable and highly luminescent white light-emitting diodes from perovskite quantum dots - Polymer nanofibers through biaxial electrospinning, APL Mater. 7 (2019), https://doi.org/10.1063/1.5124880.
[211] Y. Wang, Y. Zhu, J. Huang, J. Cai, J. Zhu, X. Yang, J. Shen, H. Jiang, C. Li, CsPbBr3 perovskite quantum dots-based monolithic electrospun fiber membrane as an ultrastable and ultrasensitive fluorescent sensor in aqueous medium, J. Phys. Chem. Lett. 7 (2016) 4253–4258, https://doi.org/10.1021/acs.jpclett.6b02045.
[212] Y. Wang, Y. Zhu, J. Huang, J. Cai, J. Zhu, X. Yang, J. Shen, C. Li, Perovskite quantum dots encapsulated in electrospun fiber membranes as multifunctional supersensitive sensors for biomolecules, metal ions and pH, Nanoscale Horiz. 2 (2017) 225–232, https://doi.org/10.1039/c7nh00057j.
[213] L. Peltonen, H. Valo, R. Kolakovic, T. Laaksonen, J. Hirvonen, Electrospraying, spray drying and related techniques for production and formulation of drug nanoparticles, Expert Opin. Drug Deliv. 7 (2010) 705–719, https://doi.org/10.1517/17425241003716802.
[214] N.F. Borrelli, D.W. Smith, Quantum confinement of PbS microcrystals in glass, J. Non. Cryst. Solids 180 (1994) 25–31, https://doi.org/10.1016/0022-3093(94)90393-X.
[215] J.T. Remillard, D.G. Steel, Narrow nonlinear-optical resonances in CdSSe-doped glass, Opt. Lett. 13 (1988) 30, https://doi.org/10.1364/ol.13.000030.
[216] K. Han, W. Bin Im, J. Heo, W.J. Chung, A complete inorganic colour converter based on quantum-dot-embedded silicate glasses for white light-emitting-diodes, Chem. Commun. 52 (2016) 3564–3567, https://doi.org/10.1039/c5cc09539e.
[217] X. Di, Z. Hu, J. Jiang, M. He, L. Zhou, W. Xiang, X. Liang, Use of long-term stable CsPbBr3 perovskite quantum dots in phospho-silicate glass for highly efficient white LEDs, Chem. Commun. 53 (2017) 11068–11071, https://doi.org/10.1039/c7cc06486a.
[218] Y. Ye, W. Zhang, Z. Zhao, J. Wang, C. Liu, Z. Deng, X. Zhao, J. Han, Highly luminescent cesium lead halide perovskite nanocrystals stabilized in glasses for light-emitting applications, Adv. Opt. Mater. 7 (2019), 1801663, https://doi.org/10.1002/adom.201801663.
[219] A.D. Andreev, E.V. Kolobkova, A.A. Lipovskii, Optical absorption in PbSe spherical quantum dots embedded in glass matrix, J. Appl. Phys. 88 (2000) 750–757, https://doi.org/10.1063/1.373733.
[220] P. Li, C. Hu, L. Zhou, J. Jiang, Y. Cheng, M. He, X. Liang, W. Xiang, Novel synthesis and optical characterization of CsPb2Br5 quantum dots in borosilicate glasses, Mater. Lett. 209 (2017) 483–485, https://doi.org/10.1016/j.matlet.2017.08.079.
[221] S. Liu, M. He, X. Di, P. Li, W. Xiang, X. Liang, Precipitation and tunable emission of cesium lead halide perovskites (CsPbX3, X = Br, I) QDs in borosilicate glass, Ceram. Int. 44 (2018) 4496–4499, https://doi.org/10.1016/j.ceramint.2017.12.012.
[222] D. Chen, Y. Liu, C. Yang, J. Zhong, S. Zhou, J. Chen, H. Huang, Promoting photoluminescence quantum yields of glass-stabilized CsPbX3 (X = Cl, Br, I) perovskite quantum dots through fluorine doping, Nanoscale 11 (2019) 17216–17221, https://doi.org/10.1039/c9nr07307h.
[223] B. Ai, C. Liu, J. Wang, J. Xie, J. Han, X. Zhao, Precipitation and optical properties of $CsPbBr_3$ quantum dots in phosphate glasses, J. Am. Ceram. Soc. 99 (2016) 2875–2877, https://doi.org/10.1111/jace.14400.
[224] D. Chen, S. Yuan, J. Chen, J. Zhong, X. Xu, Robust CsPbX3 (X = Cl, Br, and I) perovskite quantum dot embedded glasses: nanocrystallization, improved stability and visible full-spectral tunable emissions, J. Mater. Chem. C 6 (2018) 12864–12870, https://doi.org/10.1039/c8tc04786c.
[225] D. Chen, S. Yuan, X. Chen, J. Li, Q. Mao, X. Li, J. Zhong, CsPbX3 (X = Br, I) perovskite quantum dot embedded low-melting phosphosilicate glasses: controllable crystallization, thermal stability and tunable emissions, J. Mater. Chem. C 6 (2018) 6832–6839, https://doi.org/10.1039/c8tc02407c.
[226] S. Yuan, D. Chen, X. Li, J. Zhong, X. Xu, In situ crystallization synthesis of CsPbBr3 perovskite quantum dot-embedded glasses with improved stability for solid-state lighting and random upconverted lasing, ACS Appl. Mater. Interfaces 10 (2018) 18918–18926, https://doi.org/10.1021/acsami.8b05155.
[227] X. Pang, H. Zhang, L. Xie, T. Xuan, Y. Sun, S. Si, B. Jiang, W. Chen, J. Zhuang, C. Hu, Y. Liu, B. Lei, X. Zhang, Precipitating CsPbBr3 quantum dots in boro-germanate glass with a dense structure and inert environment toward highly stable and efficient narrow-band green emitters for wide-color-gamut liquid crystal displays, J. Mater. Chem. C 7 (2019) 13139–13148, https://doi.org/10.1039/c9tc04732h.
[228] V. Malgras, S. Tominaka, J.W. Ryan, J. Henzie, T. Takei, K. Ohara, Y. Yamauchi, Observation of quantum confinement in monodisperse methylammonium lead halide perovskite nanocrystals embedded in mesoporous silica, J. Am. Chem. Soc. 138 (2016) 13874–13881, https://doi.org/10.1021/jacs.6b05608.
[229] V. Malgras, J. Henzie, T. Takei, Y. Yamauchi, Stable blue luminescent $CsPbBr_3$ perovskite nanocrystals confined in mesoporous thin films, Angew. Chem. Int. Ed. 57 (2018) 8881–8885, https://doi.org/10.1002/anie.201802335.
[230] V. Malgras, J. Henzie, T. Takei, Y. Yamauchi, Hybrid methylammonium lead halide perovskite nanocrystals confined in gyroidal silica templates, Chem. Commun. 53 (2017) 2359–2362, https://doi.org/10.1039/c6cc10245j.
[231] J.Y. Sun, F.T. Rabouw, X.F. Yang, X.Y. Huang, X.P. Jing, S. Ye, Q.Y. Zhang, Facile two-step synthesis of all-inorganic perovskite $CsPbX_3$ (X = Cl, Br, and I) zeolite-Y composite phosphors for potential backlight display application, Adv. Funct. Mater. 27 (2017), 1704371, https://doi.org/10.1002/adfm.201704371.
[232] C.H. Lin, T.Y. Li, J. Zhang, Z.Y. Chiao, P.C. Wei, H.C. Fu, L. Hu, M.J. Yu, G. H. Ahmed, X. Guan, C.H. Ho, T. Wu, B.S. Ooi, O.F. Mohammed, Y.J. Lu, X. Fang, J.H. He, Designed growth and patterning of perovskite nanowires for lasing and wide color gamut phosphors with long-term stability, Nano Energy 73 (2020), 104801, https://doi.org/10.1016/J.NANOEN.2020.104801.
[233] Z. Chen, Z.G. Gu, W.Q. Fu, F. Wang, J. Zhang, A confined fabrication of perovskite quantum dots in oriented MOF thin film, ACS Appl. Mater. Interfaces 8 (2016) 28737–28742, https://doi.org/10.1021/acsami.6b11712.
[234] W. Cha, H.J. Kim, S. Lee, J. Kim, Size-controllable and stable organometallic halide perovskite quantum dots/polymer films, J. Mater. Chem. C 5 (2017) 6667–6671, https://doi.org/10.1039/c7tc01562c.
[235] J. Ghosh, R. Ghosh, P.K. Giri, Mesoporous Si nanowire templated controlled fabrication of organometal halide perovskite nanoparticles with high photoluminescence quantum yield for light-emitting applications, ACS Appl. Nano Mater. 1 (2018) 1551–1562, https://doi.org/10.1021/acsanm.8b00047.
[236] S. Demchyshyn, J.M. Roemer, H. Groiß, H. Heilbrunner, C. Ulbricht, D. Apaydin, A. Böhm, U. Rütt, F. Bertram, G. Hesser, M.C. Scharber, N.S. Sariciftci, B. Nickel, S. Bauer, E.D. Głowacki, M. Kaltenbrunner, Confining metal-halide perovskites in nanoporous thin films, Sci. Adv. 3 (2017), e1700738, https://doi.org/10.1126/sciadv.1700738.
[237] Water-resistant multicolored bioimaging probes - advanced science news, (n.d.). https://www.advancedsciencenews.com/water-resistant-multicolored-bioimaging-probes/ (accessed December 14, 2020.
[238] F.O. Saouma, C.C. Stoumpos, M.G. Kanatzidis, Y.S. Kim, J.I. Jang, Multiphoton absorption order of CsPbBr3 as determined by wavelength-dependent nonlinear optical spectroscopy, J. Phys. Chem. Lett. 8 (2017) 4912–4917, https://doi.org/10.1021/acs.jpclett.7b02286.
[239] W. Chen, S. Bhaumik, S.A. Veldhuis, G. Xing, Q. Xu, M. Grätzel, S. Mhaisalkar, N. Mathews, T.C. Sum, Giant five-photon absorption from multidimensional core-shell halide perovskite colloidal nanocrystals, Nat. Commun. 8 (2017), https://doi.org/10.1038/ncomms15198.
[240] N.G. Horton, K. Wang, D. Kobat, C.G. Clark, F.W. Wise, C.B. Schaffer, C. Xu, *In vivo* three-photon microscopy of subcortical structures within an intact mouse brain, Nat. Photonics 7 (2013) 205–209, https://doi.org/10.1038/nphoton.2012.336.
[241] K.T. Yong, J. Qian, I. Roy, H.H. Lee, E.J. Bergey, K.M. Tramposch, S. He, M. T. Swihart, A. Maitra, P.N. Prasad, Quantum rod bioconjugates as targeted probes for confocal and two-photon fluorescence imaging of cancer cells, Nano Lett. 7 (2007) 761–765, https://doi.org/10.1021/nl063031m.
[242] R. Tenne, U. Rossman, B. Rephael, Y. Israel, A. Krupinski-Ptaszek, R. Lapkiewicz, Y. Silberberg, D. Oron, Super-resolution enhancement by quantum image scanning microscopy, Nat. Photonics 132 (2018) (2018) 116–122, https://doi.org/10.1038/s41566-018-0324-z, 13.
[243] B. Luo, S.B. Naghadeh, A. Allen, X. Li, J.Z. Zhang, Peptide-passivated lead halide perovskite nanocrystals based on synergistic effect between amino and carboxylic functional groups, Adv. Funct. Mater. 27 (2017), 1604018, https://doi.org/10.1002/adfm.201604018.
[244] Z. Yang, J. Xu, S. Zong, S. Xu, D. Zhu, Y. Zhang, C. Chen, C. Wang, Z. Wang, Y. Cui, Lead halide perovskite nanocrystals-phospholipid micelles and their

biological applications: multiplex cellular imaging and *in vitro* tumor targeting, ACS Appl. Mater. Interfaces 11 (2019) 47671–47679, https://doi.org/10.1021/acsami.9b12924.
[245] M.J.H. Tan, D. Ravichandran, H.L. Ang, E.W.Y. Ong, C.Q.X. Lim, G.M.Q. Kam, A. P. Kumar, Z. Tan, Magneto-fluorescent perovskite nanocomposites for directed cell motion and imaging, Adv. Healthc. Mater. 8 (2019), 1900859, https://doi.org/10.1002/adhm.201900859.
[246] C.Y. Zhong, L. Xiao, J. Zhou, Z. Chen, Y. Chen, Z.Q. Liu, J.Z. Zhang, Two-photon photoluminescence and bio-imaging application of monodispersed perovskite-in-silica nanocrystals with high biocompatibility, Chem. Eng. J. 431 (2022), 134110, https://doi.org/10.1016/J.CEJ.2021.134110.
[247] Y. Dong, X. Tang, Z. Zhang, J. Song, T. Niu, D. Shan, H. Zeng, Perovskite nanocrystal fluorescence-linked immunosorbent assay methodology for sensitive point-of-care biological test, Matter 3 (2020) 273–286, https://doi.org/10.1016/J.MATT.2020.05.004.
[248] C. Gao, H. Yu, Y. Wang, D. Liu, T. Wen, L. Zhang, S. Ge, J. Yu, Paper-based constant potential electrochemiluminescence sensing platform with black phosphorus as a luminophore enabled by a perovskite solar cell, Anal. Chem. 92 (2020) 6822–6826, https://doi.org/10.1021/acs.analchem.0c01033.
[249] A. Babayigit, A. Ethirajan, M. Muller, B. Conings, Toxicity of organometal halide perovskite solar cells, Nat. Mater. 15 (2016) 247–251, https://doi.org/10.1038/nmat4572.
[250] Best Research-Cell Efficiency Chart | Photovoltaic Research | NREL, (n.d.). https://www.nrel.gov/pv/cell-efficiency.html (accessed July 30, 2020.
[251] A. Hazarika, Q. Zhao, E.A. Gaulding, J.A. Christians, B. Dou, A.R. Marshall, T. Moot, J.J. Berry, J.C. Johnson, J.M. Luther, Perovskite quantum dot photovoltaic materials beyond the reach of thin films: full-range tuning of a-site cation composition, ACS Nano 12 (2018), https://doi.org/10.1021/acsnano.8b05555, 0.
[252] E.M. Sanehira, A.R. Marshall, J.A. Christians, S.P. Harvey, P.N. Ciesielski, L. M. Wheeler, P. Schulz, L.Y. Lin, M.C. Beard, J.M. Luther, Enhanced mobility CsPbI3 quantum dot arrays for record-efficiency, high-voltage photovoltaic cells, Sci. Adv. 3 (2017) eaao4204, https://doi.org/10.1126/sciadv.aao4204.
[253] Q. Zhao, A. Hazarika, X. Chen, S.P. Harvey, B.W. Larson, G.R. Teeter, J. Liu, T. Song, C. Xiao, L. Shaw, M. Zhang, G. Li, M.C. Beard, J.M. Luther, High efficiency perovskite quantum dot solar cells with charge separating heterostructure, Nat. Commun. 10 (2019) 1–8, https://doi.org/10.1038/s41467-019-10856-z.
[254] K. Ji, J. Yuan, F. Li, Y. Shi, X. Ling, X. Zhang, Y. Zhang, H. Lu, J. Yuan, W. Ma, High-efficiency perovskite quantum dot solar cells benefiting from a conjugated polymer-quantum dot bulk heterojunction connecting layer, J. Mater. Chem. A 8 (2020) 8104–8112, https://doi.org/10.1039/d0ta02743j.
[255] M. Hao, Y. Bai, S. Zeiske, L. Ren, J. Liu, Y. Yuan, N. Zarrabi, N. Cheng, M. Ghasemi, P. Chen, M. Lyu, D. He, J.H. Yun, Y. Du, Y. Wang, S. Ding, A. Armin, P. Meredith, G. Liu, H.M. Cheng, L. Wang, Ligand-assisted cation-exchange engineering for high-efficiency colloidal Cs1−xFAxPbI3 quantum dot solar cells with reduced phase segregation, Nat. Energy 5 (2020) 79–88, https://doi.org/10.1038/s41560-019-0535-7.
[256] L.J. Chen, C.R. Lee, Y.J. Chuang, Z.H. Wu, C. Chen, Synthesis and optical properties of lead-free cesium tin halide perovskite quantum rods with high-performance solar cell application, J. Phys. Chem. Lett. 7 (2016) 5028–5035, https://doi.org/10.1021/acs.jpclett.6b02344.
[257] J. Xue, J.W. Lee, Z. Dai, R. Wang, S. Nuryyeva, M.E. Liao, S.Y. Chang, L. Meng, D. Meng, P. Sun, O. Lin, M.S. Goorsky, Y. Yang, Surface ligand management for stable FaPbi3 perovskite quantum dot solar cells, Joule 2 (2018) 1866–1878, https://doi.org/10.1016/j.joule.2018.07.018.
[258] K. Chen, Q. Zhong, W. Chen, B. Sang, Y. Wang, T. Yang, Y. Liu, Y. Zhang, H. Zhang, Short-chain ligand-passivated stable α-CsPbI $_3$ quantum dot for all-inorganic perovskite solar cells, Adv. Funct. Mater. 29 (2019), 1900991, https://doi.org/10.1002/adfm.201900991.
[259] P. Meredith, A. Armin, LED technology breaks performance barrier, Nature 562 (2018) 197–198, https://doi.org/10.1038/d41586-018-06923-y.
[260] P. Azarhoosh, S. McKechnie, J.M. Frost, A. Walsh, M. Van Schilfgaarde, Research update: relativistic origin of slow electron-hole recombination in hybrid halide perovskite solar cells, APL Mater. 4 (2016), 091501, https://doi.org/10.1063/1.4955028.
[261] P.R. Brown, D. Kim, R.R. Lunt, N. Zhao, M.G. Bawendi, J.C. Grossman, V. Bulović, Energy level modification in lead sulfide quantum dot thin films through ligand exchange, ACS Nano 8 (2014) 5863–5872, https://doi.org/10.1021/nn500897c.
[262] J. Song, J. Li, X. Li, L. Xu, Y. Dong, H. Zeng, Quantum dot light-emitting diodes based on inorganic perovskite cesium lead halides (CsPbX3), Adv. Mater. 27 (2015) 7162–7167, https://doi.org/10.1002/adma.201502567.
[263] J. Li, L. Xu, T. Wang, J. Song, J. Chen, J. Xue, Y. Dong, B. Cai, Q. Shan, B. Han, H. Zeng, 50-fold EQE improvement up to 6.27% of solution-processed all-inorganic perovskite CsPbBr3 QLEDs via surface ligand density control, Adv. Mater. 29 (2017) 1–9, https://doi.org/10.1002/adma.201603885.
[264] T. Chiba, K. Hoshi, Y.J. Pu, Y. Takeda, Y. Hayashi, S. Ohisa, S. Kawata, J. Kido, High-efficiency perovskite quantum-dot light-emitting devices by effective washing process and interfacial energy level alignment, ACS Appl. Mater. Interfaces 9 (2017) 18054–18060, https://doi.org/10.1021/acsami.7b03382.
[265] J. Song, T. Fang, J. Li, L. Xu, F. Zhang, B. Han, Q. Shan, H. Zeng, Organic–inorganic hybrid passivation enables perovskite QLEDs with an EQE of 16.48%, Adv. Mater. 30 (2018) 1–9, https://doi.org/10.1002/adma.201805409.
[266] T. Chiba, Y. Hayashi, H. Ebe, K. Hoshi, J. Sato, S. Sato, Y.J. Pu, S. Ohisa, J. Kido, Anion-exchange red perovskite quantum dots with ammonium iodine salts for highly efficient light-emitting devices, Nat. Photonics 12 (2018) 681–687, https://doi.org/10.1038/s41566-018-0260-y.
[267] S.W. Wen, M.T. Lee, C.H. Chen, Recent development of blue fluorescent OLED materials and devices, J. Disp. Technol. 1 (2005), https://doi.org/10.1109/JDT.2005.852802.
[268] S. Zou, Y. Liu, J. Li, C. Liu, R. Feng, F. Jiang, Y. Li, J. Song, H. Zeng, M. Hong, X. Chen, Stabilizing cesium lead halide perovskite lattice through Mn(II) substitution for air-stable light-emitting diodes, J. Am. Chem. Soc. 139 (2017) 11443–11450, https://doi.org/10.1021/jacs.7b04000.
[269] J. Zhang, Y. Yang, H. Deng, U. Farooq, X. Yang, J. Khan, J. Tang, H. Song, High quantum yield blue emission from lead-free inorganic antimony halide perovskite colloidal quantum dots, ACS Nano 11 (2017) 9294–9302, https://doi.org/10.1021/acsnano.7b04683.
[270] M. Leng, Y. Yang, K. Zeng, Z. Chen, Z. Tan, S. Li, J. Li, B. Xu, D. Li, M. P. Hautzinger, Y. Fu, T. Zhai, L. Xu, G. Niu, S. Jin, J. Tang, All-inorganic bismuth-based perovskite quantum dots with bright blue photoluminescence and excellent stability, Adv. Funct. Mater. 28 (2018) 1–11, https://doi.org/10.1002/adfm.201704446.
[271] T. Guner, M.M. Demir, A review on halide perovskites as color conversion layers in white light emitting diode applications, Phys. Status Solidi 215 (2018), 1800120, https://doi.org/10.1002/pssa.201800120.
[272] M. Lu, Y. Zhang, S. Wang, J. Guo, W.W. Yu, A.L. Rogach, Metal halide perovskite light-emitting devices: promising technology for next-generation displays, Adv. Funct. Mater. 29 (2019), https://doi.org/10.1002/adfm.201902008.
[273] N.C. George, K.A. Denault, R. Seshadri, Phosphors for solid-state white lighting, Annu. Rev. Mater. Res. 43 (2013) 481–501, https://doi.org/10.1146/annurev-matsci-073012-125702.
[274] L. Wang, R.J. Xie, T. Suehiro, T. Takeda, N. Hirosaki, Down-conversion nitride materials for solid state lighting: recent advances and perspectives, Chem. Rev. 118 (2018) 1951–2009, https://doi.org/10.1021/acs.chemrev.7b00284.
[275] T. Ogi, A.B.D. Nandiyanto, K. Okino, F. Iskandar, W.N. Wang, E. Tanabe, K. Okuyama, Towards better phosphor design: effect of SiO_2 Nanoparticles on photoluminescence enhancement of YAG:ce, ECS J. Solid State Sci. Technol. 2 (2013) R91–R95, https://doi.org/10.1149/2.021305jss.
[276] T. Erdem, H.V. Demir, Color science of nanocrystal quantum dots for lighting and displays, Nanophotonics 2 (2013) 57–81, https://doi.org/10.1515/nanoph-2012-0031.
[277] C.M. Wang, Y.M. Su, T.A. Shih, G.Y. Chen, Y.Z. Chen, C.W. Lu, I.S. Yu, Z.P. Yang, H.C. Su, Achieving highly saturated single-color and high color-rendering-index white light-emitting electrochemical cells by CsPbX3 perovskite color conversion layers, J. Mater. Chem. C 6 (2018) 12808–12813, https://doi.org/10.1039/c8tc04451a.
[278] Y.H. Ko, M. Jalalah, S.J. Lee, J.G. Park, Super ultra-high resolution liquid-crystal-display using perovskite quantum-dot functional color-filters, Sci. Rep. 8 (2018) 12881, https://doi.org/10.1038/s41598-018-30742-w.
[279] Y.H. Song, S.H. Choi, J.S. Yoo, B.K. Kang, E.K. Ji, H.S. Jung, D.H. Yoon, Design of long-term stable red-emitting CsPb(Br0.4, I0.6)3perovskite quantum dot film for generation of warm white light, Chem. Eng. J. 313 (2017) 461–465, https://doi.org/10.1016/j.cej.2016.12.087.
[280] J. Zhou, Z. Hu, L. Zhang, Y. Zhu, Perovskite CsPbBr1.2I1.8 quantum dot alloying for application in white light-emitting diodes with excellent color rendering index, J. Alloy. Compd. 708 (2017) 517–523, https://doi.org/10.1016/j.jallcom.2017.03.043.
[281] J. Zhou, F. Huang, H. Lin, Z. Lin, J. Xu, Y. Wang, Inorganic halide perovskite quantum dot modified YAG-based white LEDs with superior performance, J. Mater. Chem. C 4 (2016) 7601–7606, https://doi.org/10.1039/c6tc02405j.
[282] Y.W. Zhang, G. Wu, H. Dang, K. Ma, S. Chen, Multicolored mixed-organic-cation perovskite quantum dots (FAxMA1-xPbX3, X = Br and I) for white light-emitting diodes, Ind. Eng. Chem. Res. 56 (2017) 10053–10059, https://doi.org/10.1021/acs.iecr.7b02309.
[283] F. Palazon, F. Di Stasio, Q.A. Akkerman, R. Krahne, M. Prato, L. Manna, Polymer-free films of inorganic halide perovskite nanocrystals as UV-to-white color-conversion layers in LEDs, Chem. Mater. 28 (2016) 2902–2906, https://doi.org/10.1021/acs.chemmater.6b00954.
[284] M. Leng, Z. Chen, Y. Yang, Z. Li, K. Zeng, K. Li, G. Niu, Y. He, Q. Zhou, J. Tang, Lead-free, blue emitting bismuth halide perovskite quantum dots, Angew. Chem. Int. Ed. 55 (2016) 15012–15016, https://doi.org/10.1002/anie.201608160.
[285] J. Luo, X. Wang, S. Li, J. Liu, Y. Guo, G. Niu, L. Yao, Y. Fu, L. Gao, Q. Dong, C. Zhao, M. Leng, F. Ma, W. Liang, L. Wang, S. Jin, J. Han, L. Zhang, J. Etheridge, J. Wang, Y. Yan, E.H. Sargent, J. Tang, Efficient and stable emission of warm-white light from lead-free halide double perovskites, Nature 563 (2018) 541–545, https://doi.org/10.1038/s41586-018-0691-0.
[286] E. López-Fraguas, B. Arredondo, C. Vega-Colado, G. del Pozo, M. Najafi, D. Martín-Martín, Y. Galagan, J.M. Sánchez-Pena, R. Vergaz, B. Romero, Visible Light Communication system using an organic emitter and a perovskite photodetector, Org. Electron. 73 (2019) 292–298, https://doi.org/10.1016/j.orgel.2019.06.028.
[287] B.R. Sutherland, S. Hoogland, M.M. Adachi, P. Kanjanaboos, C.T.O. Wong, J. J. McDowell, J. Xu, O. Voznyy, Z. Ning, A.J. Houtepen, E.H. Sargent, Perovskite thin films via atomic layer deposition, Adv. Mater. 27 (2015) 53–58, https://doi.org/10.1002/adma.201403965.
[288] H. Dong, C. Zhang, X. Liu, J. Yao, Y.S. Zhao, Materials chemistry and engineering in metal halide perovskite lasers, Chem. Soc. Rev. 49 (2020) 951–982, https://doi.org/10.1039/c9cs00598f.
[289] S. Das, S. Gholipour, M. Saliba, Perovskites for laser and detector applications, Energy Environ. Mater. 2 (2019) 146–153, https://doi.org/10.1002/eem2.12044.

[290] H. Zhang, Q. Liao, Y. Wu, Z. Zhang, Q. Gao, P. Liu, M. Li, J. Yao, H. Fu, H. Zhang, Y. Wu, J. Yao, H. Fu, Q. Liao, Z. Zhang, Q. Gao, P. Liu, M. Li, 2D ruddlesden–popper perovskites microring laser array, Adv. Mater. 30 (2018), 1706186, https://doi.org/10.1002/ADMA.201706186.
[291] J. Zhao, Y. Yan, C. Wei, W. Zhang, Z. Gao, Y.S. Zhao, Switchable single-mode perovskite microlasers modulated by responsive organic microdisks, Nano Lett. 18 (2018) 1241–1245, https://doi.org/10.1021/ACS.NANOLETT.7B04834/SUPPL_FILE/NL7B04834_SI_001.PDF.
[292] A. Zhizhchenko, S. Syubaev, A. Berestennikov, A.V. Yulin, A. Porfirev, A. Pushkarev, I. Shishkin, K. Golokhvast, A.A. Bogdanov, A.A. Zakhidov, A. A. Kuchmizhak, Y.S. Kivshar, S.V. Makarov, Single-mode lasing from imprinted halide-perovskite microdisks, ACS Nano 13 (2019) 4140–4147, https://doi.org/10.1021/ACSNANO.8B08948/SUPPL_FILE/NN8B08948_SI_001.PDF.
[293] Y. Wang, X. Li, V. Nalla, H. Zeng, H. Sun, Solution-processed low threshold vertical cavity surface emitting lasers from all-inorganic perovskite nanocrystals, Adv. Funct. Mater. 27 (2017), https://doi.org/10.1002/adfm.201605088.
[294] Y. Wang, X. Li, J. Song, L. Xiao, H. Zeng, H. Sun, All-inorganic colloidal perovskite quantum dots: a new class of lasing materials with favorable characteristics, Adv. Mater. 27 (2015) 7101–7108, https://doi.org/10.1002/adma.201503573.
[295] Y. Fu, H. Zhu, C.C. Stoumpos, Q. Ding, J. Wang, M.G. Kanatzidis, X. Zhu, S. Jin, Broad wavelength tunable robust lasing from single-crystal nanowires of cesium lead halide perovskites (CsPbX3, X = Cl, Br, I), ACS Nano 10 (2016) 7963–7972, https://doi.org/10.1021/acsnano.6b03916.
[296] L. Jiang, R. Liu, R. Su, Y. Yu, H. Xu, Y. Wei, Z.K. Zhou, X. Wang, Continuous wave pumped single-mode nanolasers in inorganic perovskites with robust stability and high quantum yield, Nanoscale 10 (2018) 13565–13571, https://doi.org/10.1039/c8nr03830a.
[297] K. Wang, S. Wang, S. Xiao, Q. Song, Recent advances in perovskite micro- and nanolasers, Adv. Opt. Mater. 6 (2018) 1–27, https://doi.org/10.1002/adom.201800278.
[298] P. Brenner, M. Stulz, D. Kapp, T. Abzieher, U.W. Paetzold, A. Quintilla, I. A. Howard, H. Kalt, U. Lemmer, Highly stable solution processed metal-halide perovskite lasers on nanoimprinted distributed feedback structures, Appl. Phys. Lett. 109 (2016), 141106, https://doi.org/10.1063/1.4963893.
[299] K. Park, J.W. Lee, J.D. Kim, N.S. Han, D.M. Jang, S. Jeong, J. Park, J.K. Song, Light-matter interactions in cesium lead halide perovskite nanowire lasers, J. Phys. Chem. Lett. 7 (2016) 3703–3710, https://doi.org/10.1021/acs.jpclett.6b01821.
[300] M. Li, Q. Gao, P. Liu, Q. Liao, H. Zhang, J. Yao, W. Hu, Y. Wu, H. Fu, Amplified spontaneous emission based on 2D ruddlesden-popper perovskites, Adv. Funct. Mater. 28 (2018), 1707006, https://doi.org/10.1002/adfm.201707006.
[301] A. Pisoni, J. Jaćimović, O.S. Barišić, M. Spina, R. Gaál, L. Forró, E. Horváth, Ultra-low thermal conductivity in organic-inorganic hybrid perovskite CH3NH3PbI3, J. Phys. Chem. Lett. 5 (2014) 2488–2492, https://doi.org/10.1021/jz5012109.
[302] A. Kovalsky, L. Wang, G.T. Marek, C. Burda, J.S. Dyck, Thermal conductivity of CH3NH3PbI3 and CsPbI3: measuring the effect of the methylammonium ion on phonon scattering, J. Phys. Chem. C 121 (2017) 3228–3233, https://doi.org/10.1021/acs.jpcc.6b12231.
[303] M. Levinshtein, S. Rumyantsev, M. Shur, Handbook Series on Semiconductor Parameters, World Scientific, 1996, https://doi.org/10.1142/2046-vol1.
[304] Q. Liao, X. Jin, H. Fu, Tunable halide perovskites for miniaturized solid-state laser applications, Adv. Opt. Mater. 7 (2019), 1900099, https://doi.org/10.1002/adom.201900099.
[305] M.R. Leyden, S. Terakawa, T. Matsushima, S. Ruan, K. Goushi, M. Auffray, A.S. D. Sandanayaka, C. Qin, F. Bencheikh, C. Adachi, Distributed feedback lasers and light-emitting diodes using 1-naphthylmethylamnonium low-dimensional perovskite, ACS Photonics 6 (2019) 460–466, https://doi.org/10.1021/acsphotonics.8b01413.
[306] C.C. Boyd, R. Cheacharoen, T. Leijtens, M.D. McGehee, Understanding degradation mechanisms and improving stability of perovskite photovoltaics, Chem. Rev. 119 (2019) 3418–3451, https://doi.org/10.1021/acs.chemrev.8b00336.
[307] W. Lv, L. Li, M. Xu, J. Hong, X. Tang, L. Xu, Y. Wu, R. Zhu, R. Chen, W. Huang, Improving the stability of metal halide perovskite quantum dots by encapsulation, Adv. Mater. 31 (2019), 1900682, https://doi.org/10.1002/adma.201900682.
[308] Y. Wei, Z. Cheng, J. Lin, An overview on enhancing the stability of lead halide perovskite quantum dots and their applications in phosphor-converted LEDs, Chem. Soc. Rev. 48 (2019) 310–350, https://doi.org/10.1039/c8cs00740c.
[309] H. Yu, X. Cheng, Y. Wang, Y. Liu, K. Rong, Z. Li, Y. Wan, W. Gong, K. Watanabe, T. Taniguchi, S. Wang, J. Chen, Y. Ye, L. Dai, Waterproof perovskite-hexagonal boron nitride hybrid nanolasers with low lasing thresholds and high operating temperature, ACS Photonics 5 (2018) 4520–4528, https://doi.org/10.1021/acsphotonics.8b00977.
[310] G. Xing, M.H. Kumar, W.K. Chong, X. Liu, Y. Cai, H. Ding, M. Asta, M. Grätzel, S. Mhaisalkar, N. Mathews, T.C. Sum, Solution-processed tin-based perovskite for near-infrared lasing, Adv. Mater. 28 (2016) 8191–8196, https://doi.org/10.1002/adma.201601418.
[311] S. Yakunin, Y. Shynkarenko, D.N. Dirin, I. Cherniukh, M.V. Kovalenko, Non-dissipative internal optical filtering with solution-grown perovskite single crystals for full-colour imaging, NPG Asia Mater. 9 (2017), https://doi.org/10.1038/am.2017.163 e431–e431.
[312] M. Sytnyk, S. Deumel, S.F. Tedde, G.J. Matt, W. Heiss, A perspective on the bright future of metal halide perovskites for X-ray detection, Appl. Phys. Lett. 115 (2019), 190501, https://doi.org/10.1063/1.5125999.
[313] S. Yakunin, M. Sytnyk, D. Kriegner, S. Shrestha, M. Richter, G.J. Matt, H. Azimi, C.J. Brabec, J. Stangl, M.V. Kovalenko, W. Heiss, Detection of X-ray photons by solution-processed lead halide perovskites, Nat. Photonics 9 (2015) 444–449, https://doi.org/10.1038/nphoton.2015.82.
[314] Y.C. Kim, K.H. Kim, D.Y. Son, D.N. Jeong, J.Y. Seo, Y.S. Choi, I.T. Han, S.Y. Lee, N.G. Park, Printable organometallic perovskite enables large-area, low-dose X-ray imaging, Nature (2017) 87–91, https://doi.org/10.1038/nature24032, 2017 5507674. 550.
[315] C. Zhang, B. Wang, W. Li, S. Huang, L. Kong, Z. Li, L. Li, Conversion of invisible metal-organic frameworks to luminescent perovskite nanocrystals for confidential information encryption and decryption, Nat. Commun. 81 (8) (2017) 1–9, https://doi.org/10.1038/s41467-017-01248-2, 2017.
[316] J. Liu, Y. Zhao, X. Li, J. Wu, Y. Han, X. Zhang, Y. Xu, Dual-emissive CsPbBr3@Eu-BTC composite for self-calibrating temperature sensing application, Cryst. Growth Des. 20 (2019) 454–459, https://doi.org/10.1021/ACS.CGD.9B01374.
[317] R. Tang, S. Zhou, H. Li, R. Chen, L. Zhang, L. Yin, Halogen bonding induced aqueously stable CsPbBr3@MOFs-Derived Co3O4/N-doped-C heterostructure for high-performance photoelectrochemical water oxidation, Appl. Catal. B Environ. 265 (2020), 118583, https://doi.org/10.1016/J.APCATB.2019.118583.
[318] D.H. Kang, S.R. Pae, J. Shim, G. Yoo, J. Jeon, J.W. Leem, J.S. Yu, S. Lee, B. Shin, J. H. Park, An ultrahigh-performance photodetector based on a perovskite–transition-metal-dichalcogenide hybrid structure, Adv. Mater. 28 (2016) 7799–7806, https://doi.org/10.1002/adma.201600992.
[319] W. Deng, L. Huang, X. Xu, X. Zhang, X. Jin, S.T. Lee, J. Jie, Ultrahigh-responsivity photodetectors from perovskite nanowire arrays for sequentially tunable spectral measurement, Nano Lett. 17 (2017) 2482–2489, https://doi.org/10.1021/acs.nanolett.7b00166.
[320] L. Dou, Y.M. Yang, J. You, Z. Hong, W.H. Chang, G. Li, Y. Yang, Solution-processed hybrid perovskite photodetectors with high detectivity, Nat. Commun. 5 (2014) 1–6, https://doi.org/10.1038/ncomms6404.
[321] J. Yu, X. Chen, Y. Wang, H. Zhou, M. Xue, Y. Xu, Z. Li, C. Ye, J. Zhang, P.A. Van Aken, P.D. Lund, H. Wang, A high-performance self-powered broadband photodetector based on a CH3NH3PbI3 perovskite/ZnO nanorod array heterostructure, J. Mater. Chem. C 4 (2016) 7302–7308, https://doi.org/10.1039/c6tc02097f.
[322] L. Gao, K. Zeng, J. Guo, C. Ge, J. Du, Y. Zhao, C. Chen, H. Deng, Y. He, H. Song, G. Niu, J. Tang, Passivated single-crystalline CH3NH3PbI3 nanowire photodetector with high detectivity and polarization sensitivity, Nano Lett. 16 (2016) 7446–7454, https://doi.org/10.1021/acs.nanolett.6b03119.
[323] Y. Fang, J. Huang, Resolving weak light of sub-picowatt per square centimeter by hybrid perovskite photodetectors enabled by noise reduction, Adv. Mater. 27 (2015) 2804–2810, https://doi.org/10.1002/adma.201500099.
[324] Q. Lin, A. Armin, D.M. Lyons, P.L. Burn, P. Meredith, Low noise, IR-blind organohalide perovskite photodiodes for visible light detection and imaging, Adv. Mater. 27 (2015) 2060–2064, https://doi.org/10.1002/adma.201405171.
[325] L. Shen, Y. Fang, D. Wang, Y. Bai, Y. Deng, M. Wang, Y. Lu, J. Huang, A self-powered, sub-nanosecond-response solution-processed hybrid perovskite photodetector for time-resolved photoluminescence-lifetime detection, Adv. Mater. 28 (2016) 10794–10800, https://doi.org/10.1002/adma.201603573.
[326] Z. Li, X. Liu, C. Zuo, W. Yang, X. Fang, Z.Q. Li, X.Y. Liu, C.L. Zuo, W. Yang, X. S. Fang, Supersaturation-controlled growth of monolithically integrated lead-free halide perovskite single-crystalline thin film for high-sensitivity photodetectors, Adv. Mater. 33 (2021), 2103010, https://doi.org/10.1002/ADMA.202103010.
[327] S.O. Kasap, J.A. Rowlands, Direct-conversion flat-panel X-ray image sensors for digital radiography, Proc. IEEE 90 (2002) 591–604, https://doi.org/10.1109/JPROC.2002.1002529.
[328] M.J. Yaffe, J.A. Rowlands, X-ray detectors for digital radiography, Phys. Med. Biol. 42 (1997) 1–39, https://doi.org/10.1088/0031-9155/42/1/001.
[329] Y.C. Kim, K.H. Kim, D.Y. Son, D.N. Jeong, J.Y. Seo, Y.S. Choi, I.T. Han, S.Y. Lee, N.G. Park, Printable organometallic perovskite enables large-area, low-dose X-ray imaging, Nature 550 (2017) 87–91, https://doi.org/10.1038/nature24032.